

ANALYSIS AND DEVELOPMENT OF EXPERIMENTAL CHARACTERIZATION METHODOLOGIES OF MODE II FRACTURE TOUGHNESS ON CFRP BONDED JOINTS

Magdalena Pérez Galmés

Per citar o enllaçar aquest document:
Para citar o enlazar este documento:
Use this url to cite or link to this publication:
<http://hdl.handle.net/10803/664508>

ADVERTIMENT. L'accés als continguts d'aquesta tesi doctoral i la seva utilització ha de respectar els drets de la persona autora. Pot ser utilitzada per a consulta o estudi personal, així com en activitats o materials d'investigació i docència en els termes establerts a l'art. 32 del Text Refós de la Llei de Propietat Intel·lectual (RDL 1/1996). Per altres utilitzacions es requereix l'autorització prèvia i expressa de la persona autora. En qualsevol cas, en la utilització dels seus continguts caldrà indicar de forma clara el nom i cognoms de la persona autora i el títol de la tesi doctoral. No s'autoritza la seva reproducció o altres formes d'explotació efectuades amb finalitats de lucre ni la seva comunicació pública des d'un lloc aliè al servei TDX. Tampoc s'autoritza la presentació del seu contingut en una finestra o marc aliè a TDX (framing). Aquesta reserva de drets afecta tant als continguts de la tesi com als seus resums i índexs.

ADVERTENCIA. El acceso a los contenidos de esta tesis doctoral y su utilización debe respetar los derechos de la persona autora. Puede ser utilizada para consulta o estudio personal, así como en actividades o materiales de investigación y docencia en los términos establecidos en el art. 32 del Texto Refundido de la Ley de Propiedad Intelectual (RDL 1/1996). Para otros usos se requiere la autorización previa y expresa de la persona autora. En cualquier caso, en la utilización de sus contenidos se deberá indicar de forma clara el nombre y apellidos de la persona autora y el título de la tesis doctoral. No se autoriza su reproducción u otras formas de explotación efectuadas con fines lucrativos ni su comunicación pública desde un sitio ajeno al servicio TDR. Tampoco se autoriza la presentación de su contenido en una ventana o marco ajeno a TDR (framing). Esta reserva de derechos afecta tanto al contenido de la tesis como a sus resúmenes e índices.

WARNING. Access to the contents of this doctoral thesis and its use must respect the rights of the author. It can be used for reference or private study, as well as research and learning activities or materials in the terms established by the 32nd article of the Spanish Consolidated Copyright Act (RDL 1/1996). Express and previous authorization of the author is required for any other uses. In any case, when using its content, full name of the author and title of the thesis must be clearly indicated. Reproduction or other forms of for profit use or public communication from outside TDX service is not allowed. Presentation of its content in a window or frame external to TDX (framing) is not authorized either. These rights affect both the content of the thesis and its abstracts and indexes.



Doctoral Thesis

Analysis and development of
experimental characterization
methodologies of mode II
fracture toughness on CFRP
bonded joints

Magdalena Pérez Galmés

2018



Doctoral Thesis

**Analysis and development of experimental
characterization methodologies of mode II
fracture toughness on CFRP bonded joints**

Magdalena Pérez Galmés

2018

Doctoral Program in Technology

Advisors:

Dr. Jordi Renart Canalias
Universitat de Girona

Dr. Carlos Sarrado Molina
Universitat de Girona

Thesis submitted for the degree of Doctor of Philosophy

Magdalena Pérez Galmés

Analysis and development of experimental characterization methodologies of mode II fracture toughness on CFRP bonded joints

Doctoral Thesis, 2018

Doctoral Program in Technology

Advisors: Dr. Jordi Renart Canalias and Dr. Carlos Sarrado Molina

Universitat de Girona

AMADE Research Group

Escola Politècnica Superior

Dept. d'Enginyeria Mecànica i de la Construcció Industrial

Carrer Universitat de Girona, 4. Campus de Montilivi

17003 Girona

A ca nostra.

” *It is not important to be better than someone else, but to be better than yesterday.*

— **Jigoro Kano**
(Judo founder)

Acknowledgement

First of all, I would like to express my gratitude to my advisors, Jordi Renart and Carlos Sarrado, for their endless support. Jordi encouraged me to begin this project and always made me left his office with more work but with more confidence, and Carlos have been my mentor, from the beginning in the laboratory, after as a students and now being my advisor.

Secondly, I would like to thank the AMADE research group directors, Joan Andreu and Josep for giving me the opportunity of belonging to this group. I would also like to thank Professor Andreas J. Brunner for the valuable discussions, and all the colleagues from Empa for the excellent treatment during my research stay at Empa (Switzerland). I felt at home.

Vull agrair a tots els companys d'AMADE, des dels meus companys de laboratori, passant per tots els professors del grup, fins als companys més propers pel seu recolzament, però sobretot per tants bons moments. També als PAS que sou tan simpàtics i ho poseu tot tan fàcil.

També vull agrair a totes les bones persones que han aportat granets "d'arena" en el meu camí. Esper no haver-vos decepcionat, ja sé que volia ser inventora però mira, al final he acabat espenyant coses. Als amics del teatre per un nou llenguatge, als castellers per enfilat-me ben amunt, als santantoniers per emocionar-me, a manafoc i als xítxeros per l'empenta, als músics i 'bandidos' per ensenyar-me que ningú reconeix millor els teus errors que tu mateix. I a les meves famílies: als judoques amb qui mai érem perfectes, als papayes on la rima si que ho és, i a

les rugberes amb qui mai caminem soles, per arribar ben lluny. També agraeixo a aquells amics, companys de pis i familiars amb qui compartim aficions més extravagants com fer matances, torròn, panades, caps d'anys temàtics, viatgets, esquiadetes, nedadetes, excursionetes, sortidetes, cervesetes, verbenetes i altres locuretes.

A més, vull agrair molt sincerament a n'en Toni Pascual totes les hores que m'ha dedicat. I com no, a na Mar i n'Adrià, que sempre me doten de confiança en tot allò que faig, però me frenen un poc si fa falta.

Per acabar, el més profund agraïment és per mumpare i mumare. Ells m'han ensenyat a estimar el que faig i m'han encoratjat a perseguir tot allò que estim. Jo de gran vull ser com voltros.

The work contained in this Ph.D. thesis was concluded in the AMADE research group (Department of Mechanical Engineering and Industrial Construction, University of Girona, Spain). The thesis was carried out under a pre-doctorate grant UdG BR-GR, funded by contract ABORDA.

Part of the research presented in this thesis was developed during the Ph.D. candidate's stay at Empa, Swiss Federal Laboratories for Materials Science and Research (Dübendorf, Switzerland) which was funded by University of Girona through the grant MOB17.

List of Publications

The present Ph.D. thesis has been prepared as a compendium of peer-reviewed journal papers, according to the regulations of the Universitat de Girona. The thesis is comprised of the following papers:

- M. Pérez-Galmés, J. Renart, C. Sarrado, A. Rodríguez-Bellido, J. Costa. A data reduction method based on the J -integral to obtain the interlaminar fracture toughness in a mode II end-loaded split (ELS) test. *Composites Part A: Applied Science and Manufacturing*, 2016; 90:670-677.
<http://dx.doi.org/10.1016/j.compositesa.2016.08.020>
ISSN: 1359-835X, Impact Factor: 4.075, ranked 2/44 in the category of *Engineering, Manufacturing* and ranked 4/25 in the category of *Materials Science, Composites* (1st quartile)¹.
- M. Pérez-Galmés, J. Renart, C. Sarrado, J. Costa. Suitable specimen dimensions for the determination of mode II fracture toughness of bonded joints by means of the ELS test. *Submitted to Engineering Fracture Mechanics*, 2018.
ISSN: 0013-7944, Impact Factor: 2.151, ranked 41/133 in the category of *Mechanics* (2nd quartile)¹.
- M. Pérez-Galmés, J. Renart, C. Sarrado, A.J. Brunner, A. Rodríguez-Bellido. Towards a consensus on mode II adhesive fracture testing: experimental study.

¹ According to the 2016 Journal Citation Reports

Submitted to Theoretical and Applied Fracture Mechanics, 2018.

ISSN:0167-8442, Impact Factor: 2.659, ranked 24/130 in the category of *Engineering, Mechanical* and ranked 21/133 in the category of *Mechanics*(1st quartile)².

Conferences

- M. Pérez-Galmés, J. Renart, C. Sarrado, J. Costa, A. Rodríguez-Bellido. Obtaining the Mode II Energy Fracture Toughness in a C-ELS Test by means of the J -integral. 7th International Conference on Composites Testing and Model Identification (CompTest 2015). Madrid (Spain). International Conference. Poster.
- M. Pérez-Galmés, J. Renart, C. Sarrado, A. Turon, J. Costa, A. Rodríguez-Bellido. Aplicación de la integral J para determinar la tenacidad a la fractura en modo II mediante el ensayo C-ELS (Matcomp 2015). Móstoles (Spain). National Conference. Oral presentation.
- M. Pérez-Galmés, J. Renart, C. Sarrado, A. Turon, J. Costa, A. Rodríguez-Bellido. Configuración del ensayo ELS para la determinación de la tenacidad a la fractura en modo II en uniones adhesivas (Matcomp 2017). Donostia, San Sebastián (Spain). National Conference. Oral presentation.
- J. Renart, M. Pérez-Galmés, C. Sarrado, J. Costa, A. Rodríguez-Bellido. Definition of the operation range for the determination of mode II fracture toughness of bonded joints by means of the ELS test. 8th International Conference on Fracture Polymers, composites and Adhesives 2017. Les Diablerets (Switzerland).
- M. Pérez-Galmés, J. Renart, C. Sarrado, J. Costa, A. Rodríguez-Bellido. Towards a consensus on mode II adhesive fracture testing and data reduction

² According to the 2016 Journal Citation Reports

methods. 18th European conference on composite materials (ECCM18 2018).
Athens (Greece).
International Conference. Accepted oral communication.



Dr. Jordi Renart Canalias, Associate Professor at Universitat de Girona,

and

Dr. Carlos Sarrado Molina, R&D Project Manager at AMADE Research Group (Universitat de Girona),

hereby CERTIFY that

The work entitled *Analysis and development of experimental characterization methodologies of mode II fracture toughness on CFRP bonded joints*, submitted for the doctoral degree by Magdalena Pérez Galmés, has been conducted under their supervision and that it fulfils the requirements to aim for the *International Mention*.

Girona, May 2018.

Jordi Renart Canalias
Universitat de Girona

Carlos Sarrado Molina
Universitat de Girona

List of Figures

1.1	Example of available propagation region in a mode II End Loaded Split (ELS) test.	3
1.2	Common mode II test geometries.	4
1.3	Other mode II test geometries.	7
1.4	A through thickness crack in an constant wide plate subjected to a remote tensile stress.	9
1.5	Example of use of big specimens in adhesive ENF tests, a) [77] $2L = 1000$ mm b) [123] $2L = 800$ mm.	15
2.1	Integration paths $\Gamma_a, \Gamma_b, \Gamma_c, \Gamma_d, \Gamma_e, \Gamma_f$ and Γ_g in the ELS specimen for derivation of J -integral equations.	27
2.2	Integration paths in the ELS specimen with large displacements assumption.	32
2.3	Specimen instrumentation: inclinometers and strain gauge. Location of section $S-S'$ and edges A and B.	37
2.4	Load-displacement curve of a 4.5 mm thick specimen. $PROP_i$ point corresponds to a crack growth of i mm visually measured. The dotted line is a straight unloading curve from the maximum displacement point to the zero of load and displacement used in the AREA data reduction method.	39
2.5	LEFM-based methods fracture toughness results. 4.5 mm thick specimen.	39

- 2.6 Fracture toughness results using the J -integral (large displacements correction) and LEFM-based methods. Results from a 4.5 mm thick specimen. 41
- 2.7 Strain profiles at section $S-S'$ measured with DIC and estimated from the strain gauge (ε_g) measurements for different propagation stages. Results from a 4.5 mm thick specimen. 42
- 3.1 Schematic of LEFM $P - \delta$ curve. Example of FPZ effects in the stability. 54
- 3.2 Schematic of two $P - \delta$ curve of same geometry (a_0/L below the LEFM-based stable limit) to illustrate the instability induced by the LD during the test. 55
- 3.3 a) Undeformed geometry of ELS specimen; b) Deformed geometry of ELS specimen. v corresponds to the shear deformation of the adhesive layer and w to the deflection; c) Positive directions of sectional loads and adhesive stresses in the interval $x \in [0, b]$, where W corresponds to the specimen width. 59
- 3.4 Bilinear constitutive relation of the adhesive layer. 60
- 3.5 $P - \delta$ curve from a FE model and the proposed analytical model. Results from specimens with the same geometry ($a_0 = 80$ mm, $H = 3$ mm, $W = 25$ mm and $L = 150$ mm) but with different cohesive properties. . . . 64
- 3.6 Working range of case 5 ($\mathcal{G}_{IIc} = 8$ kJ/m² and $\tau_{sh} = 30$ MPa). Specimens of 6 mm thickness. 66
- 3.7 Working domain of each case study. 71
- 3.8 Working domain of resins of \mathcal{G}_{IIc} between 0.7 kJ/m² and 3 kJ/m² and τ_{sh} between 30 MPa and 110 MPa. Relatives to cases 1 and 2. 73
- 3.9 Working domain of paste adhesives adhesives of \mathcal{G}_{IIc} between 3 kJ/m² and 5 kJ/m² and τ_{sh} between 17 MPa and 30 MPa. Relatives to cases 2 and 3. 73
- 3.10 Working domain of film adhesives of \mathcal{G}_{IIc} between 5 kJ/m² and 8 kJ/m² and τ_{sh} between 30 MPa and 45 MPa. Relatives to cases 4 and 5. . . 74

4.1	ELS geometry and instrumentation. Supports and loading applicators are represented in black. Two inclinometers are bonded at the load application points and at section $S-S'$. Dimensions: $L = 100$ mm, $a_0 = 55$, $a_f = 95$ mm and $L_S = 10$ mm.	87
4.2	ENF specimen, test geometry and instrumentation. Black circles correspond to the bottom supports and the centered loading application roller, and white circles represent the inclinometers. Dimensions used were: $L = 60$ mm and $a_0 = 35$ mm, $a_f = 60$ mm and loading roller diameter = 10 mm.	89
4.3	4ENF test fixture.	91
4.4	4ENF geometry and instrumentation. Black circles correspond to supports and loading rollers and white circles represent the inclinometers. Dimensions used were: $L = 60$ mm, $a_0 = 35$ mm, $a_f = 60$ mm and roller radius = 5 mm.	91
4.5	MMB geometry and instrumentation. In black, the supports and the loading applicators, white circles represent the inclinometers. Dimensions used were: $L = 60$ mm, $a_0 = 35$ mm, $a_f = 60$ mm and roller radius = 5 mm.	93
4.6	Load-displacement curves of tested specimens.	96
4.7	R -curve for each data reduction method of a representative M1 specimen from each batch. The energy release rate values are normalized with respect to the averaged value of J_{IIc} from the M1 ELS batch (blue line in (a)).	98
4.8	Summary of results. Batch average and standard deviation of each batch normalized with respect to the J_{IIc} average value from all specimens tested.	102
4.1	External applied loads and integration paths Γ in 4ENF specimen for J -integral derivation.	104
5.1	Working domain in a) ELS test and b) ENF test for a 25 mm width, and 6 mm and 12 mm thick specimens with a cohesive layer properties of $\mathcal{G}_{IIc} = 8$ kJ/m ² and $\tau_{sh} = 30$ MPa. The intersection of the two specimen thicknesses is represented in red and it is the working domain of specimens between these two thicknesses ($H = 3$ mm to $H = 6$ mm).	112

List of Tables

1.1	Summary of LEFM-based data reduction expressions used in the ENF test.	11
1.2	Summary of LEFM-based data reduction expressions used in the ELS test.	12
1.3	Summary of LEFM-based data reduction expressions used in the 4ENF test.	12
1.4	Summary of J -integral-based data reduction expressions for common mode I, mode II and mixed mode I/II tests.	18
2.1	Data reduction methods nomenclature.	38
2.2	Fracture toughness propagation values obtained from different data reduction methods (LEFM and J -integral) from the batches with 3 mm and 4.5 mm thick specimens. Values obtained from the propagation range within points PROP ₇ and PROP ₁₅ of each specimen (propagation points at which the fracture toughness becomes constant). The values in brackets refer to the difference respect \mathcal{G}_{IIc} (CBTE) in %.	44
3.1	Mechanical properties (fracture toughness, shear failure strength and Young's modulus) of common adhesives used in aeronautics.	68
3.2	Cohesive properties and geometries considered in the analytical model.	69
4.1	Measurements before testing and during the test.	86
4.2	ELS data reduction methods.	88

4.3 ENF data reduction methods summary. 90

4.4 Summary of 4ENF data reduction methods. 93

4.5 ELS tests summary of results. All values are normalized with respect to the averaged value of J_{IIc} from the M1 ELS batch. 99

4.6 ENF tests summary of results. All values normalized with respect to averaged value of J_{IIc} from the M1 ELS batch. 99

4.7 4ENF summary of results. All values normalized with respect to the averaged value of J_{IIc} from the M1 ELS batch. 100

4.8 MMB tests summary of results. All values normalized with respect to the averaged value of J_{IIc} from the M1 ELS batch. 101

Contents

1	Introduction	1
1.1	Background	1
1.2	Mode II experimental tests	3
1.3	Mode II data reduction methods	7
1.3.1	Linear Elastic Fracture Mechanics	8
1.3.2	Considerations in mode II adhesive testing	12
1.3.3	Cohesive Zone Model approach	15
1.4	Motivation	18
1.5	Objectives	19
1.6	Thesis structure	20
2	A data reduction method based on the J-integral to obtain the inter-laminar fracture toughness in a mode II end-loaded split (ELS) test	21
2.1	Introduction	23
2.2	Analytical formulation	25
2.2.1	Large displacements correction	31
2.3	Experimental campaign	34
2.3.1	Test procedure	35
2.3.2	Instrumentation	36
2.3.3	Data reduction	37
2.4	Results	38
2.5	Discussion	40

2.6	Conclusions	45
3	Suitable specimen dimensions for the determination of mode II fracture toughness of bonded joints by means of the ELS test	47
3.1	Introduction	49
3.2	ELS specimen design criteria	52
3.2.1	Full FPZ development criterion	52
3.2.2	Stability criterion	53
3.2.3	Large deflections criterion	55
3.2.4	Adherend failure criterion	56
3.3	Analytical model	58
3.4	Definition of a working domain	65
3.4.1	Working domain for known adhesive properties	65
3.4.2	Definition of a general domain	67
3.5	Results	69
3.6	Discussion	74
3.7	Conclusions	76
4	Towards a consensus on mode II adhesive fracture testing typologies and data reduction methods: experimental study	79
4.1	Introduction	81
4.2	Experimental test campaign	83
4.2.1	End-Loaded Split (ELS) test	86
4.2.2	End-Notched Flexure (ENF) test	88
4.2.3	Four-point End Notched Flexure (4ENF) test	90
4.2.4	Mixed Mode Bending (MMB) test	92
4.3	Results and discussion	94
4.4	Conclusions	102
5	Discussion	107
6	Concluding remarks	117
6.1	Conclusions	117
6.2	Perspectives and future work	121

Bibliography	123
A Appendix. Generated papers	137
A.1 A data reduction method based on the J -integral to obtain the interlaminar fracture toughness in a mode II end-loaded split (ELS) test	139
A.2 Suitable specimen dimensions for the determination of mode II fracture toughness of bonded joints by means of the ELS test	149
A.3 Towards a consensus on mode II adhesive fracture testing: experimental study	181

Abstract

Adhesives have been shown to be an excellent solution for joining fibre reinforced polymer (FRP) components thanks to their capacity to redistribute loads, reduces stress concentrations and contribute to overall weight saving in the structure. Compared to other joining methods, such as mechanical fasteners, adhesive joints also reduce the number of components and the processing time, which results in a reduction in both manufacturing and operational costs of lightweight structures.

Despite all these benefits, predicting adhesive joints failure is still not fully understood, and the development and improvement of robust tools to evaluate and understand the mechanisms of fracture are required, especially when the adhesive joints are used to join structural components.

Adhesive joints work better under shear rather than traction or peel loads, and this is why, they are designed such that the joint mainly works in shear, and tensile or peel stresses are avoided. For this reason, the most relevant mechanical property in adhesive bonded joints design is the shear (mode II) fracture toughness of the adhesive.

Nowadays, most of the test methods to determine fracture toughness in mode II have been designed for the study of delamination i.e., the debonding of the matrix between the composite layers. However, directly applying these methods to adhesive joints entails some major limitations that result in severe under/over estimations of the adhesive properties and, in many cases, can even prevent results from being obtained from tests.

In view of these limitations, the main objective of the present thesis is to develop robust tools for the determination of shear (mode II) fracture toughness in adhesive joints. The applicability of the existing mode II delamination test methods to structural adhesive joints is studied. This includes studying data reduction methods as well as the test geometries.

On the one hand, two new data reduction methods for two types of mode II fracture toughness tests are presented. As these methods take into account the existence of large fracture process zones compared with the size of the specimen, they extend the applicability from delamination tests, which are well described by linear elastic fracture mechanics, to structural adhesive testing, whose analysis requires a non-linear fracture mechanics framework. The methods presented not only have a wider range of applicability than those available in the test standards, but they also decrease the uncertainty in the results.

Furthermore, a new specimen design method to define suitable specimen test geometries for test adhesives is presented. The proposed method allows for the preliminary design of specimen geometry to ensure that stable propagation results can be obtained from the test, reaching the steady state propagation of the test once the fracture process zone is fully developed.

Finally, the suitability of mode II fracture toughness test methods for structural adhesives is discussed. A test campaign including the four most widespread mode II test configurations is performed. The different test configurations and data reduction methods available and those proposed in this work are compared and discussed. Final recommendations for the mode II testing of structural adhesives are drawn from this analysis.

Resum

Els adhesius han demostrat ser una magnífica solució per unir components de polímers reforçats amb fibres (FRP) gràcies a la seva capacitat per redistribuir càrregues, reduir les concentracions de tensions i contribuir a l'estalvi general de pes en l'estructura. En comparació amb altres mètodes d'unió, com les fixacions mecàniques, les unions adhesives també redueixen la quantitat de components i el temps de processament, el que es tradueix en una reducció dels costos de fabricació de les estructures lleugeres.

Malgrat tots aquests beneficis, la predicció de ruptura de les unions adhesives encara no està ben definida, i es requereix el desenvolupament i millora d'eines robustes per avaluar i comprendre els mecanismes de fractura, especialment quan les unions adhesives s'usen per unir components estructurals.

Les unions adhesives treballen millor sota càrregues a tallant que sota càrregues de tracció o de pelat. Per aquesta raó, estan dissenyades de manera que la unió treballi principalment a tallant, mentre que s'eviten les tensions de tracció o de pelat. Per aquest motiu, la propietat mecànica més rellevant en el disseny d'unions adhesives és la tenacitat a la fractura a tallant (mode II) de l'adhesiu.

Avui en dia, la majoria dels mètodes d'assaig per a la determinació de la tenacitat a la fractura en mode II estan dissenyats per a l'estudi de la deslaminació, el desenganxament de la matriu entre les capes de compòsit. No obstant, l'aplicació directa d'aquests mètodes a les unions adhesives pot derivar en estimacions errònies, per sota o per sobre, de les propietats adhesives i, en molts casos, evitar que l'assaig es pugui realitzar satisfactòriament.

En vista d'aquestes limitacions, l'objectiu principal d'aquesta tesi és el desenvolupament d'eines robustes per a la determinació de la tenacitat a la fractura a tallant (mode II) d'unions adhesives. S'estudia l'aplicabilitat dels mètodes d'assaig de deslaminació en mode II existents a les unions adhesives estructurals. Això inclou l'estudi dels mètodes de reducció de dades i de les geometries d'assaig.

Per una banda, es presenten dos nous mètodes de reducció de dades per a dos tipus d'assajos de tenacitat a la fractura en mode II. Aquests mètodes tenen en compte l'existència de grans zones de procés de falla en comparació amb la mida de la proveta. Per tant, amplien l'aplicabilitat dels assajos de deslaminació, que estan ben descrites dins el marc de la mecànica de la fractura lineal i elàstica, a l'assaig d'adhesius estructurals, que requereixen un anàlisi dins el marc de la mecànica de la fractura no lineal. Els mètodes presentats tenen un rang més ampli d'aplicabilitat que els disponibles en els assajos estandaritzats i disminueixen la incertesa en els resultats.

També es presenta un nou mètode de disseny de provetes per definir geometries adequades per a l'assaig d'adhesius. El mètode permet dissenyar la geometria de la proveta a priori per tal de garantir l'obtenció de resultats de propagació estable durant l'assaig, aconseguint un règim estable de propagació quan la zona del procés de fractura s'ha desenvolupat completament.

Finalment, es discuteix la idoneïtat dels mètodes d'assaig de tenacitat a la fractura en mode II en l'estudi d'adhesius estructurals. Es realitza una campanya d'assajos que inclou les quatre configuracions d'assaig en mode II més esteses. A partir d'aquesta, es comparen i discuteixen les diferents configuracions d'assaig i els mètodes de reducció de dades disponibles i proposats en aquest treball. D'aquest anàlisi s'extreuen algunes recomanacions finals per a l'assaig d'adhesius estructurals en mode II.

Resumen

Los adhesivos han demostrado ser una excelente solución para unir componentes de polímeros reforzados con fibras (FRP) gracias a su capacidad para redistribuir cargas, reducir las concentraciones de tensiones y contribuir al ahorro general de peso en la estructura. En comparación con otros métodos de unión, como las fijaciones mecánicas, las uniones adhesivas también reducen la cantidad de componentes y el tiempo de procesamiento, lo que se traduce en una reducción de los costos de fabricación de las estructuras ligeras.

A pesar de todos estos beneficios, la predicción de la ruptura en las uniones adhesivas aún no está bien definida, y se requiere el desarrollo y mejora de herramientas robustas para evaluar y comprender los mecanismos de fractura, especialmente cuando las uniones adhesivas se usan para unir componentes estructurales.

Las uniones adhesivas funcionan mejor bajo cargas a cortante que bajo cargas de tracción o pelado. Por esta razón, están diseñadas de manera que la unión funcione principalmente a cortante, mientras que se evitan las tensiones de tracción o pelado. Por esta razón, la propiedad mecánica más relevante en el diseño de uniones adhesivas es la tenacidad a la fractura a cortante (modo II) del adhesivo.

Hoy en día, la mayoría de los métodos de ensayo para la determinación de la tenacidad a la fractura en el modo II están diseñados para el estudio de la delaminación, el despegue de la matriz entre las capas de composite. Sin embargo, la aplicación directa de estos métodos a las uniones adhesivas puede derivar en estimaciones erróneas, por debajo o por encima, de las propiedades adhesivas y, en muchos casos, evitar que el ensayo se pueda realizar satisfactoriamente.

En vista de estas limitaciones, el objetivo principal de esta tesis es el desarrollo de herramientas robustas para la determinación de la tenacidad de la fractura a cortante (modo II) en uniones adhesivas. Se estudia la aplicabilidad de los métodos de ensayo de delaminación en modo II existentes a las uniones adhesivas estructurales. Esto incluye el estudio de los métodos de reducción de datos y de las geometrías de ensayo.

Por una parte, se presentan dos nuevos métodos de reducción de datos para dos tipos de ensayos de tenacidad a la fractura en modo II. Estos métodos tienen en cuenta la existencia de grandes zonas de proceso de fallo en comparación con el tamaño de la probeta. Por lo tanto, amplían la aplicabilidad de los ensayos de delaminación, que están bien descritas según la mecánica de la fractura lineal y elástica, al ensayo de adhesivos estructurales, que requieren un análisis dentro del marco de la mecánica de la fractura no lineal. Los métodos presentados tienen un rango más amplio de aplicabilidad que los disponibles en los estándares de ensayo y disminuyen la incertidumbre en los resultados.

También se presenta un nuevo método de diseño de probetas para definir geometrías adecuadas para ensayar adhesivos. El método propuesto permite el diseño preliminar de la geometría de la probeta para garantizar que se puedan obtener resultados de propagación estables, alcanzando un régimen estable de propagación una vez que la zona del proceso de fallo se ha desarrollado completamente.

Finalmente, se discute la idoneidad de los métodos de ensayo de tenacidad a la fractura en modo II en el estudio de adhesivos estructurales. Se realiza una campaña de ensayos que incluye las cuatro configuraciones de ensayo de modo II más extendidas. A partir de esta, se comparan y discuten las diferentes configuraciones de ensayo y los métodos de reducción de datos disponibles y propuestos en este trabajo. De este análisis se extraen algunas recomendaciones finales para el ensayo de adhesivos estructurales en modo II.

Introduction

1.1 Background

The use of adhesives on Fibre Reinforced Polymer composite (FRP) assemblies is a natural step on composites structural design due to their capability to redistribute the loads, resulting in a reduction of the stress concentrations. For this reason, they are a suitable replacement for traditional mechanical fasteners (bolts, screws, studs, rivets, ...), while additionally reducing the number of components used in a joint, decreasing its weight-to-stiffness ratio and reducing their derived costs.

Despite the benefits, the failure prediction of such joints are still not well defined, and precise tools need to be developed or improved, specially when used in structural components. Under this context, it is essential to understand the fracture mechanisms of adhesive joints, taking special care of determining the most relevant fracture properties. The adhesive bonded joints perform better in shear loading rather than under tensile or peel loadings [68]. For this reason, they are designed such that the adhesive is mainly loaded in in-plane shear, while tension or peel stresses are usually avoided [20]. Thus, the most relevant mechanical property in their design is the shear (mode II) fracture toughness of the adhesive.

Nowadays, the majority of test methodologies used to determine structural adhesive fracture toughness are based on procedures that have been developed for studying delamination (matrix debonding between composite plies). This may result in erroneous fracture toughness measurement, or even the prevention to perform the test satisfactorily.

When a crack appears inside an adhesive, it develops a region where the material is damaged, but it is still capable of transferring stresses. Normally, these stresses decrease as the crack opens. This region is defined in the literature as the Fracture

Process Zone (FPZ). The size of this region is defined by numerous parameters, such as the loading conditions, the specimen size or the material properties [16].

During a test involving FPZ, we can distinguish three main steps; FPZ development, crack propagation and stiffening. At the first stage the FPZ starts to develop (onset) and once the FPZ is fully developed, the crack starts to propagate in a self similar way (propagation) until approaching the boundaries, when the system starts to strengthen.

When testing structural adhesives (adhesives used in load-bearing structural assemblies) under peel loads (mode I), the developed FPZ is relatively small with respect to the standard specimen dimensions. Under these circumstances, it is possible to use delamination-based procedures to measure structural adhesive fracture toughness.

On the other hand, in structural adhesives loaded in shear, the developed FPZ is of comparable size with respect to the specimen dimensions when using delamination-based procedures. Therefore, the FPZ involved may affect the specimens dimensioning and data reduction.

If the FPZ is not totally formed during the test, steady state propagation is not reached and the propagation fracture toughness can not be measured. To achieve the total FPZ development, the specimen must be sufficiently large to entail such FPZ and the test must be stable. In the majority of mode II tests, this two conditions are interrelated. The stability condition usually depend on the initial crack length to span length rate (a_0/L). The same relationship provides, for the same specimen length, the length available for the FPZ to develops and/or the crack to propagate (propagation region, $L - a_0$, c.f Figure 1.1).

In structural adhesives mode II testing, apart from the difficulties derived from the FPZ formation, another issue arises related to the test data reduction to determine the fracture toughness.

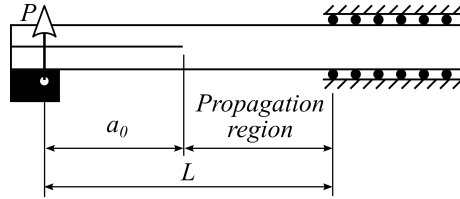


Fig. 1.1.: Example of available propagation region in a mode II End Loaded Split (ELS) test.

In that account, the existing data reduction methodologies used in mode II testing have evolved from the simplicity of Linear Elastic Fracture Mechanics (LEFM), in which a sharp crack tip is considered, to more complex models that account for the non-linear behaviour (i.e. FPZ) of the material in the formation of new crack surface, the so called Cohesive Zone Models (CZM).

Within the CZM framework, the J -integral approach, proposed by Rice [101], have been used to characterize fracture processes with large FPZs. Based on this approach, simple J -integral closed-form solutions for some specific fracture toughness tests have been developed.

1.2 Mode II experimental tests

Various mode II tests have been developed to determine the interlaminar shear fracture toughness of Fibre Reinforced Polymer composites. The current mode II fracture tests consist of a specimen containing a crack at one of its ends, that is loaded in flexure. By doing so, the shear strains in the midplane provoke the crack growing through the specimen midplane. Similarly to the mode I fracture toughness tests, mode II tests are usually run by applying the load under displacement control. As stated above, one of the main issues of fracture toughness tests in mode II is the test stability. When the test is not stable, the crack suddenly propagates and only onset fracture toughness values can be obtained. As the fracture toughness is obtained from the propagation values, the instability in mode II tests is not desired.

With the aim of avoiding unstable crack propagation, a wide variety of mode II tests have been developed.

The main differences between the tests rely on the flexural loading condition. Figure 1.2 illustrates the geometry of the most relevant mode II test geometries.

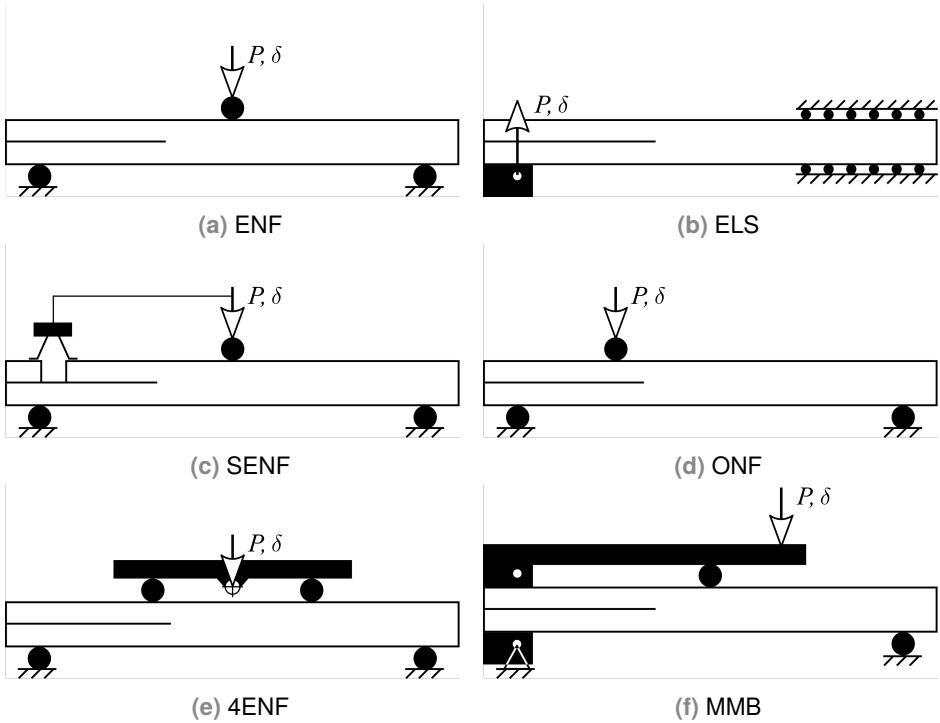


Fig. 1.2.: Common mode II test geometries.

The first existing test was the End Notched Flexure (ENF) (Figure 1.2a), which was developed by Barrett in 1977 [15] for the study of cracked wood beams. It consists of a three point bending test of a specimen that contains a crack at one of its ends. The ENF was later adapted to characterise the mode II interlaminar fracture toughness of FRP [102] and later on, given the simplicity of the test, the American Society of Composite Materials, would adopt it for standardization [11]. It has enjoyed greater success due to its test fixture simplicity, however the main drawback of this test is

that it is unstable under displacement control. Some works have been hampered with the ENF stability problem, concluding that the test configuration would be only stable for relatively long crack lengths, if the ratio between the initial crack and the half span length (a/L) does exceed 0.7 [34]. Other works have dealt with the influencing factors on mode II fracture toughness measurement such as friction [54, 74, 110], large displacements [34, 74] or bending rotations [7], including them on the data reduction methods.

The End Loaded Split (ELS) test (Figure 1.2b) was later developed at Texas A&M University [126] and adopted by European Structural Integrity Society (ESIS), Technical Committee 4 (TC4) on polymers and composites to develop a procedure that would become standardized in 2014 by the International Organization for Standardization [63]. In this test the uncracked part of the specimen is horizontally clamped and the load is applied vertically at the cracked free edge of the specimen (see Figure 1.2b). Compared with the ENF test, it has the advantage of higher stability, i.e. it is stable at lower initial crack to span length ratios, $a_0/L = 0.55$ [19, 48, 79, 129, 130]. This allows longer propagation length relative to the ENF test case [84] (Figure 1.1), providing more propagation fracture toughness values. Contrarily, its major drawback are the large deflections involved [59, 130, 133].

Another mode II test geometry of great interest was the Stabilized End Notched Flexure (SENF) test, first developed by Kageyama in 1991 [67]. It only differs from the ENF test on the displacement control, which is not constant but it depends on the measured shear displacement at the specimen cracked end, that feeds the displacement control of the machine (Figure 1.2c). Although this test requires a complex test set-up, it became the first mode II standardized test in 1993 [65].

With the aim of obtaining stable crack propagation, other specimen geometries were developed. Following their work with mode I specimens [96], Qiao et. al [95] developed the tapered ENF (TENF) test (Figure 1.3e), an ENF specimen with a variable thickness whose main advantage is that, makes the compliance rate change ($\partial C/\partial a$) independent of the crack length, thus the fracture toughness does not depend on the crack length and results constant during propagation. Its main difficulty relies on specimens manufacturing.

In the same context, Tanaka et. al [124] developed the Over-Notched flexure (ONF) test (with a similar ENF geometry, see Figure 1.2d) in which a vertical load is applied uncentred, directly to the cracked end of the specimen, resulting in stable crack propagation. It was studied by Wang et. al [131], who concluded that it is seriously affected by friction. A similar ONF test, the so called Four-End Notched Flexure (4ENF) test (Figure 1.2e) was later developed by Martin and Davidson [76], in which the load is applied distributed in two loading rollers, thus reducing the friction between the cracked arms of the specimen. Although also being affected by friction, the 4ENF test has become more popular than the ONF and the friction effects have been investigated [45, 111].

Alternatively, the Mixed Mode Bending (MMB) test (Figure 1.2f), proposed by Reeder and Crews [38, 98, 99] and standardized by ASTM [10] can be used at 100 % mode II ratio to perform pure mode II tests. By doing so, the MMB test works similarly to the original ENF test.

Even though the most used test geometries have been the ENF, SENF, ELS, 4ENF, ONF and MMB tests, other mode II test geometries were proposed to be applied to fatigue studies (i.e. Cantilever Beam Enclosed Notch (CBEN) test [93], Figure 1.3a) and impact studies (i.e. Centre Notched Flexure (CNF) test [73], Figure 1.3b).

Alternatively to the usual mode II flexure tests, other mode II test geometries have been proposed. A tensile geometry was developed by Prinz [94], so called Transverse Crack Tension (TCT) test (Figure 1.3c), where a specimen with a transversal crack inside is loaded under tensile load. Matsumoto and colleagues [78] proposed the Curvature Driven Delamination (CDD) test (Figure 1.3d) in which the specimen is punched through unaligned rollers. Cammi developed the Compact Edge Notched Shear (CENS) test [25] (Figure 1.3f) where unsymmetric compression is applied to the specimen.

The experimental determination of crack growth resistance of a certain material under in-plane shear loadings is still having issues related to stability, large deflections involved, test fixture compliance, determination of the crack length or bending rotations. This is the reason of the existence of large variety of mode II test typologies

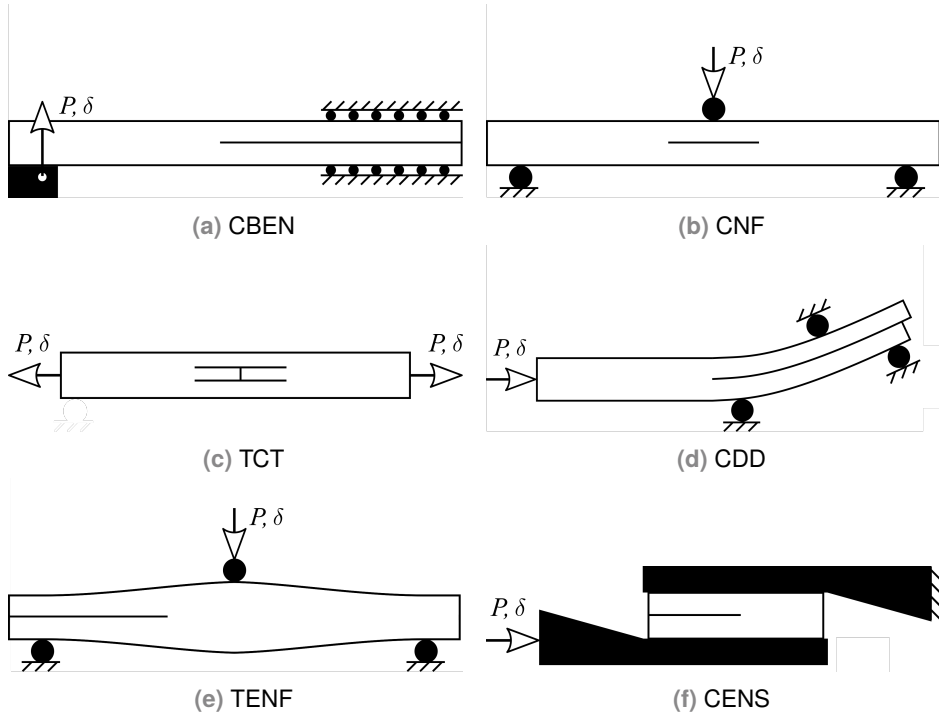


Fig. 1.3.: Other mode II test geometries.

already presented in this section. Furthermore, this has resulted in the study and development of a wide variety of data reduction methods for mode II tests, which are introduced in the following section.

1.3 Mode II data reduction methods

This section aims to introduce the existing data reduction methods used in mode II fracture tests. Firstly, those based on Linear Elastic Fracture Mechanics (LEFM), in which a sharp crack tip is considered, are presented. Secondly, some considerations in mode II adhesive testing are made in order to, thirdly, introduce the methods based on Cohesive Zone Model (CZM) approach.

1.3.1 Linear Elastic Fracture Mechanics

Griffith [55, 56] introduced the principles of fracture mechanics based on an energy approach. He postulated that the maximum load that a structure withstand depends on the size of the defects that may exist in the structural element, and not only on the material strength. This provided the basis of Linear Elastic Fracture Mechanics.

Griffith proposed the theory of the energy balance between the elastic energy of the body and the potential energy release rate (ERR) available for an increment of crack surface extension, defined as \mathcal{G} . The parameter to describe the fracture resistance per area unit of a material is the critical energy release rate, \mathcal{G}_c . The crack will grow if the available potential energy (\mathcal{G}) reaches the critical one (i.e. $\mathcal{G} \geq \mathcal{G}_c$).

The critical energy release rate, also called fracture toughness (\mathcal{G}_c), was considered by Griffith to be a material property. Although he defined it as a constant value, it was experimentally observed that \mathcal{G} may depend on the crack history. The dependence of \mathcal{G} with the crack growth (Δa) is described with the resistance curve, \mathcal{R} -curve.

In experimental interlaminar fracture tests, it is usual that the \mathcal{R} -curve increases from onset values up to a constant plateau (steady-state values), where the \mathcal{R} -curve remains constant. Then, this constant value is considered as the fracture toughness (\mathcal{G}_c) of the joint.

In common fracture toughness tests, the engineering approach for ERR expression reads

$$\mathcal{G} = \frac{P^2}{2W} \frac{\partial C}{\partial a} \quad (1.1)$$

where P is the load, W is the specimen width, a is the crack length and C is the compliance (i.e. the ratio between deflection and applied load, δ/P), which usually is crack length dependant. See figure 1.4.

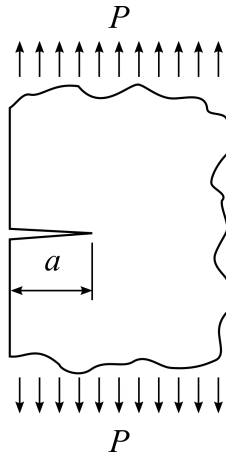


Fig. 1.4.: A through thickness crack in a constant wide plate subjected to a remote tensile stress.

In mode II tests, the load (P) and specimen width (W) are easy to measure from the machine load cell record and specimen dimensions measurements, respectively. The difficulty relies on the derivation of the compliance and its variation with respect to the crack length ($\partial C/\partial a$).

Often a closed form solution of the compliance (C) is derived based on specimen geometry using Beam Theory (BT) approaches. Alternatively, the compliance can be experimentally determined through a previous Compliance Calibration (CC) test. Another alternative, is the use of the area approach, based on the principle that the area enclosed in the load-displacement diagram (i.e. total energy dissipated) with respect to the total amount of cracked area formation (i.e. ΔaW), corresponds to the fracture toughness.

In Beam Theory (BT) based methods, the compliance of a particular geometry is derived from an expression of the compliance as a function of the crack length. Thus, this methods directly depend on crack length measurement. This measure is usually performed by visual inspection of the crack length advance during the test. However, in mode II tests, due to the difficulty in measuring the crack length, some approaches

to obtain an analytical equivalent crack length have been developed. Examples of this are the Corrected Beam Theory using Effective crack length (CBTE) data reduction method in ENF and ELS tests [20, 63], c.f. Tables 1.2 and 1.1.

In the methods based on Compliance Calibration (CC), a calibration test is performed before the actual test in order to make a correlation of the measured compliance with a given crack length. From the compliance calibration, a function that correlates the compliance with crack length advance is obtained and derived to obtain the fracture toughness using Irwin-Kies formula (equation (4.1)).

The area approach was proposed by Hashemi et al. [59]. From this approach, only a global value of shear fracture toughness (G_c) can be obtained and not the evolution of G with respect to crack length advance (\mathcal{R} -curve).

The most used mode II tests have been the ENF, ELS and 4ENF, for which a large variety of LEFM-based data reduction methods have been developed, based on the three approaches mentioned above.

The principal approaches for ENF, ELS and 4ENF tests respectively are listed, together with some of the works that make use of it, in Tables 1.1, 1.2 and 1.3. Although many other authors have used the different approaches, the provided references are representative of the methods presented.

In Tables 1.1, 1.2 and 1.3, the geometric parameters a , L , W and H are the crack length, half span length, width and half specimen thickness respectively. The load is defined as P , the displacement as δ and E_{11} and G_{13} are the specimen longitudinal and shear modulus, respectively. Some of the methods include various heuristic corrections for large deflections, bending rotations or crack length measurements.

Tab. 1.1.: Summary of LEFM-based data reduction expressions used in the ENF test.

Method		Expression for fracture toughness	Ref.
Beam Theory (BT)	Classical Beam Theory (CBT)	Load $\mathcal{G}_{IIc} = \frac{9P^2 a^2}{16W^2 H^3 E_{11}}$	[2, 44, 88, 109]
		Compliance $\mathcal{G}_{IIc} = \frac{9P^2 a^2 C_0}{2W(2L^3 + 3a_0^3)}$	[32, 44, 103]
		Load-displacement $\mathcal{G}_{IIc} = \frac{9P\delta a^2}{2W(2L^3 + 3a_0^3)}$	[39, 47, 103, 109]
	Modified Beam Theory (MBT)	Load ¹ $\mathcal{G}_{IIc} = \frac{9P^2(a+0.42\chi H)^2}{16W^2 H^3 E_{11}} F$	[59]
		Compliance $\mathcal{G}_{IIc} = \frac{9P^2 a^2 C_1}{2W(2L^3 + 3a_1^3)}$	[65]
		Load-displacement ¹ $\mathcal{G}_{IIc} = \frac{9P\delta(a+0.42\chi H)^2}{2W(2L^3 + 3(a+0.42\chi H)^3)} F$	[18, 59]
	Timoshenko Beam theory (TBT)	Load $\mathcal{G}_{IIc} = \frac{9P^2 a^2}{16W^2 H^3 E_{11}} \left[1 + 0.2 \frac{E_{11}}{G_{13}} \left(\frac{H}{a} \right)^2 \right]$	[34, 44, 88]
		Load-compliance $\mathcal{G}_{IIc} = \frac{9P^2 a^2 C_0}{2W(2L^3 + 3a^2)} \left[1 + 0.2 \frac{E_{11}}{G_{13}} \left(\frac{H}{a} \right)^2 \right]$	[86, 88]
	Corrected Beam Theory with Effective length(CBTE)	$\mathcal{G}_{IIc} = \frac{9P^2(a_e)^2}{16E_{11}W^2H^3}$; $a_e = \left(\frac{8E_{11}WH^3C_c}{3} - \frac{2L^3}{3} \right)^{1/3}$	[19, 20, 83]
	Modified Corrected Beam Theory with Effective length(MCBTE) ²	$\mathcal{G}_{IIc} = \frac{9P^2(a^I)^2}{16E_{11}W^2H^3}$	[8]
	Beam Theory including Bending Rotation (BTBR) ²	$\mathcal{G}_{IIc} = \frac{P^2(a^{II})^2}{16E_{11}W^2H^3}(1 - \chi)$	[8]
	Compliance Calibration (CC)	CC1 CC2 CC3 $\mathcal{G}_{IIc} = \frac{P^2}{2W} \frac{\partial C}{\partial a} \left\{ \begin{array}{l} C = C_\alpha + C_\beta a^3 \\ C = C_\alpha + C_\beta a + C_\gamma a^3 \\ C = C_\alpha + C_\beta a + C_\gamma a^2 + C_\delta a^3 \end{array} \right.$	[18, 32, 44, 85, 88, 109] [18, 88] [92, 111]
AREA	$\mathcal{G}_{IIc} = \frac{A10^6}{\Delta a W}$	[59]	

¹ F is a correction for large displacements [59] and χ is a crack length correction.

² a^{II} and a^I are the crack length taking and without taking into account bending rotation effects, respectively [8].

Tab. 1.2.: Summary of LEFM-based data reduction expressions used in the ELS test.

Method	Expression for fracture toughness	Ref.
Simple Beam Theory (SBT) ¹	$\mathcal{G}_{IIc} = \frac{9P^2 a^2}{4W^2 H^3 E_{11}} F$	[63]
Modified Beam Theory Load (MBT Load)	$\mathcal{G}_{IIc} = \frac{9P^2 (a+\chi H)^2}{4W^2 H^3 E_{11}}$	[59, 83, 132]
Beam Theory (BT) Modified Beam Theory Load-displacement (MBT Load-displacement) ¹	$\mathcal{G}_{IIc} = \frac{9P\delta(a+\chi H)^2}{2W[3N(a+\chi H)^3+(L+2\chi H)^3]} F$	[59]
Corrected Beam Theory using Effective crack length (CBTE) ^{1,2}	$\mathcal{G}_{IIc} = \frac{9P^2 a_e^2}{4W^2 H^3 E_{11}} F ;$ $a_e = \left(\frac{1}{3} (2WCH^3 E_{11} - (L + \Delta_{clamp})^3) \right)^{1/3}$	[19, 63, 81, 83]
Compliance Based Beam Method (CBBM) ¹	$\mathcal{G}_{IIc} = \frac{9P^2 C_{0c}}{2W(3a_0^3+L^3)} F \left[\frac{C_c}{C_{0c}} a_0^3 + \frac{L^3}{3} \left(\frac{C_c}{C_{0c}} - 1 \right) \right]^{2/3}$	[81, 83, 116]
Compliance calibration (CC) Experimental Compliance Method (ECM) ¹	$\mathcal{G}_{IIc} = \frac{3P^2 a^2 m}{2W} ; C = (C_0 + ma^3)/N$	[19, 63]
Compliance Calibration Method (CCM)	$\mathcal{G}_{IIc} = \frac{P^2}{2W} \frac{\partial C}{\partial a} ; C = C_\alpha + C_\beta a^3$	[83]
AREA	$\mathcal{G}_{IIc} = \frac{A10^6}{\Delta a W}$	[3, 19, 59]

¹ Correction factors for large displacements (F) and load-block effects (N) from [63]

² Clamp correction, Δ_{clamp} , according to [63].

Tab. 1.3.: Summary of LEFM-based data reduction expressions used in the 4ENF test.

Method	Expression for fracture toughness	Ref.
Beam Theory (BT)	$\mathcal{G}_{IIc} = \frac{9P^2 L^2}{16WH^3 E_{11}}$	[30, 76]
Compliance Calibration Method (CCM)	$\mathcal{G}_{IIc} = \frac{P^2 m}{2W}, a_e = \frac{C-C_0}{m}$	[41, 45, 110, 111]
AREA	$\mathcal{G}_{IIc} = \frac{A10^6}{\Delta a W}$	[59]

1.3.2 Considerations in mode II adhesive testing

As explained in Section 1.2, many different test methodologies have emerged in order to solve the stability problem of mode II testing, raising as a consequence, other difficulties related with the friction or the large displacements involved. Furthermore, given the difficulty in obtaining the compliance with respect to crack length rate change during propagation ($\partial C/\partial a$) in LEFM-based data reduction methods, many approaches have been derived (Section 1.3.1).

However, the existing mode II delamination test procedures aim at measuring the shear fracture toughness (G_{IIc}) of the FRP matrix, but are not designed to study shear fracture of adhesive bonded joints.

On the contrary, a standard on the determination of adhesives mode I fracture toughness exists [64], and it is essentially the same as the one addressed to delamination specimens [62].

Why a specific procedure to test structural adhesives in shear does not yet exist? The main cause is that the large FPZs involved in the test, which is a non-linear region still capable of transmitting stresses between the cracked surfaces, are not taken into account in the existing data reduction methods. Therefore, the models that consider a sharp crack tip existence are no longer valid.

When a structural adhesive is loaded in peel (mode I), the FPZ is still small compared with the standardized specimen dimensions. For this reason, the delamination-based procedures for mode I are suitable for structural adhesive testing, since the FPZ does not affect the main test parameters.

On the contrary, the shear loading of structural adhesives results in relatively larger FPZ compared with the recommended delamination-based standard specimen dimensions.

The size of the FPZ in mode II tests depends on the specimen dimensions (especially thickness), the adhesive mechanical properties (fracture toughness, G_{IIc} , and failure strength, τ_{sh}) and the adherend longitudinal Young Modulus [121]. Compared with the common resins used in FRP manufacturing, the paste and film adhesives used in structural adhesive bonding have been reported to have low shear strengths and high fracture toughness [26, 27, 29, 71, 75, 105, 113–115], which results in large FPZ. This large FPZ involved affects three main parameters of the test: the stability, the specimens dimensions and the data reduction method.

In the FPZ the material is partially damaged and it can transmit closure stresses between the crack surfaces, which may affect the stability of the test. Actually, the

FPZ is beneficial, as the closure stresses contribute to stabilize the test. Several authors experimentally observed this phenomena when using the ENF test for adhesives, obtaining stable propagation, even using a_0/L ratios below the minimum established with LEFM approach [4, 12, 71, 80–82, 108, 115].

Regarding the specimens dimensioning, it is important that the FPZ has enough space to develop inside the specimen in order to properly capture propagation fracture toughness values. During a fracture test, first the FPZ develops and secondly, after the full FPZ development, the crack propagates in a self similar way and the \mathcal{G}_c is measured. If the damaged zone (FPZ) approaches the boundaries (load application points), this provokes a system stiffening. If the propagation region (c.f. Figure 1.1) is not large enough, the FPZ can not be totally developed because of reaching the boundaries before steady state propagation. Thus, not capturing the fracture toughness. The values obtained during FPZ development (onset) underestimate the fracture toughness, and after, when FPZ approaches the boundaries, the values captured are overestimated due to the system stiffening. To overcome this, in structural adhesive testing, various authors have used bigger specimens, compared with the mode II test standard recommendations, in order to enlarge the zone available for propagation and FPZ formation [5, 31, 52, 71, 77, 112, 115, 116, 122, 123, 134]. Two examples of this are shown in Figure 1.5, where ENF specimens of total span size of a) 1000 mm and b) 800 mm are shown.

Concluding, the use of LEFM-based data reduction methods is questionable in presence of large FPZ. The FPZ development ahead of the crack tip, in conjunction with the lack of crack opening, difficult the visual inspection of the crack tip during propagation. Therefore, all the data reduction methods that depends on the visual crack measurement are not suitable. An example of this, is the recommendation of the ELS test standard [63], based on the study of Blackman et al. [19], of using an equivalent crack length method (CBTE) in data reduction instead of data reductions that depend on the crack length visual measurement. Furthermore, Linear Elastic Fracture Mechanics assumes the existence of a sharp crack tip, which is not identifiable. Thus, even adapting the data reduction and/or specimens dimensions in adhesive testing to let the FPZ fully develop, in those cases involving large FPZs,

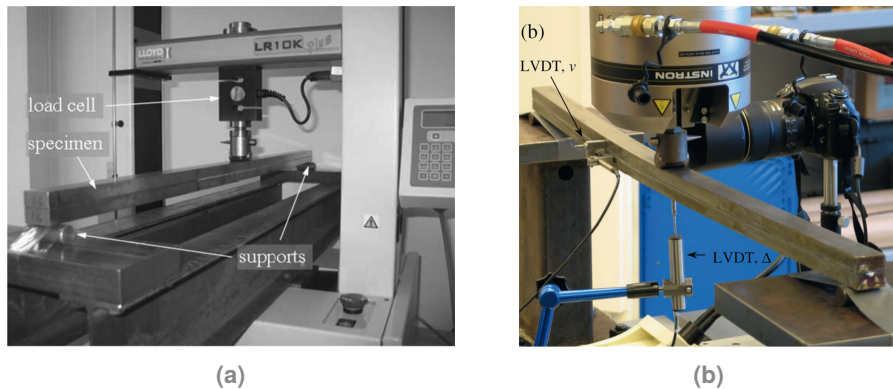


Fig. 1.5.: Example of use of big specimens in adhesive ENF tests, a) [77] $2L = 1000$ mm b) [123] $2L = 800$ mm.

more elaborated fracture models, such as the Cohesive Zone Models (CZM), are needed in order to capture properly the energy dissipation mechanisms.

1.3.3 Cohesive Zone Model approach

The previous Section 1.3.2 presents the issues when using the common mode II delamination test methodologies (test geometry and data reduction methods) to structural adhesive testing. Regarding to the data reduction, LEFM is limited by the difficulties on measuring the crack length in absence of crack opening and presence of a damaged region near the crack tip capable to transmit stresses. The Cohesive Zone Model (CZM), first proposed by Dugdale [50] and Barenblatt [13, 14], considers cohesive stresses at the crack tip in order to capture the non-linear behaviour of the material in the formation of new crack surface and it is more suitable in those cases where the damaged region is of considerable size compared with the problem dimensions (i.e. adhesive testing).

Hillerborg et al. [60] extended the model of Dugdale and Barenblatt, introducing the concept of a fictitious crack that takes place inside the FPZ. This fictitious crack is capable of transferring tension between its surfaces. The relationship between

the cohesive stress profile and the crack opening displacement is governed by a Cohesive Law (CL), that is generally considered a material property [51]. The area enclosed in the cohesive law corresponds to the fracture toughness of the material.

Within the CZM framework, the J -integral approach, proposed by Rice [101], that does not rely on LEFM assumptions, can be used to characterize fracture processes with large FPZs. The J -integral is defined as a path-independent contour integral that can be interpreted as a non-linear energy release rate [101]. The term independent means that the measured energy that is being dissipated is invariant regardless of the path enclosing the FPZ. In the specific case of two-dimensional elastic problem, the J -integral is given by

$$J = \int_{\Gamma} \left[\omega dx_2 - T_k \frac{\partial u_k}{\partial x_1} ds \right] \quad (k = 1, 2) \quad (1.2)$$

where w is the strain energy density, T_k is the tractions vector, u_k are the displacements vector and ds is the length increment along the contour path Γ .

The J -integral is a very convenient method to be applied in adhesive testing because its definition does not require any measurement or approximation of the crack length and it is applicable in cases of large FPZ. Furthermore, in cases of small FPZ, compared to other specimen dimensions (e.g. width, thickness or crack length) the J -integral is also applicable and equates to Griffith's energy release rate definition \mathcal{G} ($J \equiv \mathcal{G}$).

For cases of small FPZ within the LEFM framework, where a sharp crack tip is assumed, the \mathcal{G}_c is associated to the self similar propagation (i.e. \mathcal{R} -curve plateau). The values of \mathcal{G}_c obtained before reaching steady-state propagation are considered to be onset values. On the other hand, when testing structural adhesive joints, in most cases there is not a clear transition between undamaged material and traction-free crack, but a relatively large region where the adhesive is being damaged (large FPZ). In these cases it is possible to approach the problem from the CZM point of

view, explained as follows. During the development of the FPZ, the energy being dissipated inside of it is usually lower than the critical fracture energy. As the FPZ grows, the measured J_c also increases. Once the FPZ is fully developed, the dissipated fracture energy in the damage process equals the critical fracture energy \mathcal{G}_c . From this point on, the FPZ does not grow further, but simply translates as the crack length increases. This is what is defined as steady-state propagation in the CZM, corresponding to the point in which the J -integral curve achieves its plateau.

Several closed-form solutions for various delamination test methodologies have been developed based on the J -integral approach. In these, depending on the assumptions made to derive the J -integral (i.e. Beam Theory), the solution might still require the crack length measurement, which is undetermined in the presence of large FPZs. Examples of this, are the J -integral closed-forms for the ENF test and ELS test developed by Leffler et al. [70] and Corleto [22], respectively.

Simpler closed-forms of J -integral, that do not require any crack length measurement, have been developed for some mode I, mode II and mixed mode I/II tests as the Double Cantilever Beam (DCB), the End Notched Flexure (ENF), the Double Cantilever Beam with Uneven Bending Moments (DCB-UBM) and the Mixed Mode Bending (MMB) tests (Table 1.4). In these, only the applied load and rotation angles at load introduction points are required for the J -integral calculation. This can be simply measured by means of, for example, the machine load cell and the use of inclinometers.

Moreover, given that the area enclosed inside the Cohesive Law corresponds to the fracture toughness, the J -integral approach has been applied to the CL characterization in mode I, mode II and mixed mode I/II specimens by using the measurement of the crack opening displacements together with the J -integral measure [61, 71, 97, 106, 117, 118, 120].

Tab. 1.4.: Summary of J -integral-based data reduction expressions for common mode I, mode II and mixed mode I/II tests.

Test method	Expression for the J -integral	Ref.
Mode I, DCB	$J = \frac{2P}{W}\theta$	[57, 87, 90]
Mode II, ENF	$J = \frac{P}{2W}(\theta_1 - 2\theta_2 + \theta_3)$	[122]
Mode I/II DCB-UBM ¹	$J = \frac{21(M_1^2 + M_2^2) - 6M_1M_2}{4W^2H^3E}$ for $ M_1 > M_2$	[119]
Mode I/II MMB	$J = \frac{P}{W} \left[\left(\frac{1}{2} - \frac{c}{2L} \right) \theta_{1bottom} + \left(\frac{c}{2L} + \frac{1}{2} \right) \theta_3 + \frac{c}{L} \theta_{1top} - \left(\frac{c}{L} + 1 \right) \theta_2 \right]$	[107]

* All the rotations θ_n considered from left to right respectively, c.f. Figure 1.2.

¹ M_1 and M_2 are the bending moments applied.

1.4 Motivation

Adhesive bonded joints are now very common in FRP structures assembly due to their capability on redistributing loads, thus reducing the stress concentrations that, for instance, mechanical fasteners would induce. This improves the joint efficiency in terms of material and weight saving. The in-plane shear fracture toughness (mode II) is one of the most relevant parameters used in the design of adhesively bonded joints. This property, can be experimentally measured through a mode II test.

The existing mode II test procedures are designed to measure the interlaminar shear fracture toughness, G_{IIc} , of the resin in a FRP but not of structural adhesives.

One of the main problems encountered in structural adhesive mode II testing using delamination-based procedures has been the large FPZ involved, compared with the specimen dimensions. The FPZ can transmit stresses between the cracked surfaces and must be totally developed in order to measure the propagation fracture toughness values. Moreover, the data analysis of those situations involving large FPZ are not straightforward, since the majority of existing data reduction methods are based on the assumption of a sharp crack tip existence (i.e. LEFM) and the FPZ effects are underestimated.

The main motivation of this work is to extend the usefulness of the existing mode II test methodologies to situations where non-linear region near the crack tip is relatively large and high \mathcal{G}_{IIc} values are reached, which is the case of the adhesives used in structural adhesive joint of FRP components.

1.5 Objectives

The present thesis has as main objective the definition of reliable test methodologies and data reduction methods to determine the fracture toughness of structural adhesive bonded joints loaded in shear. In order to achieve this main goal, several specific objectives are proposed.

- Development of simple data reduction methodologies for ELS and 4ENF mode II tests based on CZM approach (J -integral), where the existence of a FPZ that transmits stresses between the cracked surfaces is taken into account. These should result in more robust data reduction methods than the existing ELS and 4ENF LEFM-based data reduction methods.
- Development of tools to define suitable ELS specimen dimensions to test structural adhesive joints in order to achieve steady-state propagation during the test. The ELS seems to be a good candidate beforehand due to its better stability compared with the ENF case that is directly related to a larger zone to permit the complete FPZ development and crack propagation.
- Study of the applicability of both existing and proposed in this work mode II test methodologies and data reduction methods for the characterization of structural adhesive joints by means of a comprehensive experimental test campaign.

1.6 Thesis structure

The present thesis has been developed as a compendium of publications, each one addressing the specific objectives of the thesis. In order to achieve the objectives described in Section 1.5, Chapters 2 to 4 present the whole text of each publication, preceded by an introductory overview to expose the coherence of the paper in the context of the thesis.

In Chapter 2, a data reduction method based on the J -integral to obtain the interlaminar fracture toughness in a mode II end-loaded split (ELS) test is presented.

Chapter 3 contains a study on the suitable specimen dimensions for the determination of mode II fracture toughness of structural adhesive joints by means of the ELS test in order to avoid unstable propagation and allow the full development of the FPZ.

In Chapter 4, an experimental study towards a consensus on mode II adhesive fracture testing is presented. In this, four mode II test types are compared, and a data reduction method based on the J -integral for the four end notched flexure test (4ENF) is presented to be compared with other existing mode II J -integral based data reduction methods.

A general discussion and concluding remarks are presented in Chapters 5 and 6, respectively. Finally, a reproduction of the generated papers are presented in the appendix.

A data reduction method
based on the J -integral to
obtain the interlaminar
fracture toughness in a mode
II end-loaded split (ELS) test

M. Pérez-Galmés ^a, J. Renart ^a, C. Sarrado ^a, A. Rodríguez-Bellido ^b, J. Costa ^a

^aAMADE, Mechanical Engineering and Industrial Construction Department, Universitat de Girona, Campus Montilivi s/n, Girona, Spain

^bComposite Technology, Materials and Processes, AIRBUS Operations SL, Paseo John Lenon s/n, E-28906 Getafe, Madrid, Spain

The paper has been published in *Composites Part A: Applied Science and Manufacturing Vol. 90 (2016) 670-677*.

Overview

One of the objectives of this thesis deals with the development of suitable data reduction methods for the determination of the mode II fracture toughness of structural adhesives.

Within the most popular mode II test methods, the ELS seems to be a good candidate to be applied to adhesive testing, since it allows large zone for crack propagation, which is needed in adhesive testing due to the large fracture process zones involved, compared with the standardized specimen dimensions.

All the data reduction methods found in the literature for the ELS test are designed for delamination tests and they are based on linear elastic fracture mechanics, thus not considering large FPZ. Therefore, a data reduction method based on non-linear fracture mechanics is required for testing adhesives (e.g. J -integral).

In this chapter a methodology based on the J -integral is presented to be used in structural adhesive tests data reduction.

Abstract

Various difficulties arise in the data reduction of the end-loaded split (ELS) test. On one hand, a small Fracture Process Zone (FPZ) at the crack front is assumed in the existing mode II end-loaded split test methodologies based on Linear Elastic Fracture Mechanics (LEFM). However, mode II fracture has been reported to involve large FPZ and a fuzzy crack tip. Furthermore, the ELS test, is usually affected by geometrical non-linearities.

This work proposes a closed-form solution based on the J -integral to determine the interlaminar fracture toughness in an ELS test. This solution avoids the need to measure the crack length, and is applicable when a large FPZ is present, as occurs in adhesive bonded joints between CFRP. In addition, because the ELS test involves large vertical deflections, a correction of the formulation for large displacements has been implemented.

This new methodology has been compared to other methods available in the literature based on LEFM by means of an experimental campaign of delamination tests using unidirectional CFRP specimens in order to make a first validation of the method.

2.1 Introduction

The end-loaded split (ELS) test is used to determine mode II fracture toughness in unidirectional fibre-reinforced polymer composites [19, 24, 48]. Among other mode II test methodologies, such as the End Notch Flexure (ENF) test [11, 49] or the 100% mode II Mixed Mode Bending (MMB) test [10], the ELS has the advantage of stable crack growth [19, 24, 48, 79]. According to the existing ISO 15114 standard [63], which is based on Linear Elastic Fracture Mechanics (LEFM), the crack length is a required parameter that must be either measured or calculated.

The main hypothesis behind LEFM is that the non-linear zone at the crack front, and thus also the Fracture Process Zone (FPZ), is small in comparison to any of

the specimen's relevant dimensions (width, thickness or crack length). Mode II fracture has been reported to involve large FPZ, which in conjunction with the lack of crack opening, hinders measuring the crack length by visual inspection [23, 59, 130]. To overcome this, a method based on an effective crack length derived from the specimen's compliance was proposed by Blackman et al. [19]. Even though this method has shown great success in measuring fracture toughness in mode II delamination, it is still based on corrected LEFM assumptions and, therefore, the analysis of those situations involving large FPZ may fall outside their scope [63]. Adhesively bonded joints have been reported to entail large FPZ due to the plasticity of the adhesive layer [20, 61], so their analysis should be based on non-linear fracture mechanics data reduction methods.

One of the methods that has enjoyed greater success on the characterization of fracture in a non-linear fracture mechanics framework is the contour integral known as the J -integral. The J -integral was first developed by Rice [101] and has been used as a data reduction method to determine fracture toughness when LEFM assumptions do not hold true, e.g. when performing a mode II fracture test of an adhesive joint [6, 89]. The J -integral has been also used to obtain fracture toughness closed-form solutions for pure mode II ENF [122] and MMB [107] tests. These closed-form solutions are derived by selecting a convenient integration path that allows the contour integral to be solved. Such J -integral closed-form solutions can be applied when large FPZ are present as they do not rely on LEFM assumptions and do not require a crack length measurement, so they are a good alternative for measuring fracture toughness when LEFM does not apply. Corleto [36] proposed a J -integral closed-form solution for the mode II ELS test, where evaluating the J -integral requires a calibration of the moment-curvature relationship for a given crack length before starting the test, making the method crack length dependent (unlike the J -integral solutions for ENF and MMB cited above [107, 122]).

Most solutions for the J -integral are valid only under the assumptions of small displacements, where the crack front is perpendicular to the applied load [101, 107, 122]. However, the ELS test may involve large vertical deflections if the fracture toughness is high enough and/or thin specimens are used (e.g. in bonded joints with structural adhesives) [59, 130, 133].

Very few studies have dealt with large deflections in DCB [87] and ELS [36] tests, and those that do consider that the crack propagates through a horizontal plane parallel to the longitudinal axis following a straight pattern. By doing this, the problem becomes 1-dimensional, and the formulation developed by Rice [101] can be used to calculate the J -integral instead of using more general and complex approaches such as the vector J -integral [35].

This work presents a data reduction scheme for the ELS test based on the J -integral to extend the usefulness of this test to situations where the non-linear region can not be neglected, i.e. where LEFM no longer applies. The method takes into account the large displacements involved in the ELS test and, unlike the method proposed by Corleto [36], the proposed closed-form solution does not depend on crack length.

In order to assess the correctness of the proposed procedure, the results of the J -integral and LEFM on delamination Carbon Fibre Reinforced Polymer (CFRP) specimens are compared. The two batches of specimens tested have different thickness in order to also compare the effect of large displacements on the results of the J -integral. For these specimens the non-linear zone is small and both LEFM and the J -integral should yield the same fracture toughness.

2.2 Analytical formulation

In the particular case of a two-dimensional elastic problem, the J -integral is defined as

$$J = \int_{\Gamma} \left[\omega dx_2 - T_k \frac{\partial u_k}{\partial x_1} ds \right] \quad (k = 1, 2) \quad (2.1)$$

where Γ is a closed path enclosing the crack tip and bounding a region R (see Figure 2.1), u_k is the displacements vector, ds an infinitesimal arc length along Γ ,

and x_1 and x_2 are the horizontal and vertical coordinates, respectively. ω is the strain energy density, defined as

$$\omega = \int_0^{\varepsilon_{ij}} \sigma_{ij} d\varepsilon_{ij} \quad (2.2)$$

where σ_{ij} and ε_{ij} are the stress and strain tensors expressed in two dimensional form, respectively.

T_k is the tractions vector defined by

$$T_k = \sigma_{ki} n_i \quad (2.3)$$

where n_i denotes the normal vector to the bounding path Γ .

For a fracture test specimen with an initial defect, the fracture toughness may be obtained by means of the J -integral computation along a remote arbitrary path Γ enclosing the crack tip [101], and in most cases the J -integral can be solved to obtain a closed-form solution [61, 107, 122].

If Γ is defined by the contour of the specimen edge, the traction vector T_k only takes into account the external forces applied to the specimen. In addition, when Γ does not cross the section of the specimen, the term of the strain energy density is zero. Therefore, the integral results in a simple expression that includes the loads applied and the rotation angles at the load application points and at the supports [107].

In the particular case of the ELS test, the specimen is loaded at the bottom arm of the pre-cracked end and clamped at the other end by a carriage, which allows unrestrained displacement along the longitudinal edge (x_1) but restricts the vertical displacement [63] (Figure 2.1). The estimation of the reaction forces induced by the carriage is not straightforward because it is a contact problem that depends on

Path Γ_g runs through a free surface parallel to the crack tip ($dx_2 = 0$). Thus, J_{Γ_g} is zero everywhere except at the load introduction point, where an external traction is applied (T_P).

Considering the tractions in Figure 2.1 as concentrated forces applied in an infinitesimal region dx_1 , $\int \sigma_{22} dx_1 = \frac{P}{b}$, where P is the external applied load and b the specimen width. These tractions can therefore be considered punctual forces, as in Figure 2.2. The derivative of the displacements is

$$\frac{\partial u_k}{\partial x_1} = \begin{bmatrix} \frac{\partial u_1}{\partial x_1} \\ \frac{\partial u_2}{\partial x_1} \end{bmatrix} = \begin{bmatrix} \varepsilon_{11} \\ \tan(\theta_P) \end{bmatrix} \quad (2.7)$$

where θ_P is the rotation angle at the load application point. The replacement of equation (2.7) into (4.2) reads:

$$J_{\Gamma_g} = \frac{P}{b} \tan(\theta_P) \quad (2.8)$$

Path Γ_a travels through a transversal section perpendicular to the crack tip. It is assumed that the strains ε_{22} are zero. Under the hypothesis of a linear elastic constitutive relationship between strains and stress, the strain energy density takes the form:

$$\omega = \frac{1}{2} \sigma_{ij} \varepsilon_{ji} = \frac{1}{2} \sigma_{11} \varepsilon_{11} + \sigma_{12} \varepsilon_{12} \quad (2.9)$$

The normal vector to path Γ_a is $n_i = [1 \ 0]^T$, therefore the tractions vector in path Γ_a is

$$T_k = \sigma_{ki} n_i = \begin{bmatrix} \sigma_{11} & \sigma_{12} \\ \sigma_{12} & \sigma_{22} \end{bmatrix} \begin{bmatrix} 1 \\ 0 \end{bmatrix} = \begin{bmatrix} \sigma_{11} \\ \sigma_{12} \end{bmatrix} \quad (2.10)$$

The product between the tractions and the displacement gradients in path Γ_a is

$$T_k \frac{\partial u_k}{\partial x} = \begin{bmatrix} \sigma_{11} & \sigma_{12} \end{bmatrix} \begin{bmatrix} \varepsilon_{11} \\ \tan \theta_g \end{bmatrix} = \sigma_{11} \varepsilon_{11} + \sigma_{12} \tan \theta_g \quad (2.11)$$

where θ_g is the rotation at section S - S' .

Replacing (2.9) and (2.11) into (4.2) the contribution of path Γ_a to the J -integral is obtained:

$$J_{\Gamma_a} = \int_{-h}^h \left(-\frac{1}{2} \sigma_{11} \varepsilon_{11} + \sigma_{12} (\varepsilon_{12} - \tan \theta_g) \right) dx_2 \quad (2.12)$$

Assuming a UD laminate, plane strain, small strains and $\varepsilon_{22} = 0$, equation (2.12) can be represented as a function of the strains as

$$J_{\Gamma_a} = \int_{-h}^h \left(-\frac{1}{2} E_{11} \varepsilon_{11}^2 + G_{12} \varepsilon_{12} (\varepsilon_{12} - \tan \theta_g) \right) dx_2 \quad (2.13)$$

where E_{11} is the Young's modulus in the fibre direction, G_{12} is the shear modulus, h is half the specimen thickness and ε_{11} and ε_{12} are the longitudinal and shear strains along the section S - S' .

Equation (2.13) can be solved by assuming a parabolic shear strain distribution along the thickness direction in section S - S' ,

$$\varepsilon_{12} = \frac{3P(h^2 - x_2^2)}{4bh^3G_{12}} \quad (2.14)$$

By adding up expressions (2.8) and the solution of (2.13) the J -integral closed-form solution for the ELS test is obtained:

$$J_{ELS} = \frac{3}{5} \frac{P^2}{G_{12}b^2h} + \frac{P}{b}(\tan \theta_P - \tan \theta_g) + \int_{-h}^h \left(-\frac{1}{2} E_{11} \varepsilon_{11}^2 \right) dx_2 \quad (2.15)$$

The last term in equation (2.15) can be addressed in three ways:

Firstly, by integrating numerically the last term of a strain profile, which can be experimentally measured by means of, for example, a Digital Image Correlation system (DIC).

Secondly, under the assumption of a linear strain profile at section S - S' , this term can be solved by measuring the longitudinal strains at the top of section S - S' with a longitudinal strain gauge. In that case equation (2.15) results in

$$J_{ELS} = \frac{3}{5} \frac{P^2}{G_{12}b^2h} + \frac{P}{b}(\tan \theta_P - \tan \theta_g) - \frac{E_{11}h}{3} \varepsilon_g^2 \quad (2.16)$$

where ε_g is the strain gauge measurement on the top face of section S - S' .

Thirdly, the longitudinal strain profile can be estimated by means of Simple Beam Theory, resulting in an expression that does not depend on the strains, but rather on the distances between the load application point and the clamp tool (L), and the distance between section S - S' and the clamp tool (L_s), (Figure 2.1):

$$J_{ELS} = \frac{3}{5} \frac{P^2}{G_{12}b^2h} + \frac{P}{b}(\tan \theta_P - \tan \theta_g) - \frac{E_{11}h}{3} \left(\frac{3P(L - L_s)}{2E_{11}bh^2} \right)^2 \quad (2.17)$$

The Young's modulus in the fibre direction (E_{11}) can be obtained from the calibration specified on the test standard [63], from a three point bending test, or from the

difference between two rotated angles along the beam. In this work the Young's modulus is obtained by taking into account the difference in rotated angles between the load application point and section $S-S'$. Thus, the Young's modulus in the fibre direction (E_{11}) is obtained by applying the second Mohr's Theorem at the linear region of the load displacement curve (before the propagation starts) where the crack length is known:

$$E_{11} = \frac{-3P(3a_0^2 + (L - L_s)^2)}{4bh^3(\theta_P - \theta_g)} \quad (2.18)$$

where a_0 is the initial crack length. Measuring the angles at section $S-S'$ (θ_g) and at the load application point (θ_P) avoids using additional tests to obtain E_{11} .

2.2.1 Large displacements correction

This section presents an extension of the formulation to account for large displacements in the bending arms. In an ELS test the crack plane is not horizontal due to the bending of the specimen, but rather it is rotated an angle θ_g with respect to the horizontal axis (x_1''), as shown in Figure 2.2. In addition, the applied load causes a vertical deflection and an horizontal displacement ($\Delta x_1''$) of the sliding fixture that tends to increase the stiffness of the system, see Figure 2.2a.

With the aim of simplifying the calculation, the test set-up has been idealized by assuming three hypotheses (Figure 2.2b): i) the crack propagates along a straight line parallel to the x_1 axis; ii) the difference in the rotation angles at section $S-S'$ and the crack front is negligible (i.e. x_1' is parallel to x_1 , or $\theta_g = \theta_g'$) and; iii) the specimen curvature is small compared to the length of the specimen and the strains caused by the horizontal component of load P (P_1) are negligible compared to the rest of the deformation, so that it does not affect the position of the neutral axis. By assuming these hypotheses, Rice's J -integral [101] can be used instead of a more general and complex formulation such as the vector J -integral [35].

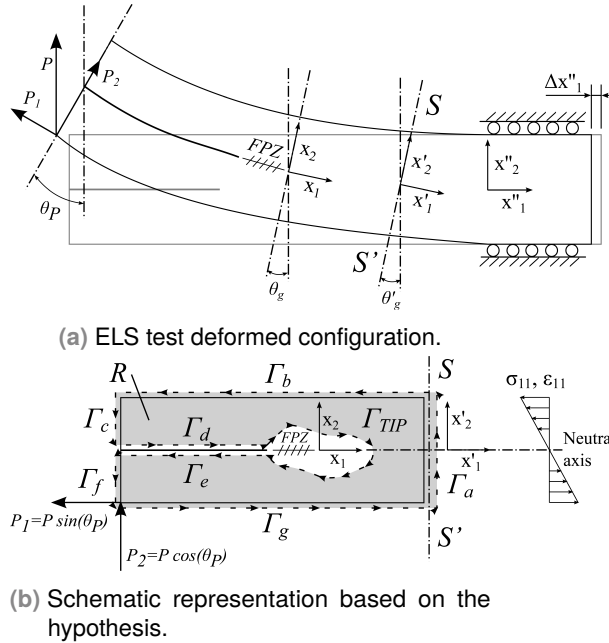


Fig. 2.2.: Integration paths in the ELS specimen with large displacements assumption.

With regards to the second hypothesis, smaller curvature is produced on the uncracked region because of its higher moment of inertia. This was checked using Mohr's Second Theorem obtaining less than 3.2 degrees difference between x_1 and x'_1 axis rotations before the crack starts to propagate. The third hypothesis is demonstrated from the DIC measured strain profile at section $S-S'$, where the neutral axis of the beam coincides with the zero intersection of the longitudinal strain profile ($\epsilon_{11}(x'_2 = 0)$), as shown in Figure 2.7.

Analogous to the situation of small displacements, from Figure 2.2b and considering the equation (4.2) $J_{\Gamma_b} = J_{\Gamma_c} = J_{\Gamma_d} = J_{\Gamma_e} = J_{\Gamma_f} = 0$, as these contours are either free surfaces or contact surfaces with no friction assumed. Therefore, only paths Γ_a and Γ_g contribute to the J -integral.

J_{Γ_g} is zero everywhere except at the load point. Considering the tractions as concentrated forces applied in an infinitesimal region:

$$\int T_i ds = \int \sigma_{ij} n_j ds = \frac{1}{b} \begin{bmatrix} -P_1 \\ P_2 \end{bmatrix} = \frac{1}{b} \begin{bmatrix} -P \sin \theta_P \\ P \cos \theta_P \end{bmatrix} \quad (2.19)$$

where $n_j = [-\sin \theta_P, -\cos \theta_P]^T$ is the normal vector to surface Γ_g at the load application point, θ_P is the rotation angle between the load P and n_i at the load application point, P_1 and P_2 are respectively, the tangent and normal components of the applied load. The derivative of the displacements is defined with respect to section S - S' , coordinate system (x'_1, x'_2) :

$$\frac{\partial u_k}{\partial x_1} = \begin{bmatrix} \varepsilon_{11} \\ \tan(\theta_P - \theta_g) \end{bmatrix} \quad (2.20)$$

where ε_{11} are the longitudinal strains in x'_1 direction and $\theta_g = \theta'_g$ is the rotation angle between section S - S' and axis x'_2 . According to the third hypothesis, the strains caused by the tangent component of load (P_1) are small compared to the rest of the deformations and can be dismissed ($\varepsilon_{11} \approx 0$). Furthermore, the bending moment at the load application point is zero. Therefore, J_{Γ_g} reads

$$J_{\Gamma_g} = \int -T_i \frac{\partial u_i}{\partial x_1} ds = \frac{P \cos(\theta_P)}{b} \tan(\theta_P - \theta_g) \quad (2.21)$$

Given the assumption of similar rotation between (x_1, x_2) and (x'_1, x'_2) , in path Γ_a the strain energy density, the traction vector and the displacement gradients take the same form as in the small displacements formulation, so J_{Γ_a} can be obtained

directly from equation (2.12). From the combination of equations (2.12) and (2.21) a general solution for the J -integral with large displacements is obtained:

$$J_{ELS} = \frac{3(P \cos(\theta_P))^2}{5G_{12}b^2h} + \frac{P \cos(\theta_P)}{b} \tan(\theta_P - \theta_g) + \int_{-h}^h \left(-\frac{1}{2} E_{11} \varepsilon_{11}^2 \right) dx_2 \quad (2.22)$$

Note that the rotation angle θ_g is the same as θ'_g . Because of that, the partial derivative of displacements is $\frac{\partial u_k}{\partial x_1} = [\varepsilon_{11} \ 0]^T$. It is worth mentioning that expression (2.22) is the same as (2.15) if small displacements are considered.

The last term of equation (2.22) can be addressed in the same way as in equation (2.15), i.e. numerically integrating the strain profile measured using DIC, as done in equation (2.16), i.e. under the assumption of a linear strain profile measured by a strain gauge placed on the top face of section S - S' or by estimating the strain profile from Simple Beam Theory, as done in equation (2.17).

2.3 Experimental campaign

The proposed methodology was validated with an experimental testing campaign. The results obtained from the J -integral closed-form solutions were compared to those provided by the methods available in the literature based on LEFM assumptions. In order to use the latter methods as a reference, the testing campaign consisted of delamination tests on unidirectional CFRP specimens, where small FPZ are expected. Therefore, the crack length could be either measured or calculated.

Two batches of 5 specimens of carbon fibre reinforced polymer (AS4/8852) unidirectional laminates were tested. The specimens in each batch differed in their total thickness (3 mm and 4.5 mm), but they had the same length (250 mm) and width (25 mm). The Young's modulus in the fibre direction (E_{11}) is 120.9 GPa and the in-plane shear modulus (G_{12}) is 4.6 GPa [100].

2.3.1 Test procedure

Before the ELS test, a clamp calibration was performed in accordance with the ISO 15114 standard [63]. This preliminary test was used to obtain the ELS clamp correction and the specimen flexural modulus (E_{11}), data required for the Simple Beam Theory (SBT) and the Corrected Beam Theory using Effective crack length (CBTE). For the J -integral method, the flexural modulus was obtained directly from the test by measuring the angles θ_P and θ_g , equation (2.18).

After the calibration, the specimen edges were prepared to be analysed both by the J -integral and the data reduction required by the ISO15114 standard [63].

In this way, edge A, was prepared to monitor the crack length. A thin coat of white paint was applied and thin vertical crack length markers at 1 mm increments were drawn. Edge B, was prepared for the DIC measurement by applying a coat of white paint and a random black speckled pattern using an airbrush in the zone around section $S-S'$. Section $S-S'$ was placed 7 mm away from the clamp fixture in order to avoid the clamping effects of the sliding fixture (carriage) and at 28 mm from the initial crack tip to make sure that the FPZ is encompassed during the test.

With the aim of avoiding an unstable crack initiation from the insert, a pre-crack in mode II was made according to the standard [63]. A load block was bonded to the specimen so that the initial crack length was 52.5 mm. After the pre-crack, the final crack length was measured with an optical microscope. The crack length after the pre-crack test was approximately 65 mm in all the specimens. Afterwards, edge A was marked every millimetre with a vertical line for the first 35 mm from the new crack tip.

The ELS test was performed in a test rig designed according to the requirements of the test standard [63]. The specimens were clamped in the sliding fixture of the test rig so that the distance between the clamping device and the load application point was of $L = 100$ mm. To ensure a stable propagation, the ratio between the

crack length a and L has to be $a/L > 0.55$ [63]. In this work the ratio was set to $a/L = 0.65$.

The tests were carried out under displacement control at a crosshead displacement rate of 1 mm/min.

2.3.2 Instrumentation

During the test, the crack length was optically monitored at edge A with a video acquisition system consisting of a Canon 550D camera with a macro lens mounted on a travelling fixture. The longitudinal strains (ε_{11}) at section S - S' zone were measured using two methods: a 3 mm longitudinal strain gauge with a resistance of 350 Ω and a Digital Image Correlation (DIC) system.

The strain gauge was placed on top face of the specimen and it was centred at section S - S' . The DIC cameras were focused on a region near section S - S' on edge B, covering the entire thickness of the specimen and a propagation zone of 17 mm. In order to obtain a stereoscopic image of section S - S' , two Stingray F504B ASG cameras with a resolution of 2452x2056 pixels were used. They were placed at a distance of about 250 mm away from the specimen edge B [37]. During the test, the data acquisition frequency of the images taken by the cameras was 2.5 Hz.

Two inclinometers were used to measure the rotation angles at section S - S' (θ_g , inclinometer 2), and at the loading application point (θ_P , inclinometer 1). In order to correct the small rotation of the carriage, two additional inclinometers, named 03 and 04, were situated at the top and bottom part of the clamping tool on the carriage (see Figure 2.3). The inclinometers used were the capacitive inclinometers NA3-30, from SEIKA Mikrosystemtechnik GmbH, with a resolution of 0.005 degrees and a maximum linearity deviation over the whole measurement range (± 30 degrees) of 0.06 degrees, in accordance with the manufacturer's specifications. A detail of the specimen instrumentation is shown in Figure 2.3.

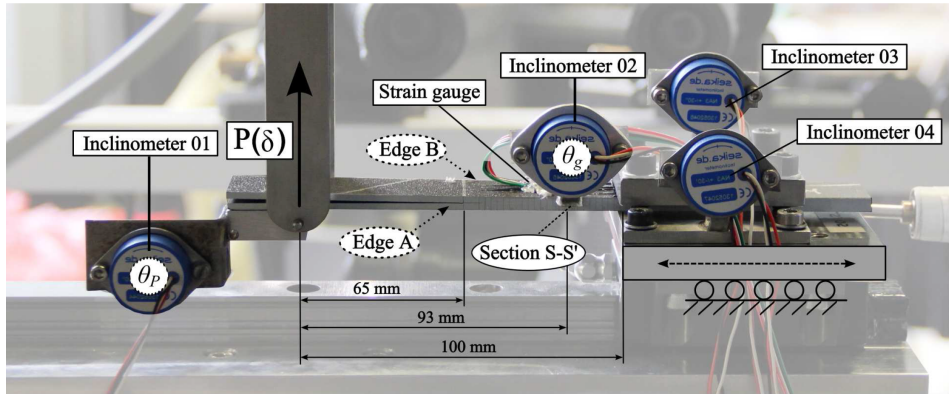


Fig. 2.3.: Specimen instrumentation: inclinometers and strain gauge. Location of section $S-S'$ and edges A and B.

2.3.3 Data reduction

The fracture toughness was obtained from the three LEFM data reduction methods proposed in the ISO 15114 standard [63]: i) Experimental Compliance Method (ECM), ii) Simple Beam Theory (SBT) and iii) Corrected Beam Theory using Effective crack length (CBTE). Following the standard, the values of \mathcal{G}_{IIc} obtained from these methods were corrected taking into account large deflections in the specimen and the stiffness induced by the loading blocks [63]. For comparative purposes, \mathcal{G}_{IIc} was also obtained from the area method (AREA) [59].

With regards to the J -integral, three different methods were used to obtain the mode II fracture toughness: i) a numerical integration of the strain profile at section $S-S'$ measured using Digital Image Correlation (DIC), equation (2.15); ii) an estimation of the strain profile by means of the strain gauge (SG), equation (2.16); and iii) an estimation of the strain profile from the Simple Beam Theory (BT), equation (2.17). Furthermore, the results were obtained from the same data reduction methods but including large displacements correction (DIC-LD, SG-LD and BT-LD).

Tab. 2.1.: Data reduction methods nomenclature.

	Method	Identifier Code	Equation/Reference
Linear Elastic Fracture Mechanics (G_{IIc})	Area	AREA	Hashemi et. al. [59]
	Corrected Beam Theory using Effective crack length	CBTE	
	Experimental Compliance Method	ECM	ISO 15114 [63]
	Simple Beam Theory	SBT	
J -integral (Small Displacements)	Digital Image Correlation	DIC	equation (2.15)
	Strain Gauge	SG	equation (2.16)
	Beam Theory	BT	equation (2.17)
J -integral (Large Displacements)	Digital Image Correlation	DIC-LD	equation (2.22)
	Strain Gauge	SG-LD	equation (2.22) ¹
	Beam Theory	BT-LD	equation (2.22) ²

¹ Last term of the equation addressed in the same way as in equation (2.16).

² Last term of the equation addressed in the same way as in equation (2.17).

The data reduction methods used, and their corresponding equations, are shown in Table 2.1.

2.4 Results

The load-displacement curve of one representative specimen is shown in Figure 2.4. The load and displacement values of five propagation points are included in the curve. These points correspond to five propagation points (PROP₁, PROP₁₂, PROP₁₈, PROP₂₀ and PROP₂₈). The last propagation point coincides with the location of section $S-S'$, where the strain gauge is bonded and the DIC measurements are made. These points are taken as a reference and will be identified in the results for discussion purposes. Apart from these, other propagation points were obtained, but are not depicted for clarity.

Figure 2.5 shows the \mathcal{R} -curve of the same representative specimen used in Figure 2.4, obtained from LEFM-based methods. The location of the propagation points

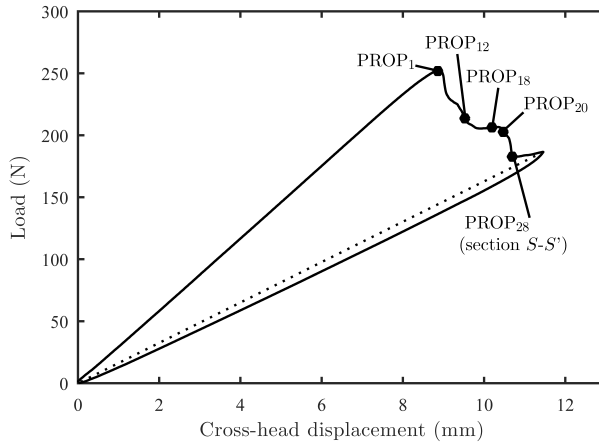


Fig. 2.4.: Load-displacement curve of a 4.5 mm thick specimen. $PROP_i$ point corresponds to a crack growth of i mm visually measured. The dotted line is a straight unloading curve from the maximum displacement point to the zero of load and displacement used in the AREA data reduction method.

previously marked in the load-displacement curve in Figure 2.4 are indicated by vertical dotted lines.

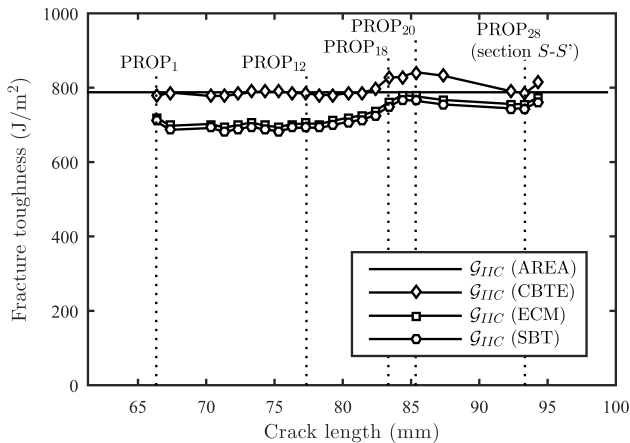


Fig. 2.5.: LEFM-based methods fracture toughness results. 4.5 mm thick specimen.

During propagation \mathcal{G}_{IIc} (CBTE) remains around 800 J/m².

In terms of the data reduction methods, the SBT yields the lowest value of \mathcal{G}_{IIc} while the CBTE provides the highest. The difference between them is around 12% for the 3 mm thick specimens and 3% for the 4.5 mm thick specimens.

The ISO15114 standard [63] recommends using the values of \mathcal{G}_{IIc} obtained from CBTE data reduction method, because it has the best reproducibility. In Figure 2.5, the results obtained from the CBTE data reduction method are very close to those from the area method. These two methods are used in the comparison to those obtained from the J -integral. The comparison between the J -integral and the LEFM data reduction methods is shown in Figure 2.6 for the same specimen used in Figures 2.4 and 2.5.

In spite of the fact that methods based on the J -integral do not make use of the crack length in the calculations, the fracture toughness in Figure 2.6 is represented against the crack length a in order to be compared with the data reduction method CBTE, which is usually expressed in terms of crack length (\mathcal{R} -curve). The vertical dotted lines represent the same propagation points indicated in Figures 2.4 and 2.5.

The J -integral results are in close agreement with the CBTE and the AREA method during the first 18 mm of propagation, when section $S-S'$ is situated 10 mm away from the optically measured crack length tip. At this plateau region the dispersion between the data reduction methods based on the J -integral (Figure 2.6) is smaller than the dispersion between the methods based on the LEFM (Figure 2.5).

2.5 Discussion

In Figure 2.6, only the results of the first 18 mm of propagation have been represented because from this point on the values of the J -integral start to deviate from the other data reduction methods. This deviation is caused by the non-linearities in the strain

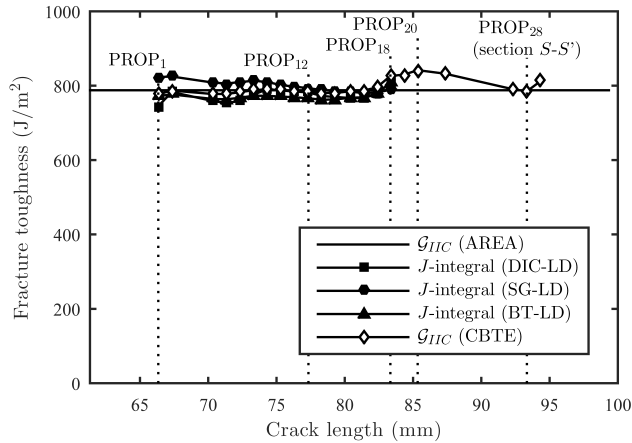


Fig. 2.6.: Fracture toughness results using the J -integral (large displacements correction) and LEFM-based methods. Results from a 4.5 mm thick specimen.

profile at section $S-S'$ caused by the crack front stresses. The closed-form solutions of the J -integral presented in this work are based on the hypothesis that the crack front is far enough from the integration contours so that the strain profile is linear, which means that the paths defined to calculate the J -integral encompass the total FPZ involved. Therefore, as the crack front approaches section $S-S'$ and the strain profile loses its linearity, the formulations developed are no longer valid.

In order to further analyse this effect, a comparison between the strain profile at section $S-S'$ for different propagation stages of the same specimen as before is shown in Figure 2.7. The strain profile measured with DIC is compared to a linear estimation of the strain profile obtained from the strain gauge measurements (SG).

The whole strain profile along section $S-S'$ can not be obtained using DIC because of an inherent lack of measurement points near the edges of this technique. Only the central part is measured (80% of the strain profile) and the other 20% of the profile has to be estimated. The estimation of the strain at the top and bottom faces is carried out with a linear extrapolation of the last two external strain measurements taken with the DIC.

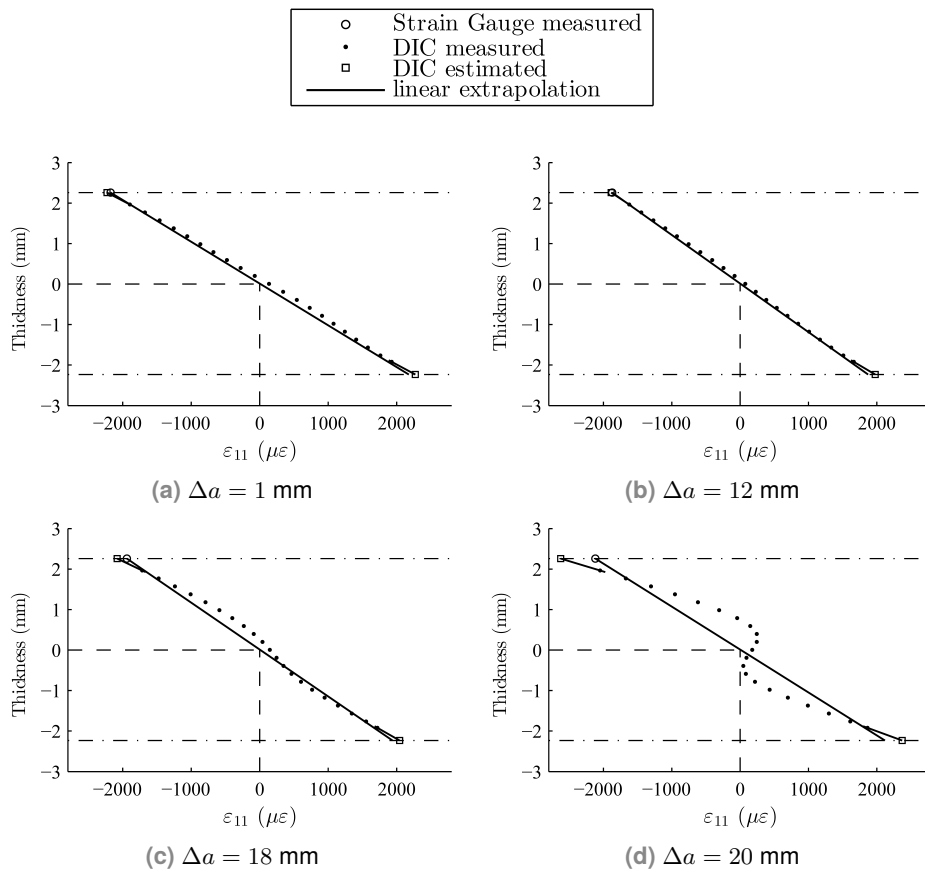


Fig. 2.7.: Strain profiles at section $S-S'$ measured with DIC and estimated from the strain gauge (ε_g) measurements for different propagation stages. Results from a 4.5 mm thick specimen.

During the first 18 mm of propagation the strain profile is almost linear and there are no appreciable differences between the measured values (DIC) and the prediction (SG), Figure 2.7. As the crack front approaches section $S-S'$ (10 mm away, Figure 2.7c), the strain profile tends to deviate from the linearity, as evidenced by the DIC

and the strains measured with the strain gauge. From this point, despite capturing almost the full strain profile with the DIC, it is not possible to determine the fracture toughness by means of the proposed method because the strain at section $S-S'$ is affected by the crack front stresses and, thus, part of the strain field generated by the FPZ falls outside the integration paths.

The average results of the propagation values of the \mathcal{G}_{IIc} and J -integral for each 3 mm and 4.5 mm thick specimen batches are listed in Table 2.2. For each specimen, the average accounts for the propagation points in the range between $\Delta a = 7$ mm and $\Delta a = 15$ mm, see Figures 2.5 and 2.6.

The difference between the CBTE data reduction method and the J -integral (DIC) diminishes when the large displacements correction is taken into account. The relative error between both data reduction methods (CBTE and J -integral (DIC-LD)) decreases from 5.1% to 1.5% for the 3 mm thick specimens, and from 4.1% to 0.8% for the 4.5 mm thick specimens.

A very good agreement is obtained between the results from the LEFM data reduction method \mathcal{G}_{IIc} (CBTE) and the J -integral (LD), having differences of less than 2.3%. With regards to the results of the J -integral (LD), the three proposed methodologies provide similar results of the mode II fracture toughness, having variation of less than 2.3% between them.

Furthermore, after comparing the results of the 3 mm and 4.5 mm thick specimens, it can be concluded that the results of the fracture toughness for the delamination in these specimens do not depend on specimen thickness. This is evidenced by all the data reduction methods. However, thinner specimens can cause larger deflections which then have to be taken into account in the data reduction methods.

The proposed data reduction methods are limited to unidirectional specimens. However, this work includes some general equations that can be particularized for the case of multidirectional laminates. To adapt the formulation to a multidirectional

Tab. 2.2.: Fracture toughness propagation values obtained from different data reduction methods (LEFM and J -integral) from the batches with 3 mm and 4.5 mm thick specimens. Values obtained from the propagation range within points PROP₇ and PROP₁₅ of each specimen (propagation points at which the fracture toughness becomes constant). The values in brackets refer to the difference respect G_{IIC} (CBTE) in %.

Specimen thickness		G_{IIC} AREA	G_{IIC} CBTE	
3 mm	Mean (J/m ²)	744 (3.4)	771	
	St dev (J/m ²)	33.6	25.7	
	CV (%)	4.5	3.3	
4.5 mm	Mean (J/m ²)	789 (0.2)	791	
	St dev (J/m ²)	47.8	29.9	
	CV (%)	6.1	3.8	
		J -integral (SD)		
		DIC	SG	BT
3 mm	Mean (J/m ²)	810 (5.1)	839 (8.9)	788 (2.3)
	St dev (J/m ²)	43.5	30.6	31.8
	CV (%)	5.4	3.6	4.0
4.5 mm	Mean (J/m ²)	823 (4.1)	807 (2.0)	795 (0.5)
	St dev (J/m ²)	33.3	63.5	34.7
	CV (%)	4.0	7.9	4.4
		J -integral (LD)		
		DIC	SG	BT
3 mm	Mean (J/m ²)	759 (1.5)	788 (2.2)	758 (1.7)
	St dev (J/m ²)	40.3	28.0	30.0
	CV (%)	5.3	3.6	4.0
4.5 mm	Mean (J/m ²)	797 (0.8)	781 (1.3)	775 (2.0)
	St dev (J/m ²)	31.8	61.8	33.6
	CV (%)	4.0	7.9	4.3

laminate, the path Γ_a in equation (2.12) has to be divided as a sum of integrations of each layer.

$$J_{\Gamma_a} = \sum_{j=1}^n \int_{-h_j}^{h_j} \left(-\frac{1}{2} \sigma_{11} \varepsilon_{11} + \sigma_{12} (\varepsilon_{12} - \tan \theta_g) \right) dx_2 \quad (2.23)$$

where σ_{11} , σ_{12} , ε_{11} and ε_{12} correspond to the layer stress and strain at the corresponding directions, n is the number of layers and h_j is the half thickness of the layer. The constitutive relationship between the stresses and the strains may be defined from the laminate theory.

With regards the data reduction methods based on the J -integral presented in this work, the simplest one is the J -integral based on Simple Beam Theory (BT-LD), where the last term in equation (2.22) is addressed by estimating the longitudinal strain profile at section $S-S'$ by means of Simple Beam Theory without the need for extra equipment besides two inclinometers. With this method, similar results of fracture toughness from LEFM methods are obtained, with errors of less than 2%. From these experimental results, it can be asserted that this methodology (J -integral (BT-LD)) is a good candidate for determining fracture toughness in ELS tests, thus providing a suitable and robust method for an industrial environment. The methodology can be used in delamination tests of laminated composite materials, as well as adhesively bonded joints.

It is worth mentioning that the specimen dimensions are critical because section $S-S'$ has to be situated far enough away from the FPZ. This means that the specimen dimensions depend on the expected FPZ length.

2.6 Conclusions

The end-loaded split (ELS) test, was recently standardized [63] as a result of its suitability for measuring mode II fracture toughness with stable crack growth. The standard method requires calibrating the clamp fixture beforehand and is based on LEFM assumptions, that is, the Fracture Process Zone (FPZ) ahead of the crack tip is small compared to the other dimensions of the problem. This paper presents a new methodology based on the J -integral which is not restricted to small FPZ, so it can be used, for example, to analyze adhesive joints.

The methodology relies on measuring load, displacement, rotation at the load application point and the section close to the clamping end (section $S-S'$), as well as the strain profile at this section. While the rotations may be measured in a simple way using inclinometers, three alternative methods are proposed for assessing the strain profile in section section $S-S'$: i) Digital Image Correlation (DIC), ii) a Strain

Gauge on the top face of the specimen and iii) an estimation based on Simple Beam Theory assumptions.

This new method is more objective than LEFM based approaches as it requires neither directly measuring nor calculating crack length. It requires less preparation because it does not need the clamp fixture to be calibrated beforehand. The proposed formulation accounts for large deflections in the ELS test.

The outcome of the LEFM based scheme and J -integral methodology on the data reduction of delamination tests are compared to check for correctness of the proposed formulation (both methods should reproduce the same fracture toughness), and a difference of less than 2.3% between the CBTE and any of the J -integral methods has been observed. In addition, the different methods used to assess the strain profile in section $S-S'$ result in a deviation in fracture toughness of less than 4%.

Suitable specimen
dimensions for the
determination of mode II
fracture toughness of bonded
joints by means of the ELS
test

M. Pérez-Galmés ^a, J. Renart ^a, C. Sarrado ^a, J. Costa ^a

^aAMADE, Mechanical Engineering and Industrial Construction Department, Universitat de Girona, Campus Montilivi s/n, Girona, Spain

The paper has been submitted to *Engineering Fracture Mechanics*

Overview

In the work of Chapter 2 it has been realized that the large FPZ involved in adhesive testing must be taken into account in specimens dimensioning in addition to the data reduction method, because to obtain the fracture toughness, the FPZ must be fully developed and this may involve larger specimens.

For this reason, this chapter presents a method to define suitable specimen dimensions for the determination of mode II fracture toughness of bonded joints by means of the ELS test.

In this chapter, the ELS test is selected instead of the ENF test for the same reason why a data reduction method was developed for the ELS test in Chapter 2: the ELS test allows large zone for the complete fracture process zone development, which is typical of mode II adhesive testing. Nevertheless, the presented method can be adjusted to define the ENF specimen dimensions for adhesive testing, since the same limitations (stability, FPZ development, large deflections and adherend failure) are applicable to the ENF test.

Abstract

The definition of the specimen dimensions in mode II fracture tests of bonded joints, where large Fracture Process Zones (FPZ) occur, is still an issue to be solved.

Several conditions shall be met in order to obtain propagation values in bonded joints testing; stability of the test, full FPZ formation, and avoidance of large deflections and adherend failure.

This work presents a methodology that indicates the specimen dimensions needed to obtain propagation values in End Loaded Split (ELS) tests.

In addition, suitable specimen dimensions for a wide range of thin bonded joints between CFRP adherends is presented, solving the issue of defining suitable specimen dimensions to test adhesives to ensure steady state propagation.

3.1 Introduction

The use of Fibre Reinforced Polymer composites (FRP) has become very popular in aerospace and automotive industries since their use results in the structure weight reduction. The joining of FRP parts through the use of adhesives instead of other mechanical fasteners is of great interest due to the adhesives capability to redistribute the loads, resulting in a reduction of the stress concentrations.

The adhesive bonded joints perform better in shear loading than under tensile or peel loadings, reason why they are designed such that the adhesive is mainly loaded in shear. Thus, the most relevant mechanical property in the FRP bonded joints design is the shear (mode II) fracture toughness of the bonded joint.

Several mode II tests have been developed in order to solve the main problem of mode II testing: stability of the test. The highly used End Notched Flexure (ENF) test [11] is mainly unstable, and other tests have been developed such as the tapered

ENF (TENF) test [95], the stabilized ENF (SENF) test [65], the Over-Notched flexure (ONF) test [124], the four ENF (4ENF) test [76] or the recent inverse ELS test [66] among others, in order to achieve stable propagation. However, other problems arise from these tests: specimen manufacturing (TENF), complex test set-up (SENF) or friction (4ENF and ONF).

The end-loaded split (ELS) test is used to determine the mode II fracture toughness in unidirectional Fibre-Reinforced Polymer composites (FRP). Unlike other tests, it has the advantage of stable crack growth under displacement control if the ratio between the initial crack (a_0) and the span length (L) is higher than 0.55 [19, 48, 79, 129, 130], allowing longer propagation length relative to the mode II ENF test case [84].

According to ISO 15114 standard [63], the crack length is a required parameter that has to be either measured or estimated during the test. In standard delamination tests it is assumed the existence of a neat crack or, in its absence, that the non-linear zone at the crack front, the so called Fracture Process Zone (FPZ), is small in comparison to any specimen relevant dimensions (width, thickness or crack length) [108]. Therefore, the steady state propagation is reached just after the initiation values.

Generally, adhesively bonded joints have been reported to entail large FPZ under shear loadings, compared to other specimen dimensions, induced by the plasticity of the adhesive layer [20, 61]. The large FPZ involved, in conjunction with the lack of crack opening, hinders the measurement of the crack length by visual inspection [23, 59, 130]. To overcome this, a method based on an effective crack length (a_e) derived from the specimen compliance was proposed by Blackman et al. [19] and a non crack dependant method, based on the J -integral, was later developed by Pérez-Galmés et al. [91].

Notwithstanding the improvement in fracture toughness calculation of bonded joints with methods that do not depend on crack measurements, other problems arise when testing adhesives because of the large FPZs involved. During the test, the energy release rate increases while the FPZ develops, attaining its maximum value (\mathcal{G}_{IIc})

when the FPZ has been totally formed. Thus, for large FPZs, several millimeters of propagation region are required to reach the propagation steady state [84]. Taking into account the specimen dimensions recommended by ISO 15114 [63], the steady state is not always achieved even after the crack front reaches the support, as occurs e.g. in bonded joints with a high toughness adhesive. Several authors performed mode II tests of adhesives without reaching the steady state propagation, either reporting propagation values that are below the self similar ones, or just providing initiation values [52, 53, 108, 115]. Unfortunately, those initiation values lead to very conservative results because they are several times lower than the propagation ones.

On the positive side, having large FPZ increases the stability of mode II tests. It allows the use of smaller a_0/L ratios and consequently, the propagation region to develop the total FPZ becomes larger (i.e. for a same L case, $L-a_0$ is increased). Such examples can be found in the works of different authors who used the ENF test with ratios of a_0/L below 0.7 (the minimum stable ratio established by Carlsson et al. [34]) in adhesive testing resulting in stable crack propagation [4, 12, 71, 80–82, 108, 115].

Moreover, due to the high fracture toughness of the adhesives and/or the dimensions of the specimens commonly used, the ELS test may involve Large Deflections (LD) [59, 130, 133]. Although the effects of LD in fracture toughness measurement appears to be solved in the ISO 15114 standard [63] by the use of the F correction factor proposed by Williams [133] or in other data reduction methodologies such as the use of J -integral [91], these large deflections stiffen the system and the test tends to be less stable. Regarding this, some authors have used thicker specimens to prevent exceeding the LD limit of $\delta = 0.2L$ [83, 116].

The previous considerations of using larger and/or thicker specimens to let the FPZ to fully develop or reach a steady-state crack propagation are intuitive and they follow a trial-and-error procedure. For this reason, a prediction of the test configuration needed beforehand would avoid repeating the tests.

In this work, a method to predict the specimen dimensions and the test configuration to get propagation values in ELS mode II fracture test, is proposed. The method establishes a design region (working domain), defined by four criteria: full development of FPZ, stability of the test, avoidance of large deflections and prevention of adherend failure. The first three criteria are evaluated through an analytical model based on the work of Alfredsson [4] which predicts the load-displacement curve of an ENF test by assuming the adhesive behaviour with a linear cohesive law. The last criterion is evaluated by considering Linear Elastic Fracture Mechanics (LEFM). A set of design regions is proposed for a wide range of existing commercial adhesives. As a result, the method provides a practical methodology for anyone who want to obtain the mode II fracture toughness in bonded joints with the ELS test.

3.2 ELS specimen design criteria

To obtain crack propagation when testing adhesives with the ELS test, some conditions must be accomplished. Firstly, to reach the steady-state crack propagation and thus the resistance curve plateau, ensuring the formation of the whole FPZ (i), secondly, to guarantee the stability of the test under displacement control (ii), thirdly, to avoid Large Deflections (LD) (iii) and, lastly, to prevent the Adherend Failure (AF) during testing (iv).

All these conditions shall be met by adjusting the ELS geometry: span length (L), initial crack length (a_0) and, if necessary, the specimen total thickness ($2H$).

3.2.1 Full FPZ development criterion

In order to obtain at least one propagation point, the propagation region ($L - a_0$) must be large enough to let the FPZ fully develop. Based on a previous work [91] a

minimum distance of 10 mm have been be left in order to avoid clamping effects. The aforementioned conditions are satisfied if,

$$L - a_0 > l_{FPZ} + 10mm \quad (3.1)$$

where a_0 is the initial crack length, L is the span length and, l_{FPZ} is the length of the FPZ when the propagation begins. It is worth mentioning that the pre-crack test has not been taken into account in the previous condition (equation 3.1), since it is considered a previous test.

To define this criterion, the corresponding l_{FPZ} for a particular L and a_0 has to be estimated, which can be done by means of the analytical model presented in section 3.3. It is worth noticing that, when the end of the FPZ approximates the clamp tool, compressive stresses can influence the crack propagation. On that account, the initial crack length (a_0) should be approximated to the minimum allowed by the other criteria.

3.2.2 Stability criterion

When the test becomes unstable, the crack jumps, and propagation values can not be obtained. Various studies dealt with the stability of ELS test under displacement control assuming Simple Beam Theory (SBT) and Linear Elastic Fracture Mechanics (LEFM) and they concluded that the propagation will be stable using a minimum a_0/L ratio of 0.55 [46, 59, 128–130]. The stability can be improved by using larger a_0/L ratios, reducing however the length available for the crack to grow (or by requiring a larger specimen to maintain the propagation distance, $L-a_0$)

In adhesive testing, test stability cannot be simply obtained under the assumptions of LEFM. By studying the FPZ effect in mode II testing, several authors concluded that the closure stresses ahead of the crack tip due to FPZ development contribute to the crack growth stability [4, 12, 81, 115]. Alfredsson [4] estimated, for an ENF

test, a minimum a_0/L ratio by assuming an specific cohesive law for the adhesive, and he demonstrated that the critical a_0/L ratio is less restrictive, when large FPZ are involved, than the LEFM-based ENF stability limit $a_0/L > 0.7$ [34].

In order to explain how the FPZ improves the test stability, Figure 3.1 shows the schematic Load-displacement ($P - \delta$) curves of two specimens with the same fracture toughness but different l_{FPZ} .

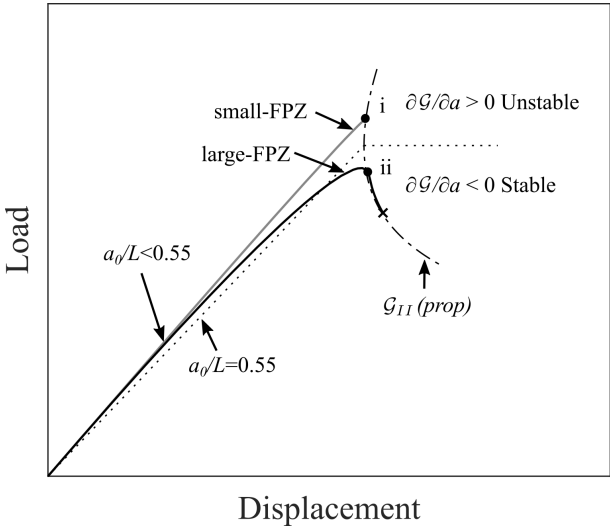


Fig. 3.1.: Schematic of LEFM $P - \delta$ curve. Example of FPZ effects in the stability.

In Figure 3.1, the dotted line marks the stability limit according to LEFM [59]. It is observed that a test on a specimen with large FPZ can be stable even if the ratio of a_0/L is smaller than 0.55. Therefore, in presence of large FPZ, the LEFM stability limit based on Griffith's energy balance approach, $\partial G / \partial a < 0$, is too conservative. A snap-back in the Load-displacement curve ($P - \delta$) always occurs in an unstable test. Therefore, the proposed stability criterion relies on avoiding snap-back in the Load-displacement curve. However, the only way to determine the stability limit is by predicting the $P - \delta$ curve beforehand, which in this work is done with an analytical model of the ELS test presented in section 3.3.

3.2.3 Large deflections criterion

In the case of specimens with thin adherends, the ELS test configuration results in Large Deflections (LD) [59, 130, 133]. In presence of LD, the compliance decreases with the displacement, and the test becomes less stable. To illustrate this behaviour, Figure 3.2 shows the schematic $P - \delta$ curves of two specimens with the same geometry but with different adhesive properties. The curves are represented assuming a LEFM approach.

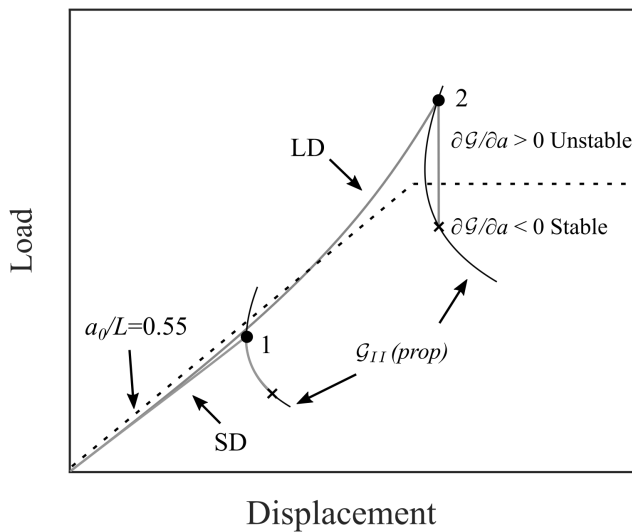


Fig. 3.2.: Schematic of two $P - \delta$ curve of same geometry (a_0/L below the LEFM-based stable limit) to illustrate the instability induced by the LD during the test.

Specimen 1 (Small Deflections) has stable propagation but specimen 2 becomes unstable due to LD effects (i.e. specimen stiffening).

As previously stated, the presence of FPZ reduces the stiffness of the specimen, so larger deflections for the same initial specimen geometry are produced. For this reason the analytical study of LD is not straightforward.

Williams [133] proposed a F correction factor that introduces the effect of the reduction on the moment arm due to large displacements in ELS test. The F correction factor used in this work has been obtained by adding the FPZ length when the propagation begins, l_{FPZ} and disregarding the effect of the loading blocks, reading

$$F = 1 - \frac{3}{20} \left(\frac{15 + 50 \left(\frac{a+l_{FPZ}}{L} \right)^2 + 63 \left(\frac{a+l_{FPZ}}{L} \right)^4}{\left(1 + 3 \left(\frac{a+l_{FPZ}}{L} \right)^3 \right)^2} \right) \left(\frac{\delta_{prop}}{L} \right)^2 \quad (3.2)$$

where δ_{prop} is the vertical deflection when propagation starts, calculated by the SBT method defined in ISO15114 [63]. Equation (3.2) takes into account the effect that the FPZ has on the stiffness of the specimen.

The same limit for the F correction factor as in ISO 25217 standard [64] is used as a LD criterion in this work ($F > 0.9$), where F is calculated according to equation (3.2).

Considering the l_{FPZ} in the F calculation results in a more restrictive criterion than William's [133], because a less rigid system is assumed (i.e. the cohesive strains do not contribute to the structure stiffening).

3.2.4 Adherend failure criterion

When testing high fracture toughness adhesives, Adherend Failure (AF) can occur due to bending stresses, even before the crack starts to propagate.

As the compression strength is lower than the tensile value in unidirectional composite laminates, the maximum compression stress (σ_c) is considered as the critical parameter for the rupture of the specimen substrates.

The maximum compression stress may take place either at the top face near the clamp section or near the crack tip ($x = 0$ or $x = b$ in Figure 3.3). By considering that the maximum compressive stress at clamp end section (σ_c) must be smaller than the ultimate normal compression strength of the adherend ($\sigma_u \geq \sigma_c$), and assuming beam's theory and LEFM, the maximum compressive stress at clamp end section ($x = b$) can be expressed in function of the a_0/L ratio

$$\frac{a_0}{L} \geq \sqrt{\frac{E_{11}\mathcal{G}_{IIc}}{H\sigma_u^2}} \quad (3.3)$$

where H is the arm specimen thickness, E_{11} is the adherend longitudinal Young's modulus, \mathcal{G}_{IIc} is the adhesive fracture toughness, and σ_u is the normal compression strength of the adherend.

On the other hand, the critical compression stress at the crack tip section ($x = 0$) defines the minimum thickness for each substrate to prevent its rupture

$$H \geq \frac{4E_{11}\mathcal{G}_{IIc}}{\sigma_u^2} \quad (3.4)$$

Moreover, shear stresses can also lead to adherend failure. Under the same assumptions than previous equations, a minimum value for a_0 is obtained:

$$a_0 \geq \frac{\sqrt{E_{11}\mathcal{G}_{IIc}H}}{2\tau_u} \quad (3.5)$$

where τ_u is the ultimate shear strength of the adherend laminate.

By assuming an specific failure strength of the adherends, a limit case can be set for each geometry, based on equations (3.3), (3.4) and (3.5).

Equation (3.4) is independent of a_0 and L constraining the maximum \mathcal{G}_{IIc} that can be tested with a determined specimen thickness, while the other two, equations (3.3) and (3.5), restrict a_0 depending on the span length L .

3.3 Analytical model

The analysis of the stability of the test and evolution of FPZ formation criteria require the estimation of a Load-displacement curve accounting for the FPZ length. The most important parameter to describe the fracture process is the fracture toughness. If combined with the shear strength, both the energy dissipated and the length of the FPZ can be controlled. These two parameters, represented in a linear cohesive law, can provide reliable descriptions of the fracture process. Using cohesive law shapes would complicate the analytical developments of the model, to obtain a small improvement in its accuracy. Furthermore, the adhesive properties available in the literature are mainly the shear fracture toughness and failure shear strength and very few information can be found about the cohesive law shape.

In this work, the Load-displacement curve is obtained from an analytical model adapted from the work of Alfredsson [4] to an ELS test configuration. The model simulates a mode II test of a bonded joint in which the adhesive is a thin layer capable to transmit pure shear.

The geometry considered for the ELS test is shown in Figure 3.3.

For small values of the slope ($|w'| \ll 1$) the shear deformation $v(x)$ of the adhesive layer is given by

$$v(x) = 2u(x) + Hw'(x) \quad (3.6)$$

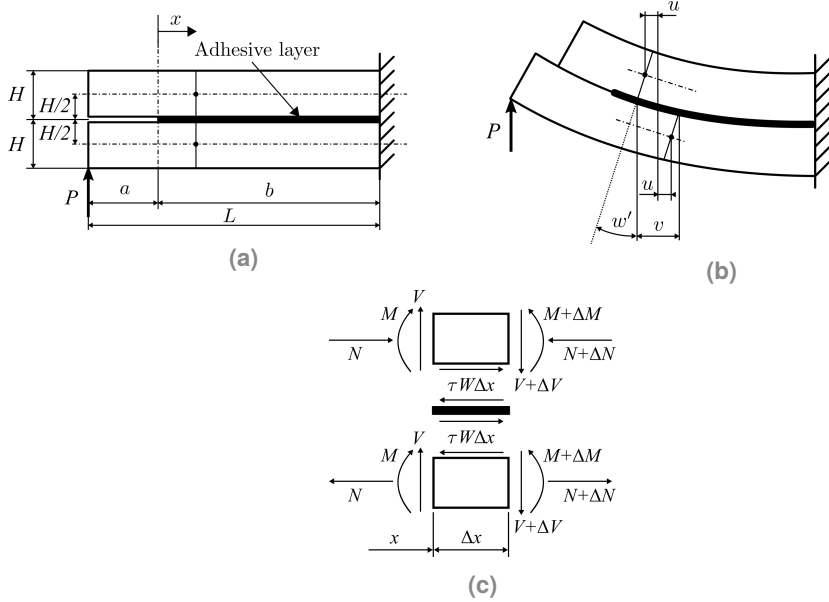


Fig. 3.3.: a) Undeformed geometry of ELS specimen; b) Deformed geometry of ELS specimen. v corresponds to the shear deformation of the adhesive layer and w to the deflection; c) Positive directions of sectional loads and adhesive stresses in the interval $x \in [0, b]$, where W corresponds to the specimen width.

The constitutive behaviour of the adhesive layer is entirely described by a bilinear law (see Figure 3.4) defined by,

$$\tau(v) = \begin{cases} kv & \text{for } 0 \leq v \leq v_a \\ \bar{k}(v_c - v) & \text{for } v_a \leq v \leq v_c \\ 0 & \text{for } v \geq v_c \end{cases} \quad (3.7)$$

being $k = \tau_{sh}/v_a$ and $\bar{k} = \tau_{sh}/(v_a - v_c)$.

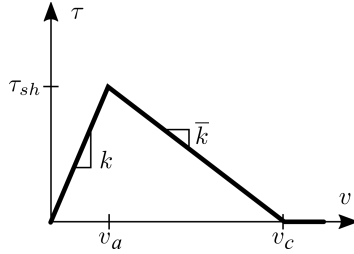


Fig. 3.4.: Bilinear constitutive relation of the adhesive layer.

The equilibrium equations obtained from the interval forces of two adjacent sections of the adhesive layer, $x \in [0, b]$, are the same than in [4], see Figure 3.3c,

$$N'(x) = W\tau[v(x)] \quad (3.8a)$$

$$V'(x) = 0 \quad (3.8b)$$

$$V(x) = M'(x) + \frac{1}{2}WH\tau[v(x)] \quad (3.8c)$$

where geometric parameters, H , b , v and x are defined in Figure 3.3, W is the specimen width, $\tau[v(x)]$ is the constitutive relationship of the adhesive layer defined in equation (3.7), N denotes the normal force of the adherends, and M and V are the bending moment and shear force respectively.

By assuming elastic adherend deformation and according to Euler-Bernoulli beam's theory, the normal force, the shear and the bending moment are given by [4],

$$N(x) = EWHu'(x) \quad (3.9a)$$

$$V(x) = \frac{P}{2} \quad (3.9b)$$

$$M(x) = -\frac{EWH^3}{12}w''(x) \quad (3.9c)$$

where E is the longitudinal Young's modulus of the adherend material and P is the applied load, represented in Figure 3.3.

Equations (3.6) to (3.9) define a system of two ordinary differential equations in $w(x)$ and $v(x)$ that describe the mathematical problem:

$$\begin{cases} EHv''(x) = 8\{\tau[v(x)] - 2\bar{\tau}\} & \text{for } 0 \leq x < b \\ EwH^3w''(x) = -6\{P(x+a) - HW \int_0^x \tau[v(\tilde{x})]d\tilde{x}\} & \text{for } -a \leq x < b \end{cases} \quad (3.10)$$

where $\bar{\tau} = 3P/(8WH)$ is the shear stress in solid beam sections (e.g. Beer et al., 2002 [17])

In order to obtain $v(x)$ and $w(x)$ the following boundary conditions are considered:

$$N(0) = 0 \quad (3.11a)$$

$$M(0) = Pa/2 \quad (3.11b)$$

$$v(b) = 0 \quad (3.11c)$$

$$w(b) = 0 \quad (3.11d)$$

$$w'(b) = 0 \quad (3.11e)$$

According to equation (3.7) the boundary conditions (equation (3.11)) transforms to

$$v'(0) = \frac{-16\bar{\tau}a}{EH} \quad (3.12)$$

Assuming the presence of a cohesive zone of length d at the crack tip ($d < b$), the general solution to the shear deformation equation (3.10) is:

$$v(x) = \begin{cases} A_1 \sin(\bar{\kappa}x) + A_2 \cos(\bar{\kappa}x) + v_c - 2\bar{\tau}/\bar{k} & \text{for } 0 \leq x \leq d \\ A_3 e^{\kappa x} + A_4 e^{-\kappa x} + 2\bar{\tau}/k & \text{for } d \leq x \leq b \end{cases} \quad (3.13)$$

where $\bar{\kappa} \equiv \sqrt{8\bar{k}/(EH)}$ and $\kappa = \sqrt{8k/(EH)}$.

The integration constants A_1, A_2, A_3 and A_4 are determined from boundary conditions (equation (3.11) and equation (3.12)) and the continuity equations at $x = d$, for $v(d)$ and $v'(d)$.

The solution of $v(x)$ is divided in 3 parts.

Firstly, when $v(0) \leq v_a$ the adhesive has a linear response and there is no FPZ, thus $d = 0$. Only the elastic part of $v(x)$ is considered:

$$v(x) = A_3 e^{\kappa x} + A_4 e^{-\kappa x} + 2\bar{\tau}/k \quad \text{for } 0 \leq x \leq b \quad (3.14)$$

Secondly, if $v_a \leq v(0) \leq v_c$ the FPZ is under development. A relationship between d and the applied load, represented by $\bar{\tau}$, can be determined by knowing that the deformation of the right end of the process zone is $v(d) = v_a$.

And thirdly, if the shear displacement $v(x)$ exceeds the critical value v_c , the crack propagates. The crack growth length a is increased in equation (3.13) and a new size of the process zone, d , is calculated using equation (3.13) and knowing the shear deformation of both sides of the FPZ; $v(0) = v_c$, and $v(d) = v_a$. For each increment of a , a value of P is obtained.

It is worth noticing that in this later part d must be kept as a dependent value, because as it is shown in [4] there is a small variation of d with the increment of the crack length, a .

Once $v(x)$ is known, $w(x)$ can be obtained by solving the differential equation (3.10) taking into account boundary conditions (equations (3.11) and (3.12)). The displacement at the loading application point is $w(-a)$.

A comparison between the analytical model and FEM for three different adhesive cohesive properties is shown in Figure 3.5, demonstrating that $P - \delta$ curve from the analytical model fits well with the FEM results.

The finite element model was developed in Abaqus implicit [1] using four-node, 2D plane strain elements (CPE4). A row of zero-thickness four-node cohesive elements (COH2D4) was placed ahead of the notch tip to model crack propagation. The same boundaries and cohesive properties used in the analytical model were used in the FEM.

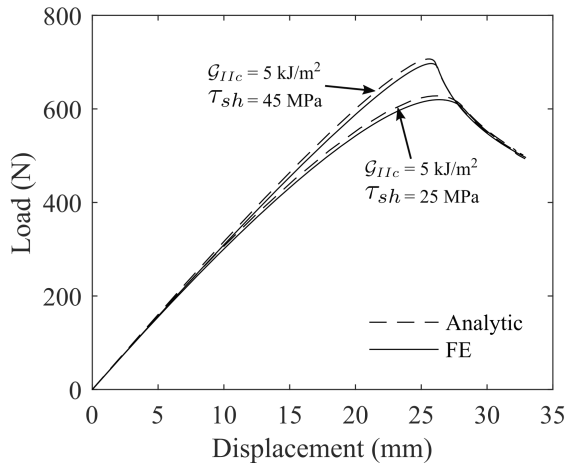


Fig. 3.5.: $P - \delta$ curve from a FE model and the proposed analytical model. Results from specimens with the same geometry ($a_0 = 80$ mm, $H = 3$ mm, $W = 25$ mm and $L = 150$ mm) but with different cohesive properties.

In the proposed analytical model the assumed boundaries do not take into account clamp effects, caused by the imperfect encastre of the ELS test rig, because they have to be evaluated once the specimen geometry is defined [63]. In Section 3.6 the clamp effects on the working domain definitions are discussed. It is worth noticing that the analytical model do not take into account the shear deformations of the adherends, since Euler Bernoulli assumptions are considered and the results show good agreement.

3.4 Definition of a working domain

3.4.1 Working domain for known adhesive properties

Assuming the constitutive properties of the adhesive layer, τ_{sh} and \mathcal{G}_{IIc} , a specimen thickness, H , and the mechanical properties of the adherends, we can define a relationship between a_0 and L for the specimen that fulfils the criteria defined in section 3.2.

Each criterion (Stability, full FPZ formation, LD: Large Deflections, AF: Adherend Failure) defines a boundary curve that, together, enclose a working domain defined by a_0 and L . These boundary curves are defined by using the analytical model described in section 3.3.

For a given adherend thickness H , a set of models with different span lengths L and a short a_0 are run. From the results, the a_0 at which the test is no longer stable (Stability criterion) is determined.

On the other hand, a set of geometries with different L and a_0 are defined for a given H and the corresponding initial l_{FPZ} and the displacement when the propagation starts (δ_{prop}) are obtained.

This data in combination with equations (3.1) and (3.2) define the onset of crack propagation (full FPZ formation criterion) and the values of a_0 for which the assumption of small deflections, is no longer valid (LD criterion).

Repeating this procedure for different H , the curves that define the Stability, full FPZ formation and LD criteria are obtained.

The AF criteria are represented directly on the a_0 vs. L or a_0 vs. a_0/L graphs from equations (3.3) and (3.5). Equation (3.4) defines the minimum thickness ($2H$) of the specimen to prevent the arm failure near the crack front before the propagation.

Figure 3.6a exemplifies how the ELS working domain is defined in an a_0 vs L plot. The grey area represents the working domain of a bonded joint with an adhesive with $G_{IIC} = 8 \text{ kJ/m}^2$, $\tau_{sh} = 30 \text{ MPa}$, $k = 10^4 \text{ GN/m}^3$, $H = 6 \text{ mm}$, $E_{11} = 120 \text{ GPa}$, $\sigma_u = 1500 \text{ MPa}$ and $\tau_u = 100 \text{ MPa}$.

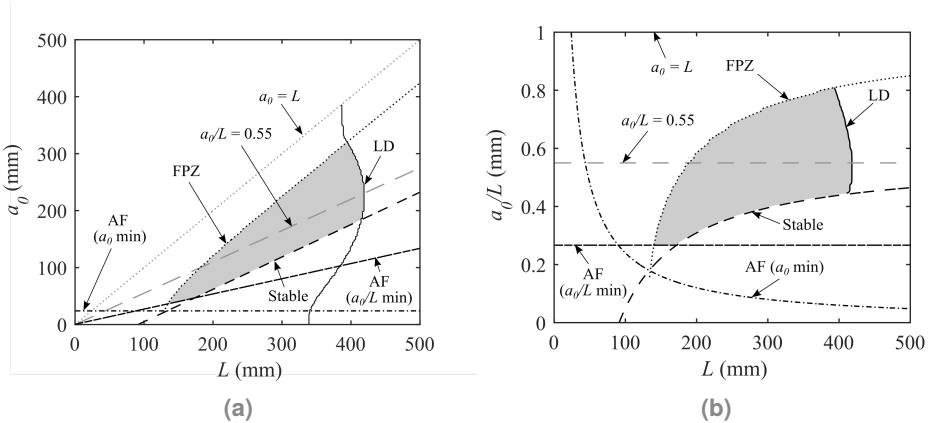


Fig. 3.6.: Working range of case 5 ($G_{IIC} = 8 \text{ kJ/m}^2$ and $\tau_{sh} = 30 \text{ MPa}$). Specimens of 6 mm thickness.

The working domain is the area enclosed by all the criteria boundaries, each one represented by a curve, except the AF boundaries that are represented by 2 curves, defined by equations (3.3) and (3.5). In Figure 3.6a, equation (3.3) does not limit the working domain.

The same results are represented in a a_0/L versus L plot for an easier viewing of each limit, see Figure 3.6b.

Additionally, the propagation ($a_0 = L$) and the stability ($a_0/L \geq 0.55$) boundaries based on LEFM assumptions have been added to Figures 3.6a and 3.6b to highlight the effect of the FPZ on the working domain. In Figure 3.6b the boundaries based on LEFM define a domain for the ratio a_0/L from 0.55 to 1, whereas when large FPZ applies, this domain is reduced and shifted down. The LD criterion limits the maximum span length (L) that can be used.

3.4.2 Definition of a general domain

Figure 3.6 can only be obtained if the constitutive properties of the adhesive layer are known in advance. In case they are not, they must be estimated.

Table 3.1 summarizes the cohesive properties of common adhesives used in aeronautics found in the literature, they are divided into three main groups: resins, pastes and films.

Tab. 3.1.: Mechanical properties (fracture toughness, shear failure strength and Young's modulus) of common adhesives used in aeronautics.

Type	Name	Supplier	G_{IIC} (kJ/m ²)	τ_{sh} (MPa)	E_{11} (GPa)
Resin	TEXIPREG HS-160 RM	SEAL [®]	0.79 [26] ³ , 0.84 [28]	80 [12] ¹ ³	-
	MCP1110	Maruhachi Corp.	1.89 [72]	49.9 [69]	3.2 [72]
	8551-7	Hexcel [®]	-	100-107 ¹	-
	8552	Hexcel [®]	1.33-1.76 [58]	128 ¹	-
Paste	M21	Hexcel [®]	-	110 ¹	-
	Araldite [®] 2015	Araldite [®]	3.18 [27], 4.3 [115], 4.7 [26] ³	17.9 [113], 22.8 [26] ³	1.85 [29]
	AV138/HV998	Araldite [®]	4.91 [115]	30.2 [75]	4.59 [113], 4.89 [29]
	EA 9361 (Hysol)	Henkel [®]	5.22 [114] ²	20.6 [114] ²	0.723 ¹ , 0.67 [114]
Film	FM-300MÄ	CYTEC	7.0 [71], 7.9 [105]	45 [71], 47.5 [105]	2.921 [105]
	EA9628	Henkel [®]	-	40-41.3 ¹	2.377 ¹
	EA9695	Henkel [®]	-	31.7-34.5 ¹	-

¹ Manufacturer's data.

² The interlaminar shear strength reported in [114] depends on the adhesive thickness, so the value shown is the result of the linear extrapolation of the failure load to a zero adhesive thickness.

³ Data used in numerical modelling.

Tab. 3.2.: Cohesive properties and geometries considered in the analytical model.

	\mathcal{G}_{IIc} (kJ/m ²)	τ_{sh} (MPa)
Case 1	0.7	110
Case 2	3	30
Case 3	5	45
Case 4	5	17
Case 5	8	30

It is observed that the paste and film adhesives have middle failure shear strengths ($\tau_{sh} = 17.9$ MPa to 47.5 MPa) and middle to high fracture toughnesses ($\mathcal{G}_{IIc} = 2.18$ kJ/m² to 7.9 kJ/m²), while the resins are of middle to high failure shear strengths ($\tau_{sh} = 49.9$ MPa to 128 MPa) and low fracture toughnesses ($\mathcal{G}_{IIc} = 0.79$ kJ/m² to 1.89 kJ/m²).

Moreover, according to [16, 121, 125] the size of the FPZ is proportional to \mathcal{G}_{IIc} and inversely proportional to τ_{sh} .

By taking this into account, and based on the literature data presented in Table 3.1, typical interlaminar constitutive behaviour of a bonded joint or an adhesive are represented by the 5 cases presented in Table 3.2.

Cases 1 and 2 are a combination of the maximum and minimum properties of the resins of Table 3.1. Cases 2 and 3 encompass the properties of low to medium toughness adhesives. And finally, cases 4 and 5 concern medium to high toughness adhesives. The combination of two cases can define an overlapped working domain for an interface (adhesive / resin) with a wider range of properties.

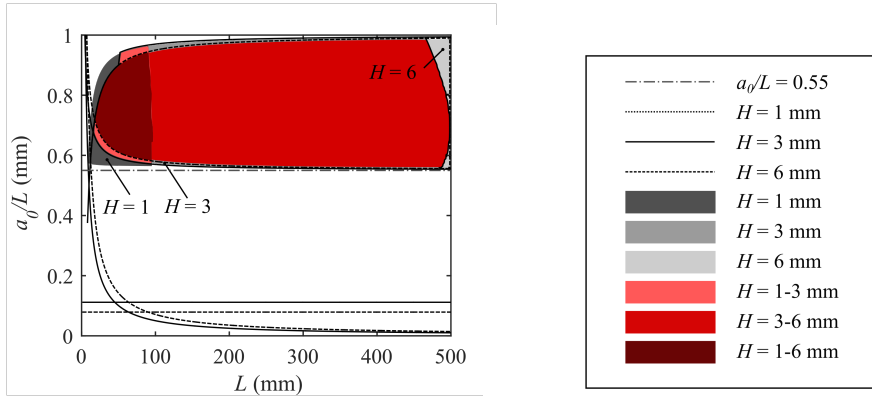
3.5 Results

A series of working domains were defined for 3 different adherend thicknesses ($H = 1, 3$ and 6 mm) and for each case of Table 3.2. The same width, W , was considered in all the cases (25 mm).

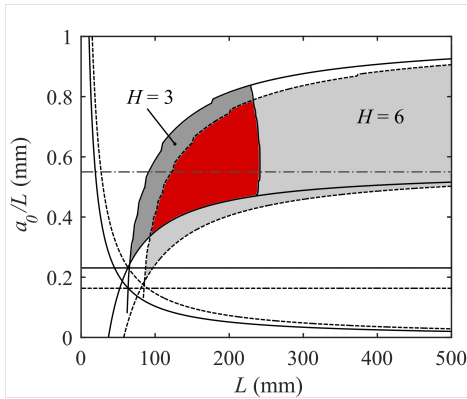
As not being crucial in fracture toughness calculation of a thin adhesive layer, k is fixed to 10^4 GN/m³ for all models, by considering an adhesive layer thickness of $t = 0.15$ mm and an adhesive shear modulus of $G_{adh} = 1500$ MPa [113], and $k = G_{adh}/t$ according to Alfredsson [4]. The elastic properties of the adherends considered are typical values of unidirectional CRFP: $E_{11} = 120$ GPa, $E_{22} = E_{33} = 7.8$ GPa and $G_{12} = 4$ GPa [71], where subscript 1 denotes x direction (c.f. Figure 3.3). The ultimate values considered to calculate the adherend failure limits are $\sigma_u = 1500$ MPa and $\tau_u = 100$ MPa.

To construct the domains, the span length was varied in the interval $L \in [50, 500]$ mm, and $a_0 \in [0, L]$.

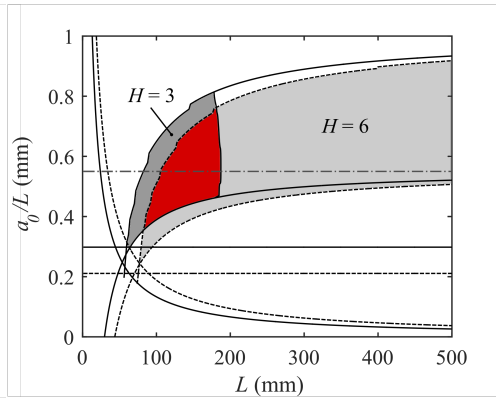
Figure 3.7 shows the working domains for the configurations described in Table 3.2. Each Figure includes the working domains for the 3 different thicknesses, 1, 3 and 6 mm.



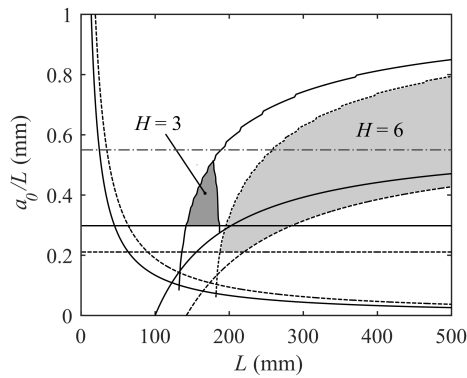
(a) $\mathcal{G}_{IIc} = 0.7 \text{ kJ/m}^2$, $\tau_{sh} = 110 \text{ MPa}$



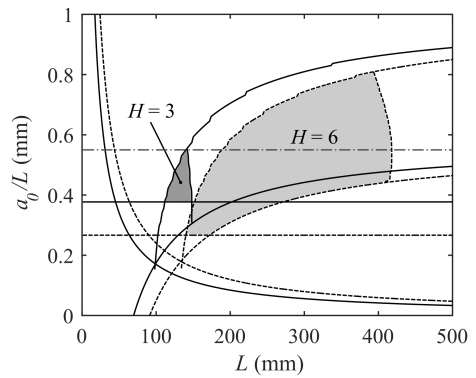
(b) $\mathcal{G}_{IIc} = 3 \text{ kJ/m}^2$, $\tau_{sh} = 30 \text{ MPa}$



(c) $\mathcal{G}_{IIc} = 5 \text{ kJ/m}^2$, $\tau_{sh} = 45 \text{ MPa}$



(d) $\mathcal{G}_{IIc} = 5 \text{ kJ/m}^2$, $\tau_{sh} = 17 \text{ MPa}$



(e) $\mathcal{G}_{IIc} = 8 \text{ kJ/m}^2$, $\tau_{sh} = 30 \text{ MPa}$

Fig. 3.7.: Working domain of each case study.

In case 1 (Figure 3.7a) the working domains of the three thicknesses intersect. In case 2 this intersection does not occur due to the LD limitation in $2H = 2$ mm thick specimens. In cases 3, 4 and 5, for a $2H = 2$ mm thick specimens, the boundary criteria do not define a working domain and they are not represented.

Figures 3.8, 3.9 and 3.10 show the intersection of two cases of Table 3.2 for the same adherend thickness. It is worth noticing that indications of what criterion is defining each limit are made in Figure 3.6, but not in Figures 3.7 to 3.10, since they only aim to show the working domain for the studied cases. Figure 3.8 shows the intersection between cases 1 and 2, defining a working domain for low toughness adhesives (0.7 to 3 kJ/m²).

Figure 3.9 plots the intersection between cases 2 and 4, defining the working domain for medium toughness adhesives (3 to 5 kJ/m²). Finally, Figure 3.10 shows the intersection between cases 3 and 5, defining the working domain for high toughness adhesives (5 to 8 kJ/m²).

For each intersection only two thicknesses are considered: $H = 1$ and 3 mm in Figure 3.8; $H = 3$ and 6 mm in Figures 3.9 and 3.10. The thickness chosen depends on the LD and AF criteria.

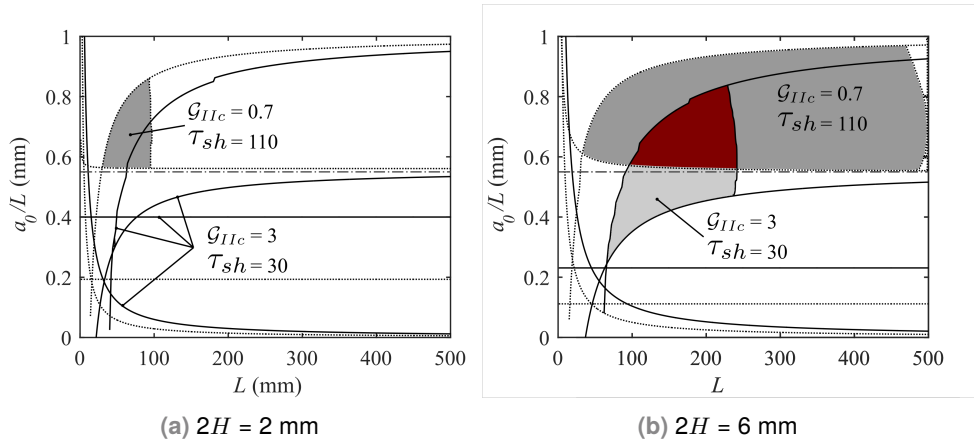


Fig. 3.8.: Working domain of resins of \mathcal{G}_{IIc} between 0.7 kJ/m² and 3 kJ/m² and τ_{sh} between 30 MPa and 110 MPa. Relatives to cases 1 and 2.

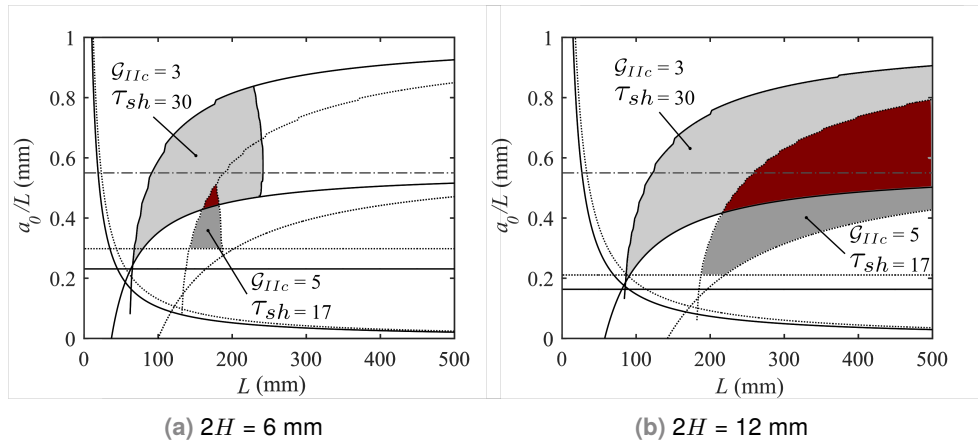


Fig. 3.9.: Working domain of paste adhesives adhesives of \mathcal{G}_{IIc} between 3 kJ/m² and 5 kJ/m² and τ_{sh} between 17 MPa and 30 MPa. Relatives to cases 2 and 3.

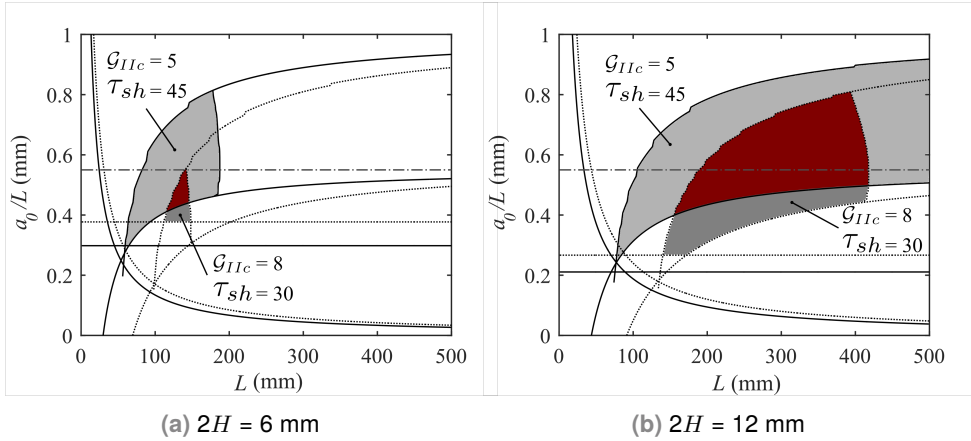


Fig. 3.10.: Working domain of film adhesives of \mathcal{G}_{IIc} between 5 kJ/m² and 8 kJ/m² and τ_{sh} between 30 MPa and 45 MPa. Relatives to cases 4 and 5.

3.6 Discussion

As it results in short FPZ lengths, the lower stable limit of case 1 ($\mathcal{G}_{IIc} = 0.7$ kJ/m² and τ_{sh} 110 MPa, represented in Figure 3.7a) approximates the LEFM-based stable limit of $a_0/L = 0.55$ and the higher FPZ formation limit approximates the geometric limit $a_0 = L$. Therefore, the recommended geometries of the standard ISO 15114 [63] would be valid and only the LD limit must be taken into account to define the specimen geometry.

In the general case of resins (Figure 3.8, combination of cases 1 and 2) the minimum a_0/L ratio to maintain the stability is 0.55 and the full FPZ development criterion restricts the minimum L and maximum a_0 . Furthermore, as including high toughness resins ($\mathcal{G}_{IIc} = 3$ kJ/m²), thicker specimens must be used in order to reduce large deflections. Notice that there is not intersection of working domains of cases 1 and 2 for thin specimens (c.f. Figure 3.8a).

On the other hand, the results of paste and film adhesives of high fracture toughness and low failure shear strengths (cases 2 to 5) show that, when the l_{FPZ} is enlarged,

the upper (full FPZ formation) and lower (stability) domain boundaries decrease requiring the use of larger and thicker specimens.

In view of the results (Figures 4.8, 3.8, 3.9 and 3.10) effects on the proposed criteria can be described.

The \mathcal{G}_{IIc} value has significant effect on the LD and AF criteria because higher deflections are produced before the propagation starts. This reduces the maximum span length (L) and minimum specimen thickness ($2H$) allowed. The \mathcal{G}_{IIc} also restricts the minimum a_0/L ratio to avoid adherend failure.

Low shear strengths, τ_{sh} , enlarge the FPZ length making the test more stable but limiting the minimum span length L and maximum a_0/L ratio (uppermost full FPZ formation criterion).

The use of thick specimens enlarge the l_{FPZ} reducing the a_0/L ratio that allows the full FPZ development criterion but relaxing the large deflections and adherend failure criteria (minimum a_0). On the contrary, the use of thin specimens increase the minimum a_0 defined by the AF criteria. Despite this, the AF criteria does not significantly limit any working domain.

Once the working domain is defined for a particular case, it is important to consider the physical background of the domain boundaries in order to make a correct choice of an experimental ELS test geometry.

First of all, the use of as small as possible geometries inside the working domain is recommended in order to avoid the early onset of Large Deflections.

Secondly, the use of a_0/L ratios adjoining the lower stability criteria boundary is recommended providing a larger propagation zone ($L - a_0$). As mentioned in Section 3.3 clamp effects are not taken into account in the analytical model to define the working domain, since they can not be evaluated before defining the specimen. Thus, before the test, a clamp calibration may be performed in order to obtain Δ_{clamp} [63]. Then, the minimum initial crack length a_0 can be defined taking into account that

for the stable criterion limit, the considered L in the horizontal axis of the working domain plot is $L + \Delta_{clamp}$.

Notice also that when approaching the upper full FPZ formation limit, any propagation of the crack is accomplished and only the initiation range of the resistance curve is obtained, i.e. FPZ development but there is no need of take into account the clamp effect.

3.7 Conclusions

The large FPZ involved in adhesive testing directly affects the suitability of the ELS test. This paper presents a methodology to define the working domain of the ELS test based on four limiting criteria: i) stability, ii) full FPZ formation, iii) Large Deflections and iv) Adherend Failure. The presented methodology ensures successful tests by providing a tool for the design of specimens. To do so, an analytical model that considers a linear constitutive relation in the cohesive zone expressed in terms of fracture toughness (G_{IIc}) and failure shear strength (τ_{sh}) is presented and used to evaluate the proposed criterion.

With the presented methodology, suitable ELS specimens dimensions to ensure steady state propagation in adhesive testing can be obtained by assuming the adherend properties and a range the adhesive mechanical properties to be tested, i.e. the working domain of specimen dimensions to perform the ELS test satisfactorily.

It has been shown that large FPZ make the LEFM based stable criterion less restrictive but demand larger zones for the crack to propagate and may induce larger deflections. Therefore, in cases of small FPZ, the standard ELS dimensions are suitable but larger FPZ demand the use of thicker and larger specimens. On the other hand, high toughness adhesives demands the use of thicker and stronger adherends since higher stresses are reached during the test.

Although particular cases have been studied (Table 3.2), the results presented in section 3.5 show the working domains for a combination of resins, paste and film adhesive properties (Table 3.1). These can be used as a guide, along with the recommendations presented in the discussion section 3.6, to define ELS specimens dimensions to satisfactorily test a wide range of adhesives with no need of further analysis. The present work therefore presents a practical methodology for all those who need to obtain the mode II fracture toughness in bonded joints.

Towards a consensus on mode II adhesive fracture testing typologies and data reduction methods: experimental study

M. Pérez-Galmés ^a, J. Renart ^a, C. Sarrado ^a, A.J. Brunner ^b, A. Rodríguez-Bellido ^c

^aAMADE, Mechanical Engineering and Industrial Construction Department, Universitat de Girona, Campus Montilivi s/n, Girona, Spain

^bEmpa, Swiss Federal Laboratories for Materials Science and Technology, Laboratory for Mechanical Systems Engineering, Überlandstrasse 129, CH-8600 Dübendorf, Switzerland

^cComposite Technology, Materials and Processes, AIRBUS Operations SL, Paseo John Lenon s/n, E-28906 Getafe, Madrid, Spain

The paper has been submitted to *Theoretical and Applied Fracture Mechanics*

Overview

In this chapter, several mode II test methodologies are compared through an experimental test campaign in order to define and discuss the suitability of mode II test methodologies to test structural adhesives, which is the main objective of the present thesis.

To achieve this, the developed J -integral for the ELS test and the existing J -integral closed-forms for the ENF and the MMB tests have been applied on the data reduction in an experimental test campaign of a structural adhesive.

Even not having the same level of popularity, the 4ENF test have been also studied in the test campaign, since it is always stable providing a large propagation zone. For comparison purposes, a J -integral closed-form have been developed for this test.

The J -integral have been compared with other data reduction methods from the literature and the results obtained have been discussed.

Abstract

Mode II fracture toughness is crucial in the design of structural bonded joints between fibre reinforced polymers (FRP). This is mainly because adhesives are designed to work under shear, rather than peel, loading. However, one of the main problems encountered in mode II experimental testing is the poor reproducibility between the most common test methodologies: End-Notched Flexure (ENF), End-Load Split (ELS), 4-point End-Notched Flexure (4ENF), and the Mixed Mode Bending (MMB) test at 100% of mode II.

The objective of this work is to define reliable test methodologies and data reduction methods to obtain comparable results among the aforementioned tests.

For this reason, an experimental test campaign consisting of the abovementioned four mode II test methods was carried out. The J -integral was implemented in all the tests as a data reduction method, and it was compared to the data reduction methods based on Linear Elastic Fracture Mechanics (LEFM). The results obtained from the J -integral based methods were independent from the test methodology and obtained very good agreement among the tests.

In addition, from the experimental results the advantages and drawbacks of the different test procedures are analysed and discussed, concluding that the ELS test is the most suitable to measure mode II fracture toughness.

[SUBMITTED PAPER. EMBARGO UNTIL PUBLICATION DATE]

Discussion

This chapter discusses the developed work as a whole in accordance with the proposed objective of the present thesis: definition of reliable test methodologies to determine the mode II fracture toughness of structural adhesive bonded joints.

As explained in Chapter 1, when testing structural adhesives under mode II loadings, large FPZ may develop compared with the delamination-based tests specimens dimensions. The large FPZ has to be taken into account not also in the data reduction for the computation of the fracture toughness, but also on specimens design.

The traditional LEFM-based data reduction methods assume a sharp crack tip and the effects of the FPZ are not taken into account. More elaborated methods have been developed in order to account for the stresses transmitted within the cracked parts in the FPZ region. One example, are the J -integral closed form solutions developed for fracture tests such as the DCB in mode I, the ENF in mode II and the MMB in mode I/II mixed mode. Despite LEFM-based methods can provide fairly good results under some particular scenarios, they are not as reliable as those based on the J -integral, because they ignore the existence of a FPZ.

In mode II testing, only a J -integral closed form solution was available in the literature for the ENF test but not for other highly used tests, such as the 4ENF or the ELS. Both ELS and 4ENF tests have the advantage over ENF test of providing a larger propagation zone for the same specimen.

Methods based on the J -integral to determine the shear fracture toughness have been developed in this thesis for ELS and 4ENF tests, with the aim of having robust data reduction methods to test structural adhesives. In the ELS test, a correction for large displacements (LD) have been applied, since it is typical of this test. In 4ENF test the effect of friction is included in the J -integral calculation. These methods are presented in Chapters 2 and 4, respectively.

The J -integral closed form solution for the ELS proposed in this work requires the strain measurement at section $S-S'$ (Figure 2.1). This strain was measured by means of Digital Image Correlation (DIC), a strain gauge (SG) and calculated by means of Beam Theory (BT).

The proposed J -integral method for the ELS test was validated by comparing the results to those of LEFM methods in a delamination test campaign with CFRP, where LEFM methods are applicable. In general, the three J -integral proposed methodologies (DIC, SG and BT) provide similar results of mode II fracture toughness when LD correction is applied. A very good agreement between the J -integral and the CBTE method (recommended by the delamination standard) were obtained (Figure 2.6) but not with methods that depends on crack tip positioning such as the ECM and the SBT (Figure 2.5). Moreover, very few differences were encountered between results of specimens with different thickness.

Furthermore, it was observed that if the LD correction is not used in J -integral calculation, the relative error with respect to the CBTE method increases significantly in thin specimens. The LD has lower influences on the measured fracture toughness of thicker specimens due to the lower deflection values achieved during the test.

Although providing good results, the J -integral (DIC) and the J -integral (SG) data reduction methods require the use of DIC and a strain gauge, respectively, apart from the inclinometers. This results in high test time and equipment costs. On the contrary, in the J -integral (BT), the longitudinal strain profile at section $S-S'$ is calculated and there is no need of extra equipment besides the two inclinometers. And it was demonstrated in section 2.5 (Chapter 2) that if the crack front is far enough from section $S-S'$, the strain profile calculated from BT is identical to that obtained from DIC.

Furthermore there is no need of extra tests, unlike the CBTE method recommended by the standard which requires a previous set of calibration tests. Given the accuracy of the J -integral (BT) method, it can be considered the most appropriate method for determining fracture toughness with the ELS test in case of large FPZ.

A part from the use of appropriate data reduction methods, the length of the FPZ must be taken into account in the specimen sizing of bonded joints. If the propagation zone is not large enough to let the FPZ completely develop, steady-state propagation values are not obtained. During FPZ development the fracture toughness is underestimated, since in mode II testing the onset values are lower than the propagation ones. For this reason, the propagation zone must be large enough in order to allow a self-similar crack growth (the full FPZ development) before the FPZ reaches the boundary of the specimen, where a stiffening of the system occurs, invalidating the results.

The FPZ length depends on the specimen thickness, adhesive layer constitutive properties and adherend mechanical properties. The specimen geometry defines the propagation zone of the test ($L - a_0$) but, in cases of large FPZ, the stability of the ENF and ELS tests is affected by the stresses transmitted within the FPZ, allowing the use of smaller a_0/L ratios, compared to the previous ones, based on LEFM. As a result, decreasing the a_0/L ratio provides larger propagation zone ($L - a_0$) for the same specimen dimensions. For this reason, the definition of ELS test and ENF test specimens dimensions needed to obtain propagation values in case of large FPZ involved compared with the specimen dimensions is not straightforward.

This issue is addressed in Chapter 3, where a methodology to define suitable ELS specimen dimensions to test adhesives is developed. The ELS test is selected due to the fact that it is more stable than the ENF test and it is not affected by friction (4ENF case), allowing large propagation regions for the same specimen. The suitability of the test relies on the accomplishment of several conditions: i) ensure the formation of the whole FPZ (FPZ criterion), providing sufficient propagation distance ($L - a_0$), ii) guarantee the stability of the test under displacement control (stable criterion), using a minimum a_0/L ratio which results in stable propagation, iii) limit the Large Deflections involved (LD criterion), since a large span length to specimen thickness ratio (L/H) result in large deflections, and iv) prevent the Adherend Failure (AF criterion), which depends on the adherend mechanical properties (ultimate strength), the specimen thickness and the adhesive layer constitutive properties (shear fracture toughness and failure shear strength).

The working domain is defined as the area enclosed by all the previous criteria boundaries, represented in an a_0/L versus L plot, as shown in Figure 3.6. This working domain establishes the specimens dimensions that allow for the measurement of the mode II fracture toughness. This methodology enables a reliable design of the specimens before any test is conducted, which in turn, results in time and material savings.

Based on literature findings, several working domains are obtained for most of the existing bonded joint configurations. The methodology can be extended to define new domains such as the analysis of extremely tough adhesives. It is also useful in the analysis of the different mechanisms that affect the size of the FPZ. For example, results show that, for the same adherend, the FPZ length is increased when increasing the adherend thickness and/or the shear fracture toughness, and shortened when increasing the failure shear strength.

When testing delamination specimens (resins of low fracture toughness and high shear strength compared with film and paste adhesives), it results in short FPZ lengths compared with the standard recommended specimen dimensions. In these scenarios LEFM applies, and the existing mode II standard recommended dimensions and data reduction methods are suitable. In Figure 3.8, it is shown that the ELS standard recommended dimensions ($L = 100$ mm, $a_0 > 55$ mm and thickness between 3 mm and 5 mm) fall into the working domain of resins. In the same manner, with regards to data reduction, the results of Table 2.2 in Chapter 2, show very good agreement between LEFM-based and J -integral-based results.

In the case of high toughness resins (case 2 in Table 3.2), the specimen must be thick enough in order to avoid large deflections. Observing Figure 3.7b, it can be seen that the range of dimensions is small due to the large displacements criteria limit.

On the other hand, when testing paste and film adhesives, which have higher fracture toughness and lower shear strengths (cases 2 to 5 in Table 3.2), it results in large FPZ compared with the typical specimens dimensions. In these cases were the FPZ length is larger, the upper (FPZ criterion) and lower (stable criterion) domain

boundaries decrease requiring the use of larger and thicker specimens but allowing smaller a_0/L ratios. It is shown in Figures 3.9 and 3.10.

Even though the suitable working domain is determined, there are still some other considerations to take a correct specimen dimensions choice. The use of small geometries inside the working domain decreases the onset of large deflection. Moreover, within the defined working domain, it is preferable to use a a_0/L ratio as small as possible in order to achieve the largest propagation region before the FPZ reaches the loading boundaries.

An analogous procedure for the determination of a specimen working domain for ENF test have been followed. It only differs on the boundary conditions defined in the analytical model. By doing so, the working domain of ELS and ENF tests for an specific adhesive layer cohesive properties ($G_{IIC} = 8 \text{ kJ/m}^2$, $\tau_{sh} = 30 \text{ MPa}$) are compared in Figure 5.1. It is observed that longer specimens for the same thickness are required in ENF test. Furthermore, the propagation region for an specific span length choice (difference between limiting criteria in the vertical axis) is smaller in ENF test compared with ELS test. This makes the ELS test a more convenient method to test structural adhesives, since smaller specimens would be required with the corresponding material costs savings.

Chapters 2 and 3 present a method to obtain the fracture toughness in tests with large FPZ. Taking into account the advantages of the J -integral in comparison to other data reduction methods (i.e. it is independent of crack length and accounts for non-linear fracture processes), the final objective of this thesis is the obtention of reliable test procedures, in which the fracture toughness is not influenced by the test. Thus, obtaining a result that could be considered as material property.

For this reason, in the work of Chapter 4, four common mode II test methods, the ENF, the ELS, the 4ENF and the MMB used at 100% mode II ratio, were used in an experimental test campaign of CFRP bonded joints. The procedure developed in Chapter 3 was applied to define the specimen dimensions for the ELS and ENF tests, and these test configurations were applied to the 4ENF and MMB tests. Different data reduction methods were used for each test type: LEFM-based and the J -

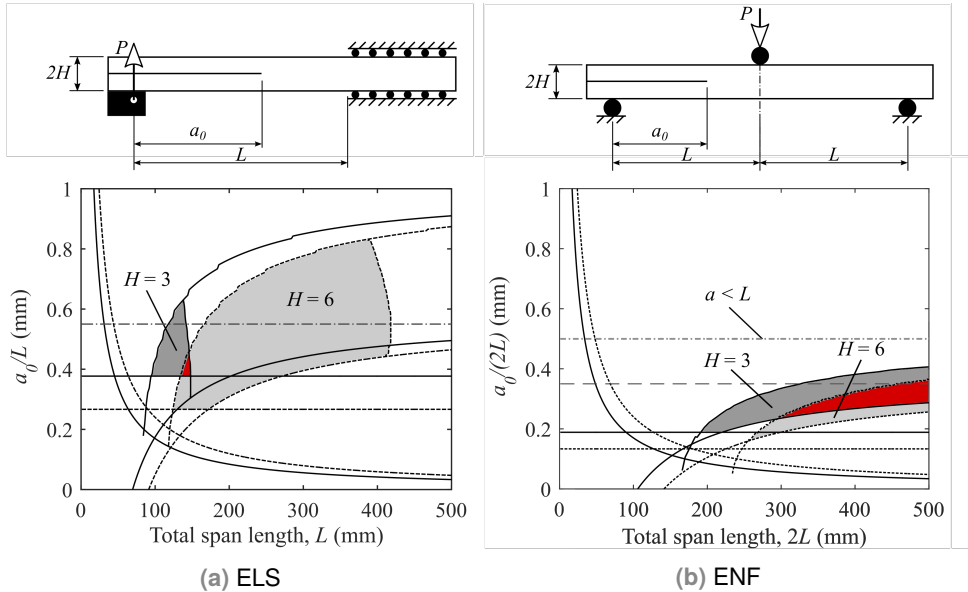


Fig. 5.1.: Working domain in a) ELS test and b) ENF test for a 25 mm width, and 6 mm and 12 mm thick specimens with a cohesive layer properties of $G_{IIc} = 8 \text{ kJ/m}^2$ and $\tau_{sh} = 30 \text{ MPa}$. The intersection of the two specimen thicknesses is represented in red and it is the working domain of specimens between these two thicknesses ($H = 3 \text{ mm}$ to $H = 6 \text{ mm}$).

integral (Tables 4.2, 4.3 and 4.4). The LEFM-based methods were based on three main approaches: Beam Theory (BT), Compliance Calibration (CC) and the area (AREA) method. Regarding the J -integral, the methods available in the literature for the ENF and MMB tests [107, 122], and the method developed in Chapter 2 for the ELS test were used. A closed form solution for the 4ENF test, which takes into account friction effects, was developed. The results obtained from two types of bonded specimens, denominated as M1 and M2, which differ on the CFRP adherend type but have the same adhesive, were compared.

Like what was obtained in previous works, large differences in the fracture toughness obtained from the data reduction methods as shown in Figure 4.7 and Tables 4.5 to 4.8. Specifically:

- In ELS test, the two methods with better agreement were the CBTE and the J -integral. The disagreement of ECM and SBT results compared with those obtained with CBTE method was expected, as Blackman et al. concluded after performing a round-robin study on carbon-fibre epoxy material [19].
- In ENF case, despite large differences were obtained between most of the LEFM-based methods (BT, CBT and AREA), the higher order LEFM-based compliance calibration methods (CC2 and CC3), the J -integral and the CCM resulted in good agreement with those results obtained in ELS test.
- In 4ENF tests, again the J -integral provided the lowest differences to the rest of the tests. Results from compliance calibration method (CCM) and experimental compliance method (ECM) methods were also in fairly good agreement with the J -integral. On the other hand, large differences were encountered between the results from BT and AREA approaches and the J -integral results. The discrepancies on BT-based and AREA-based methods are explained by the friction effects and the crack length measurement difficulties.
- In MMB tests, the results obtained following test standard were higher than the ones obtained in other tests, while the J -integral provided close values to the rest of the tests.

In general, very good agreement between J -integral-based results was observed for all test typologies, having differences below 10% between all the tests and below 6% adherend materials. This contradicts the dependence of the fracture toughness on the test typology and reinforces the idea of requiring reliable data reduction methods.

On the other hand, the CC-based data reduction methods were also providing similar results of fracture toughness regardless the test used (CBTE in ELS, CCM in ENF and CCM in 4ENF), despite not providing the same accuracy of J -integral-based methods. However, larger differences, compared with the J -integral case were observed between the batches M1 and M2 (made with different CFRP adherends

bonded with the same adhesive) when using CC-based methods (differences up to 16% in ELS test).

In short, the methods based on the visual crack length monitoring (i.e. LEFM-based with exception of CC-based cases) do not provide accurate results of fracture toughness. This is caused by their dependence on the crack tip position, which is not identifiable when testing adhesives under mode II loadings. The LEFM methods based on compliance calibration (CBTE in ELS, and CCM in ENF and 4ENF) resulted in acceptable small differences between different test typologies and within batches (c.f. Figure 4.8). Although the compliance calibration methods do not depend on the direct visual crack length measurement during the test, the crack length is an important input parameter that may influence the calibration results. Thus, it depends indirectly on the crack length measurement before the test. As the J -integral approach is totally independent of the crack length, since assumes a FPZ existence, better agreement in J -integral results (compared with compliance calibration ones) between test types and adherend materials was obtained.

Unlike compliance calibration based methods, the J -integral data reduction methods do not require any previous test (e.g. compliance calibration), apart from a pre-crack, if desired, requiring only the specimen width the load and rotations at the load application points during the test, it has been demonstrated the most robust and simple data reduction methods. Furthermore, the agreement between all J -integral results, supports the idea of the fracture toughness being a material property, independent of the adherend material, thickness and test type.

To conclude the discussion, some advantages and disadvantages of the use of the ELS, ENF, MMB and 4ENF tests in adhesive testing are summarized next.

- The ELS test configuration provides large propagation region ($L - a_0$) and relatively small specimens, compared with the common ENF test making it suitable for paste or film adhesive testing. On the other hand, the ELS test fixture system is complex compared with the ENF and the large deflections induced affect the ELS specimen dimensioning.

- The ENF test is very simple, only requiring a common 3 point bending test fixture, reason why it became popular. However, the propagation region length ($L - a_0$) is significantly smaller compared with ELS test, and when testing adhesives with the ENF test, very big specimens (compared with the ELS case) are required to let the FPZ fully develop maintaining the stability of the test.
- The MMB test used at 100% mode II ratio has essentially the same geometry of the ENF and the same issue with regards to the small propagation zone to let the full FPZ development in adhesive testing is encountered. Furthermore, it involve a complex test fixture and it is more prone to cause a premature failure to the adherend before any propagation occurs.
- The main advantage of the 4ENF test is its intrinsic stable configuration that allows large propagation regions, independently of the specimens dimensions. On the contrary, high loads are needed to provoke the crack growing. This makes it very affected by friction and more prone to the adherent failure. Therefore, the friction coefficient between the adherends must be known or estimated beforehand for each tested material in order to account for friction effects in data reduction.

In summary, the most advantageous test to be applied in structural adhesive testing is the End-Loaded Split test, using the J -integral (BT) in data reduction.

Concluding remarks

6.1 Conclusions

This thesis deals with the experimental analysis of mode II fracture toughness in CFRP adhesive bonded joints. This is the study of the crack growth, due to shear loads, inside the midplane of an FRP specimen formed by two FRP adherends that embed an adhesive layer bonding the two parts. The work focuses on the study of experimental mode II procedures and their corresponding application to adhesive testing.

The first contribution of the present work is the introduction of a new data reduction method, based on the J -integral, to obtain the interlaminar fracture toughness in a mode II end-loaded split (ELS) test.

A new methodology, based on the J -integral has been developed for the ELS test. It is not restricted to small FPZ, compared with the specimen dimensions, and can be used to analyze adhesive joints.

The methodology relies on measuring load, displacement, rotations at two points of the specimen, as well as the strain profile at a given elastic section of the specimen. While the rotations may be measured in a simple way using inclinometers, three alternative methods are proposed for assessing the strain profile required: i) Digital Image Correlation (DIC), ii) a strain gauge, and iii) an estimation based on Simple Beam Theory assumptions.

- The accuracy of the three ELS J -integral-closed forms is demonstrated through a delamination test campaign of CFRP specimens by comparing the J -integral with LEFM-based methods.

- This new method is less prone to human error than LEFM, as it requires neither measuring nor calculating the crack length. It requires less preparation because it does not need the clamp fixture to be calibrated beforehand. Furthermore, it accounts for large deflections.
- The simplest J -integral data reduction method is the one based on Beam Theory, since it only requires the measurement of the load and rotations at the load application point and at a given section of the specimen with no need of extra equipment apart from the two inclinometers. It is the most appropriate for its simplicity, rapidity and accuracy, since the equipment and time costs get reduced with respect to the CBTE proposed by the standard [63], and it is applicable in case of large FPZ (adhesive testing).

In the same manner, a J -integral-based data reduction method was developed for the four End Notched Flexure (4ENF) test. It takes into account friction effects and can be applied to adhesive testing, since it accounts for large FPZ, which are typical in mode II adhesive testing. The methodology relies on measuring the load and the rotations at the load application edges.

- The accuracy of the 4ENF J -integral-closed form is demonstrated in a test campaign with CFRP bonded joints, in which the 4ENF J -integral results were compared with the ones obtained with the ELS test, the ENF test and the MMB test used at 100% mode II ratio. The same type of specimens were used for all the tests.
- The J -integral is more simple and provides closer results to other test methodologies than LEFM-based approaches, since LEFM does not take into account large FPZ. However it requires measuring the friction coefficient between of the bonded joint beforehand.

The main difficulty on adhesive mode II testing are the large FPZ involved, compared with the specimen dimensions. The large FPZs involved in adhesive testing require the use of specimens with sufficient propagation zone to let the FPZ fully develop

and, at the same time, it has an effect on the stability of the test. The prediction of the FPZ length is not straightforward, since it depends on the adhesive layer constitutive properties, the specimens dimensions and adherend mechanical properties.

Given that the wrong specimen sizing (a_0 , L and H definition) may prevent from reaching self-similar propagation or promote unstable propagation of the test, this thesis addressed the ELS specimen dimensioning for adhesive testing.

- A methodology to define the ELS specimen dimensions to test adhesives was developed based on four limiting criteria: i) full FPZ formation, ii) stability, iii) Large Deflections and iv) Adherend Failure have been developed.
- An analytical model that considers a linear constitutive relation in the cohesive zone expressed in terms of fracture toughness (G_{IIc}) and failure shear strength (τ_{sh}) have been developed and used to evaluate the proposed criterion.
- Five case studies are defined based on adhesive properties found in the literature. The corresponding working domains (suitable specimen dimensions) for typical resin, paste and film adhesives cohesive properties were defined for three different specimen thicknesses.
- Although the exact properties of an adhesive are not known before testing, several guidelines for ELS specimen design are given based on known literature cohesive properties of common used adhesives, the obtained working domains and the physical definition of the four proposed criteria.

Furthermore, this thesis has provided some evidence of the robustness of the non-linear methods (J -integral) in front of those that assume a sharp crack tip (LEFM). An experimental test campaign of bonded joints between CFRP have been carried out using four test typologies, consisting of ENF, ELS, MMB and 4ENF test used at 100% of mode II ratio. Two specimen typologies were tested, with the same adhesive but each with different adherend. For each test, different data reduction methods were used to obtain the fracture toughness, LEFM and J -integral-based.

- The data reduction methods based on the visual crack length monitoring (LEFM-based with exception of compliance calibration (CC) based cases) have been shown not to provide accurate results of fracture toughness because they depend on the crack tip position, which is not defined when testing adhesives under mode II loadings.
- The compliance calibration based methods (CBTE in ELS, and CCM in ENF and 4ENF) have resulted in acceptable small differences between different test typologies and adherend materials.
- Very good agreement was observed using the J -integral for all test types and adherend materials.
- Unlike compliance calibration LEFM-based methods, the J -integral-based data reduction methods do not require any previous test (e.g. compliance calibration), apart from a pre-crack test, if desired.
- The measurements required in the J -integral can be easily obtained, consisting in measurement of the width, the load and the rotations at the loading application points during the test.
- The J -integral approach is the only method totally independent of the crack length. The compliance calibration methods do not depend directly on visual crack measurement during the test, but the crack length is an important input parameter that may influence the calibration results.
- With the J -integral the same fracture toughness is obtained for all the test geometries and adherend materials. This evidences the independence of the fracture toughness on the test typology and reinforces the idea of the fracture toughness being a material property independent of the adherend material, thickness and geometry (test type).
- J -integral-based data reduction methods are more robust than the LEFM-based methods in adhesive testing, since the LEFM do not takes into account

the FPZ, which in adhesive testing it is typically large compared with the specimen dimensions.

It is concluded that the most suitable test to measure the fracture toughness of structural adhesives is the End-Loaded Split (ELS) test. The test can be designed in advance by means of the methodology proposed in this work to guarantee that stable propagation toughness values are obtained. As stated above, the J -integral (BT) data reduction method proposed in this thesis is the most suitable for the fracture toughness determination.

6.2 Perspectives and future work

In this section, lines of future research and extension of the work developed in this thesis are presented.

This thesis is devoted to study the mode II fracture toughness measurement of adhesive joints. Fracture toughness is one of the two main parameters required in cohesive law characterization. If the measurement of the crack shear displacement is coupled with the J -integral measurement, the cohesive law can be totally defined [61, 71, 97, 106, 117, 118, 120].

Analogously, further research could be devoted to extend the proposed J -integral closed forms to a cohesive law measurement method for the ELS test and the 4ENF test by measuring the crack shear displacement (e.g. with Digital Image Correlation). Within the same framework, measuring the strains in the crack tip vicinity (e.g. with DIC) may provide information about the FPZ size evolution. The expected FPZ size is an important parameter in FEM analysis, since it may determine for example, the minimum element size to be used. However, many difficulties concerning the accuracy of DIC in the measurements near cracked interfaces must be addressed to be able to conduct such analysis.

Although the Chapter 3 of this thesis is devoted to the specimens dimensioning for the ELS test, given its better stability in front of the ENF test, the 4ENF test is always stable for any specimen dimensions, thus allowing larger propagation zones with respect to the ELS case. However, the main drawback of the 4ENF test are the friction effects caused by the high loads required to induce the crack growth, compared with other mode II tests. Very large and thick ELS specimens are required to test high toughness adhesives. Therefore, the use of the 4ENF test is more appropriate in these cases. Within this framework, further research could be conducted in the experimental investigation of friction effects in the 4ENF test, for example, defining a test methodology to measure the friction coefficient at the adhesive layer, for example adapting the ASTM D1894 standard [9] to adhesive surfaces.

The work developed in this thesis is an on-going effort in the road towards the development of a standardized test procedure for the determination of mode II fracture toughness of bonded joints. Therefore, conducting a round robin test program using the ELS test for bonded joints may be of great interest to pursue the required consensus for the determination of this property.

Bibliography

- [1]Abaqus. 6.12. *Documentation*. Dassault Systèmes Simulia Corp., Providence. 2012 (cit. on p. 63).
- [2]AITM 1.0006:1994. „Carbon Fibre Reinforced Plastics Determination of interlaminar fracture toughness energy (Mode II GIIC-TEST).“ In: *Airbus Industries Test Method 2* (1994), pp. 1–8 (cit. on pp. 11, 89, 90).
- [3]AITM1-0068:2014. „Carbon Fibre Reinforced Plastics Determination of mode II fracture toughness energy of bonded joints (GIIC Test).“ In: *Airbus Industries Test Method 1* (), pp. 1–21 (cit. on p. 12).
- [4]K. S. Alfredsson. „On the instantaneous energy release rate of the end-notch flexure adhesive joint specimen“. In: *International Journal of Solids and Structures* 41.16-17 (2004), pp. 4787–4807 (cit. on pp. 14, 51–53, 58, 60, 61, 63, 70).
- [5]K. S. Alfredsson, A. Biel, and S. Salimi. „Shear testing of thick adhesive layers using the ENF-specimen“. In: *International Journal of Adhesion and Adhesives* 62 (2015), pp. 130–138 (cit. on p. 14).
- [6]T. Andersson and U. Stigh. „The stress elongation relation for an adhesive layer loaded in peel using equilibrium of energetic forces“. In: *International Journal of Solids and Structures* 41 (2004), pp. 413–434 (cit. on p. 24).
- [7]A. Arrese and F. Mujika. „Influence of bending rotations on three and four-point bend end notched flexure tests“. In: *Engineering Fracture Mechanics* 75.14 (2008), pp. 4234–4246 (cit. on p. 5).
- [8]A. Arrese, N. Carbajal, G. Vargas, and F. Mujika. „A new method for determining mode II R-curve by the End-Notched Flexure test“. In: *Engineering Fracture Mechanics* 77.1 (2010), pp. 51–70 (cit. on p. 11).

- [9]ASTM D1894 - 93. „Standard Test Method for Static and Kinetic Coefficients of Friction of Plastic Film and Sheeting“. In: October 2000 (1995), pp. 455–460 (cit. on p. 122).
- [10]ASTM D6671/D6671M. „Standard Test Method for Mixed Mode I-Mode II Interlaminar Fracture Toughness of Unidirectional Fiber Reinforced Polymer Matrix Composites“. In: *American Society for Testing and Materials*. (2013) (cit. on pp. 6, 23, 82, 92–94, 101).
- [11]ASTM D7905M-14. „Standard Test Method for Determination of the Mode II Interlaminar Fracture Toughness of Unidirectional Fiber-Reinforced Polymer“. In: *American Society for Testing and Materials*. (2014) (cit. on pp. 4, 23, 49, 82, 88).
- [12]J.C.S. Azevedo, R.D.S.G. Campilho, F.J.G. da Silva, T.M.S. Faneco, and R.M. Lopes. „Cohesive law estimation of adhesive joints in mode II condition“. In: *Theoretical and Applied Fracture Mechanics* 80 (2015), pp. 143–154 (cit. on pp. 14, 51, 53).
- [13]G.I Barenblatt. „The formation of equilibrium cracks during brittle fracture. General ideas and hypotheses. Axially-symmetric cracks“. In: *Journal of Applied Mathematics and Mechanics* 23.3 (1959), pp. 622–636. arXiv: 0021-8928(59)90157-1 [10.1016] (cit. on p. 15).
- [14]G.I Barenblatt. „The Mathematical Theory of Equilibrium Cracks in Brittle Fracture“. In: *Advances In Applied Mechanics* 7. Ed. by H. L. Dryden, T. Von Kármán, G. Kuertim, F. H. Van Den Dungen, and L. Howarth. 1962, pp. 55–129 (cit. on p. 15).
- [15]J.D. Barrett and R.O. Foschi. „Mode II stress intensity factors for cracked wood beams“. In: *Engineering Fracture Mechanics* 9 (1977), pp. 371–378 (cit. on p. 4).
- [16]Z.P. Bažant and J. Planas. *Fracture and size effect in concrete and other quasibrittle materials*. CRC Press LLC, 1998, p. 616 (cit. on pp. 2, 69).
- [17]J. T. Beer, F. P., Johnson, E. R., DeWolf. *Mechanics of Materials*. third. New York: McGraw-Hill, 2002 (cit. on p. 61).
- [18]S. Bhashyam and B.D. Davidson. „Evaluation of data reduction methods for the mixed mode bending test“. In: *Aiaa J.* 35.3 (1997), pp. 546–552 (cit. on pp. 11, 89, 90).
- [19]B. R K Blackman, A.J. Brunner, and J.G. Williams. „Mode II fracture testing of composites: a new look at an old problem“. In: *Engineering Fracture Mechanics* 73.16 (2006), pp. 2443–2455 (cit. on pp. 5, 11, 12, 14, 23, 24, 50, 99, 113).
- [20]B. R K Blackman, A.J. Kinloch, and M. Paraschi. „The determination of the mode II adhesive fracture resistance, GIIC, of structural adhesive joints: an effective crack length approach“. In: *Engineering Fracture Mechanics* 72.6 (2005), pp. 877–897 (cit. on pp. 1, 10, 11, 24, 50, 82).

- [21]B. R K Blackman, A. J. Kinloch, F. S. Rodriguez-Sanchez, and W. S. Teo. „The fracture behaviour of adhesively-bonded composite joints: Effects of rate of test and mode of loading“. In: *International Journal of Solids and Structures* 49.13 (2012), pp. 1434–1452 (cit. on p. 82).
- [22]W.L. Bradley, C.R. Corleto, and D.P. Goetz. „Studies of mode I and mode II delamination using a J-integral analysis and in-situ observations of fracture in the sem.“ In: (1989) (cit. on p. 17).
- [23]A.J. Brunner. „Experimental aspects of Mode I and Mode II fracture toughness testing of fibre-reinforced polymer-matrix composites“. In: *Computer Methods in Applied Mechanics and Engineering* 185.2-4 (2000), pp. 161–172 (cit. on pp. 24, 50).
- [24]A.J. Brunner, B. R K Blackman, and P. Davies. „A status report on delamination resistance testing of polymer-matrix composites“. In: *Engineering Fracture Mechanics* 75.9 (2008), pp. 2779–2794 (cit. on p. 23).
- [25]F. Caimmi, R. Frassine, and A. Pavan. „A new jig for mode II interlaminar fracture testing of composite materials under quasi-static and moderately high rates of loading“. In: *Engineering Fracture Mechanics* 73.16 (2006), pp. 2277–2291 (cit. on p. 6).
- [26]R.D.S.G. Campilho, M.F.S.F. de Moura, D.A. Ramantani, J.J.L. Morais, and J.J.M.S. Domingues. „Buckling Behaviour of Carbon-Epoxy Adhesively-Bonded Scarf Repairs“. In: *Journal of Adhesion Science and Technology* 23 (2009), pp. 1493–1513 (cit. on pp. 13, 68).
- [27]R.D.S.G. Campilho, A.C.C. Leitão, R.L. Fernandes, J.C.S. Azevedo, and M.D. Banea. „Cohesive law estimation in mode II of a ductile adhesive“. In: *Annals of "Dunarea de Jos" University of Galati, Fascicle XII, Welding Equipment and Technology* 26 (2015), pp. 27–32 (cit. on pp. 13, 68).
- [28]R.D.S.G. Campilho, M.F.S.F. de Moura, A.M.G. Pinto, and D.A. Ramantani. „Interlaminar Fracture Characterization of a Carbon-Epoxy Composite in Pure Mode II“. In: *Materials Science Forum* 636 - 637 (2010), pp. 1518–1524 (cit. on p. 68).
- [29]R.D.S.G. Campilho, A.M.G. Pinto, M.D. Banea, R.F. Silva, and L.F.M. da Silva. „Strength Improvement of Adhesively-Bonded Joints Using a Reverse-Bent Geometry Strength Improvement of Adhesively-Bonded Joints Using“. In: *Journal of Adhesion Science and Technology* 25 (2011), pp. 23510–02368 (cit. on pp. 13, 68).
- [30]D. Carité, P. Davies, M. Peleau, and I K Partridge. „The influence of hydrostatic pressure on the interlaminar fracture toughness of carbon/epoxy composites TITRE“. In: *Composites Part B: Engineering* 37.4-5 (2006), pp. 292–300 (cit. on pp. 12, 82).

- [31]T. Carlberger, A. Biel, and U. Stigh. „Influence of temperature and strain rate on cohesive properties of a structural epoxy adhesive“. In: *International Journal of Fracture* 155.2 (2009), pp. 155–166 (cit. on p. 14).
- [32]L. A. Carlsson, J. W. Gillespie, and B. R. Trethewey. „Mode II Interlaminar Fracture of Graphite/Epoxy and Graphite/PEEK“. In: *Journal of Reinforced Plastics and Composites* 5.3 (1986), pp. 170–187 (cit. on pp. 11, 89, 90).
- [33]L.A. Carlsson and J.W. Gillespie. „Mode-II Interlaminar Fracture of Composites“. In: *Application of Fracture Mechanics to Composite Materials*. Ed. by K. Friedrich. 1989. Chap. 4, pp. 113–157 (cit. on p. 82).
- [34]L.A. Carlsson, J.W. Gillespie, and R.B. Pipes. „On the Analysis and Design of the End Notched Flexure (ENF) specimen for Mode II Testing“. In: *Journal of Composite Materials* 20.6 (1986), pp. 594–604 (cit. on pp. 5, 11, 51, 54).
- [35]Z. Chen, R.D. Adams, and L.F.M. Da Silva. „The use of the J-integral vector to analyse adhesive bonds with and without a crack“. In: *International Journal of Adhesion and Adhesives* 31.1 (2011), pp. 48–55 (cit. on pp. 25, 31).
- [36]C.R. Corleto. „Mode II Delamination Fracture Characterization of Fiber Reinforced Composite Materials, a Ph. D. Dissertation, Mechanical Engineering. Texas A&M University (1990)“. In: (1990) (cit. on pp. 24, 25).
- [37]Correlated Solutions. *Vic-3D Testing guide*. 2010 (cit. on p. 36).
- [38]Crews J and Reeder JR. „A mixed-mode bending apparatus for delamination testing“. In: *Tech. Rep.; NASA TM/100662* (1988) (cit. on p. 6).
- [39]B. D. Davidson, R. Krüger, and M. König. „Effect of stacking sequence on energy release rate distributions in multidirectional DCB and ENF specimens“. In: *Engineering Fracture Mechanics* 55.4 (1996), pp. 557–569 (cit. on p. 11).
- [40]B.D. Davidson and X.K. Sun. „Effects of friction, geometry, and fixture compliance on the perceived toughness from three- and four-point bend end-notched flexure tests“. In: *Journal of Reinforced Plastics and Composites* 24.15 (2005), pp. 1611–1628 (cit. on p. 82).
- [41]B.D. Davidson, X. Sun, and A.J. Vinciguerra. „Influences of Friction, Geometric Nonlinearities, and Fixture Compliance on Experimentally Observed Toughnesses from Three and Four-point Bend End-notched Flexure Tests“. In: *Journal of Composite Materials* 41.10 (2007), pp. 1177–1196 (cit. on pp. 12, 82, 90, 92, 93, 100).
- [42]P. Davies. „Review of standard procedures for delamination resistance testing“. In: *Delamination Behaviour of Composites*. 2008, pp. 65–86 (cit. on p. 82).

- [43]P. Davies. „Summary of results from the second VAMAS mode II round robin test exercise using the 4ENF specimen.“ In: *IFREMER Report TMSI/RED/MS 99.82* (1999) (cit. on p. 82).
- [44]P. Davies, G.D. Sims, B. R K Blackman, et al. „Comparison of test configurations for the determination of GIIC: results from an international round robin“. In: *Plastics, Rubber and Composites* 28.September (1999), pp. 432–437 (cit. on pp. 11, 82, 89, 90).
- [45]P. Davies, P. Casari, and L. A. Carlsson. „Influence of fibre volume fraction on mode II interlaminar fracture toughness of glass/epoxy using the 4ENF specimen“. In: *Composites Science and Technology* 65.2 (2005), pp. 295–300 (cit. on pp. 6, 12).
- [46]P. Davies, B.R.K. Blackman, and A.J. Brunner. „Mode II delamination“. In: *Fracture mechanics Testing Methods for Polymers, Adhesives and Composites*. Ed. by D.R. Moore, A. Pavan, and J.G. Williams. Elsevier, 2001. Chap. 4.2, pp. 307–333 (cit. on p. 53).
- [47]P. Davies, H.H. Kausch, J.G. Williams, et al. „Round-robin interlaminar fracture testing of carbon-fibre-reinforced epoxy and PEEK composites“. In: *Composites Science and Technology* 43.2 (1992), pp. 129–136 (cit. on pp. 11, 82).
- [48]P. Davies, B. R K Blackman, and A.J. Brunner. „Standard test methods for delamination resistance of composite materials: current status“. In: *Applied Composite Materials* 5.Iso 4585 (1998), pp. 345–364 (cit. on pp. 5, 23, 50, 82).
- [49]DIN EN 6034:1996. „Aerospace series - Carbon fibre reinforced plastics - Test method - Determination of interlaminar fracture toughness energy - Mode II - GIIC“. In: *Deutsches Institut für Normung* (1996) (cit. on p. 23).
- [50]D.S. Dugdale. „Yielding of steel sheets containing slits“. In: *Journal of the Mechanics and Physics of Solids* 8.2 (1960), pp. 100–104 (cit. on p. 15).
- [51]M. Elices, G. J. Guinea, J. Gómez, and J. Planas. „The cohesive zone model: advantages, limitations and challenges“. In: *Engineering Fracture Mechanics* 69.2 (2002), pp. 137–163 (cit. on p. 16).
- [52]R.L. Fernandes, M.F.S.F. de Moura, and R.D. F. Moreira. „International Journal of Adhesion & Adhesives Effect of moisture on pure mode I and II fracture behaviour of composite bonded joints“. In: *International Journal of Adhesion and Adhesives* 68 (2016), pp. 30–38 (cit. on pp. 14, 51).

- [53]I. S. Floros, K. I. Tserpes, and T. Löbel. „Mode-I, mode-II and mixed-mode I+II fracture behavior of composite bonded joints: Experimental characterization and numerical simulation“. In: *Composites Part B: Engineering* 78.October (2015), pp. 459–468 (cit. on p. 51).
- [54]J. W. Gillespie, L. A. Carlsson, and R. B. Pipes. „Finite element analysis of the end notched flexure specimen for measuring mode II fracture toughness“. In: *Composites Science and Technology* 27.3 (1986), pp. 177–197 (cit. on p. 5).
- [55]A.A. Griffith. „The Phenomena of Rupture and Flow in solids“. In: *Philosophical Transactions of the Royal Society of London* 221 (1921), pp. 163–198 (cit. on p. 8).
- [56]A.A. Griffith. „The theory of rupture“. In: *Proceedings of the First International Conference of Applied Mechanics*. Ed. by C.B. Biereno and J.M. Burgers. 1924, pp. 54–63 (cit. on p. 8).
- [57]J.D. Gunderson, J.F. Brueck, and A.J. Paris. „Alternative test method for interlaminar fracture toughness of composites“. In: *International Journal of Fracture* 143.3 (2007), pp. 273–276 (cit. on p. 18).
- [58]P. Hansen and R. Martin. „DCB , 4ENF and MMB delamination Characterisation of S2 / 8552 and IM7 / 8552 MERL Report No. N68171-98-M-5177“. In: (1999) (cit. on p. 68).
- [59]S. Hashemi, A.J. Kinloch, and J.G. Williams. „The analysis of interlaminar fracture in uniaxial fiber-polymer composites“. In: *Proceedings of the Royal Society A* 427 (1990), pp. 173–199 (cit. on pp. 5, 10–12, 24, 37, 38, 50, 51, 53–55, 82, 87–90, 93).
- [60]A. Hillerborg, M. Modéer, and P. E. Petersson. „Analysis of crack formation and crack growth in concrete by means of fracture mechanics and finite elements“. In: *Cement and Concrete Research* 6 (1976), pp. 773–781 (cit. on p. 15).
- [61]J.L. Högberg, B.F. Sørensen, and U. Stigh. „Constitutive behaviour of mixed mode loaded adhesive layer“. In: *International Journal of Solids and Structures* 44.25-26 (2007), pp. 8335–8354 (cit. on pp. 17, 24, 26, 50, 82, 121).
- [62]ISO 15024:2001. „Fibre-reinforced plastic composites. Determination of mode I interlaminar fracture toughness, G_{Ic} , for unidirectionally reinforced materials“. In: *International Standard Organization* (2001) (cit. on p. 13).
- [63]ISO 15114:2014. „Fibre-reinforced plastic composites - Determination of the mode II fracture resistance for unidirectionally reinforced materials using the calibrated end-loaded split (C-ELS) test and an effective crack length approach.“ In: *International Standard Organization, Geneva, Switzerland* 1 (2014), pp. 1–26 (cit. on pp. 5, 10, 12, 14, 23, 24, 26, 27, 30, 35–38, 40, 45, 50, 51, 56, 64, 74, 75, 82, 86–88, 118).

- [64]ISO 25217:2014. „Adhesives - Determination of the mode 1 adhesive fracture energy of structural adhesive joints using double cantilever beam and tapered double cantilever beam specimens“. In: *International Organization for Standardization, Geneva, Switzerland* (2009) (cit. on pp. 13, 56, 84).
- [65]JIS K 7086. „Testing methods for interlaminar fracture toughness of carbon fibre reinforced plastics.“ In: *Japanese Standard association* (1993) (cit. on pp. 5, 11, 50).
- [66]J. Jumel and M. K. Budzik. „Inverse end-loaded-split test analysis effect of small scale yielding“. In: *Theoretical and Applied Fracture Mechanics* May (2017), pp. 1–15 (cit. on p. 50).
- [67]K. Kageyama, M. Kikichi, and N. Yanagisawa. „Stabilized end notched flexure test: characterization of model interlaminar crack growth“. In: *Composite Materials: Fatigue and Fracture (Third volume) ASTM STM 1110*. Ed. by T.K. O'Brien. 1991, pp. 210–225 (cit. on p. 5).
- [68]A.J. Kinloch. *Adhesion and Adhesives: science and Technology*. City: London, Chapman and Hall, 1987 (cit. on p. 1).
- [69]C.M. Landis, I.J. Beyerlein, and R.M. McMeeking. „Micromechanical simulation of the failure of fiber reinforced composites“. In: *Journal of the Mechanics and Physics of Solids* 48 (2000), pp. 621–648 (cit. on p. 68).
- [70]K. Leffler, K. S. Alfredsson, and U. Stigh. „Shear behaviour of adhesive layers“. In: *International Journal of Solids and Structures* 44.2 (2007), pp. 530–545 (cit. on p. 17).
- [71]F.A. Leone. „Progressive Damage Analysis of Bonded Composite Joints“. In: *NASA/TM-2012-217790* (2012) (cit. on pp. 13, 14, 17, 51, 68, 70, 121).
- [72]Y. Ma, Y. Yang, T. Sugahara, and H. Hamada. „A study on the failure behavior and mechanical properties of unidirectional fiber reinforced thermosetting and thermoplastic composites“. In: *Composites Part B* 99 (2016), pp. 162–172 (cit. on p. 68).
- [73]H. Maikuma, J. W. Gillespie, and D. J. Wilkins. „Mode II Interlaminar Fracture of the Center Notch Flexural Specimen under Impact Loading“. In: *Journal of Composite Materials* 24.2 (1990), pp. 124–149 (cit. on p. 6).
- [74]S. Mall and N.K. Kochhar. „Finite element analysis of end notch flexure specimen. NASA contractor report 178113“. In: (1986) (cit. on p. 5).
- [75]E.A.S. Marques and L.F.M. da Silva. „Joint Strength Optimization of Adhesively Bonded Patches“. In: *The Journal of Adhesion* 84 (2008), pp. 915–934 (cit. on pp. 13, 68).

- [76]R.H. Martin and B.D. Davidson. „Mode II fracture toughness evaluation using four point bend, end notched flexure test“. In: *Plastics, Rubber and Composites* 28.8 (1999), pp. 401–406 (cit. on pp. 6, 12, 50, 82, 92, 93, 95).
- [77]S. Marzi, A. Biel, and U. Stigh. „On experimental methods to investigate the effect of layer thickness on the fracture behavior of adhesively bonded joints“. In: *International Journal of Adhesion and Adhesives* 31.8 (2011), pp. 840–850 (cit. on pp. 14, 15).
- [78]D. S. Matsumoto, M. A. Vallance, and S. K. Gifford. „A new curvature-driven delamination test for measuring the mode II toughness of composites“. In: *Polymer Composites* 17.2 (1996), pp. 171–179 (cit. on p. 6).
- [79]A.B. de Morais and M.F.S.F. de Moura. „Evaluation of initiation criteria used in interlaminar fracture tests“. In: *Engineering Fracture Mechanics* 73.16 (2006), pp. 2264–2276 (cit. on pp. 5, 23, 50).
- [80]A.B. de Morais and A. B. Pereira. „Application of the effective crack method to mode I and mode II interlaminar fracture of carbon/epoxy unidirectional laminates“. In: *Composites Part A: Applied Science and Manufacturing* 38.3 (2007), pp. 785–794 (cit. on pp. 14, 51).
- [81]M.F.S.F. de Moura. „Numerical simulation of the ENF test for the mode-II fracture characterization of bonded joints“. In: *Journal of Adhesion Science and Technology* 20.1 (2006), pp. 37–52 (cit. on pp. 12, 14, 51, 53).
- [82]M.F.S.F. de Moura and J.A.G Chousal. „Cohesive and continuum damage models applied to fracture characterization of bonded joints“. In: *International Journal of Mechanical Sciences* 48 (2006), pp. 493–503 (cit. on pp. 14, 51).
- [83]M.F.S.F. de Moura and A.B. de Morais. „Equivalent crack based analyses of ENF and ELS tests“. In: *Engineering Fracture Mechanics* 75.9 (2008), pp. 2584–2596 (cit. on pp. 11, 12, 51).
- [84]M.F.S.F. de Moura, N. Dourado, J.J.L. Morais, and F. A M Pereira. „Numerical analysis of the ENF and ELS tests applied to mode II fracture characterization of cortical bone tissue“. In: *Fatigue and Fracture of Engineering Materials and Structures* 34.3 (2011), pp. 149–158 (cit. on pp. 5, 50, 51).
- [85]M.F.S.F. de Moura, R. D S G Campilho, and J. P M Gonçalves. „Pure mode II fracture characterization of composite bonded joints“. In: *International Journal of Solids and Structures* 46.6 (2009), pp. 1589–1595 (cit. on pp. 11, 89, 90).

- [86]G. B. Murri and R.H. Martin. „Effect of Initial Delamination on Mode I and Mode II Interlaminar Fracture Toughness and Fatigue Fracture Threshold“. In: *Composite Materials: Fatigue and Fracture (4th Volume)*, ASTM STP 1156. Ed. by W. W. Stinchcomb Ashbaugh and N. E. ASTM International, West Conshohocken, PA, 1991, pp. 239–256 (cit. on p. 11).
- [87]F. Nilsson. „Large Displacement Aspects on Fracture Testing with Double Cantilever Beam Specimens“. In: *International Journal of Fracture* 139.2 (2006), pp. 305–311 (cit. on pp. 18, 25).
- [88]T. K. O'Brien, G. B. Murri, and S. A. Salpekar. „Interlaminar Shear Fracture Toughness and Fatigue Thresholds for Composite Materials“. In: *Composite Materials: Fatigue and Fracture ASTM STP 1012, (2nd Volume)*. Ed. by P. A. Lagace. 1989, pp. 222–250 (cit. on p. 11).
- [89]T.K. O'Brien. „Composite interlaminar shear fracture toughness, GIIc: shear measurement or sheer myth?“ In: *ASTM STP 1330* (1998), pp. 3–18 (cit. on p. 24).
- [90]A.J. Paris and P.C. Paris. „Instantaneous evaluation of J and C“. In: *International Journal of Fracture* 38 (1988), pp. 19–21 (cit. on p. 18).
- [91]M. Pérez-Galmés, J. Renart, C. Sarrado, A. Rodríguez-Bellido, and J. Costa. „A data reduction method based on the J-integral to obtain the interlaminar fracture toughness in a mode II end-loaded split (ELS) test“. In: *Composites Part A: Applied Science and Manufacturing* 90 (2016), pp. 670–677 (cit. on pp. 50–52, 82, 85, 87, 88).
- [92]J.J. Polaha, B.D. Davidson, R.C. Hudson, and A. Pieracci. „Effects of Mode Ratio, Ply Orientation and Precracking on the Delamination Toughness of a Laminated Composite.“ In: *Journal of Reinforced Plastics and Composites* 15.2 (1996), pp. 141–173 (cit. on pp. 11, 89, 90).
- [93]YJ Prel, P Davies, ML Benzeggagh, and FX de Charentenay. „Mode I and Mode II Delamination of Thermosetting and Thermoplastic Composites“. In: *Composite Materials: Fatigue and Fracture, ASTM STP 1012*. Ed. by A. Lagace Paul. Vol. 2. 1989, pp. 251–269 (cit. on p. 6).
- [94]R. Prinz and M. Gädke. „Characterization of interlaminar mode I and mode II fracture in CFRP laminates“. In: *Proceedings of International Conference on Spacecraft Structures and Mechanical Testing*. 1991, pp. 97–102 (cit. on p. 6).
- [95]P. Qiao, J. Wang, and J. F. Davalos. „Analysis of tapered ENF specimen and characterization of bonded interface fracture under Mode-II loading“. In: *International Journal of Solids and Structures* 40.8 (2003), pp. 1865–1884 (cit. on pp. 5, 50).

- [96]P. Qiao, J. Wang, and J.F. Davalos. „Tapered beam on elastic foundation model for compliance rate change of TDCB specimen“. In: *Engineering Fracture Mechanics* 70.2 (2003), pp. 339–353 (cit. on p. 5).
- [97]M. Rask and B.F. Sørensen. „Determination of the J integral for laminated double cantilever beam specimens: The curvature approach“. In: *Engineering Fracture Mechanics* 96 (2012), pp. 37–48 (cit. on pp. 17, 121).
- [98]J R Reeder and J H Crews. „Mixed-Mode Bending Method for Delamination Testing“. In: *Aiaa Journal* 28.7 (1990), pp. 1270–1276 (cit. on p. 6).
- [99]J R Reeder and J H Crews. „Redesign of the mixed-mode bending delamination test to reduce nonlinear effects“. In: *Journal of Composites Technology Research* 14.1 (1992), pp. 12–9 (cit. on p. 6).
- [100]J. Renart, N. Blanco, E. Pajares, et al. „Side Clamped Beam (SCB) hinge system for delamination tests in beam-type composite specimens“. In: *Composites Science and Technology* 71.8 (2011), pp. 1023–1029 (cit. on p. 34).
- [101]J.R. Rice. „A Path Independent Integral and the Approximate Analysis of Strain Concentration by Notches and Cracks“. In: *Journal of Applied Mechanics* 35 (1968), pp. 379–386 (cit. on pp. 3, 16, 24–26, 31, 82).
- [102]A.J. Russell and K.N. Street. „Factors affecting the interlaminar fracture energy of graphite/epoxy laminates“. In: *ICCM4, Tokyo ASM International*. 1982, pp. 279–286 (cit. on p. 4).
- [103]A.J. Russell and K.N. Street. „Moisture and Temperature Effects on the Mixed-Mode Delamination Fracture of Unidirectional Graphite/Epoxy.“ In: *ASTM STP 876* (1985), pp. 349–370 (cit. on p. 11).
- [104]A.J. Russell and K.N. Street. „Moisture and Temperature Effects on the Mode I and Mode II Interlaminar Fracture of Graphite/Epoxy Composites“. In: *Key Engineering Materials* 37 (1989), pp. 199–208 (cit. on pp. 89, 90).
- [105]C. Sarrado. „Experimental characterization and numerical simulation of composite adhesive joints using the cohesive zone model approach (PhD thesis), University of Girona“. In: (2015) (cit. on pp. 13, 68).
- [106]C. Sarrado, A. Turon, J. Costa, and J. Renart. „An experimental analysis of the fracture behavior of composite bonded joints in terms of cohesive laws“. In: *Composites Part A: Applied Science and Manufacturing* 90 (2016), pp. 234–242 (cit. on pp. 17, 121).

- [107]C. Sarrado, A. Turon, J. Renart, and J. Costa. „An experimental data reduction method for the Mixed Mode Bending test based on the J-integral approach“. In: *Composites Science and Technology* 117.117 (2015), pp. 85–91 (cit. on pp. 18, 24, 26, 82, 85, 94, 104, 112).
- [108]C. Sarrado, A. Turon, J. Costa, and J. Renart. „On the validity of linear elastic fracture mechanics methods to measure the fracture toughness of adhesive joints“. In: *International Journal of Solids and Structures* 81 (2016), pp. 110–116 (cit. on pp. 14, 50, 51).
- [109]J. Schön, T. Nyman, A. Blom, and H. Ansell. „Numerical and experimental investigation of a composite ENF-specimen“. In: *Engineering Fracture Mechanics* 65.4 (2000), pp. 405–433 (cit. on p. 11).
- [110]C. Schuecker and B.D. Davidson. *Effect of Friction on the Perceived Mode II Delamination Toughness from Three- and Four-Point Bend End-Notched Flexure Tests*. 2000 (cit. on pp. 5, 12).
- [111]C. Schuecker and B.D. Davidson. „Evaluation of the accuracy of the four-point bend end-notched flexure test for mode II delamination toughness determination“. In: *Composites Science and Technology* 60 (2000), pp. 2137–2146 (cit. on pp. 6, 11, 12, 82, 89, 90).
- [112]F.G.A. Silva, J.J.L. Morais, N. Dourado, et al. „Determination of cohesive laws in wood bonded joints under mode II loading using the ENF test“. In: *International Journal of Adhesion & Adhesives* 51 (2014), pp. 54–61 (cit. on p. 14).
- [113]L.F.M. da Silva, R.A.M. da Silva, J.A.G. Chousal, and A.M.G. Pinto. „Alternative Methods to Measure the Adhesive Shear Displacement in the Thick Adherend Shear Test“. In: *Journal of Adhesion Science and Technology* 22 (2008), pp. 15–29 (cit. on pp. 13, 68, 70).
- [114]L.F.M. da Silva, T.N.S.S. Rodrigues, M.A.V. Figueiredo, M.F.S.F. de Moura, and J.A.G. Chousal. „Effect of Adhesive Type and Thickness on the Lap Shear Strength“. In: *The Journal of Adhesion* 82.November 2012 (2006), pp. 1091–1115 (cit. on pp. 13, 68).
- [115]L.F.M. da Silva, F.a. C.R.G. de Magalhães, F.J.P. Chaves, and M.F.S.F. de Moura. „Mode II Fracture Toughness of a Brittle and a Ductile Adhesive as a Function of the Adhesive Thickness“. In: *The Journal of Adhesion* 86.9 (2010), pp. 891–905 (cit. on pp. 13, 14, 51, 53, 68).
- [116]M.A.L. Silva, J.J.L. Morais, M.F.S.F. de Moura, and J.L. Lousada. „Mode II wood fracture characterization using the ELS test“. In: *Engineering Fracture Mechanics* 74.14 (2007), pp. 2133–2147 (cit. on pp. 12, 14, 51).

- [117]B.F. Sørensen. „Cohesive law and notch sensitivity of adhesive joints“. In: *Acta Materialia* 50.5 (2002), pp. 1053–1061 (cit. on pp. 17, 121).
- [118]B.F. Sørensen and T.K. Jacobsen. „Determination of cohesive laws by the J integral approach“. In: *Engineering Fracture Mechanics* 70 (2003), pp. 1841–1858 (cit. on pp. 17, 121).
- [119]B.F. Sørensen, K. Jørgensen, T.K. Jacobsen, and R.C. Østergaard. „DCB-specimen loaded with uneven bending moments“. In: *International Journal of Fracture* 141 (2006), pp. 163–176 (cit. on p. 18).
- [120]B.F. Sørensen, S. Goutianos, and T.K. Jacobsen. „Strength scaling of adhesive joints in polymer-matrix composites“. In: *International Journal of Solids and Structures* 46 (2009), pp. 741–761 (cit. on pp. 17, 121).
- [121]A. Soto, E. V. González, P. Maimí, et al. „Cohesive zone length of orthotropic materials undergoing delamination“. In: *Engineering Fracture Mechanics* 159 (2016), pp. 174–188 (cit. on pp. 13, 68, 69).
- [122]U. Stigh, K. S. Alfredsson, and A. Biel. „Measurement of cohesive laws and related problems“. In: *IMECE2009: Proceedings of the ASME International Mechanical Engineering Congress and Exposition* 11 (2009), pp. 293–8 (cit. on pp. 14, 18, 24, 26, 82, 85, 89, 90, 112).
- [123]U. Stigh, A. Biel, and T. Walander. „Shear strength of adhesive layers - Models and experiments“. In: *Engineering Fracture Mechanics* 129 (2014), pp. 67–76 (cit. on pp. 14, 15).
- [124]K. Tanaka, K. Kageyama, and M. Hojo. „Prestandardization study on mode II interlaminar fracture toughness test for CFRP in Japan“. In: *Composites* 26.4 (1995), pp. 243–255 (cit. on pp. 6, 50).
- [125]A. Turon, C.G. Dávila, P.P. Camanho, and J. Costa. „An engineering solution for mesh size effects in the simulation of delamination using cohesive zone models“. In: *Engineering Fracture Mechanics* 74 (2007), pp. 1665–1682 (cit. on p. 69).
- [126]P.S. Vanderkley. „Mode I-Mode II Delamination Fracture Toughness of a Unidirectional Graphite/Epoxy Composite“. In: *Master's Thesis, Texas A&M University, College Station TX* (1981) (cit. on p. 5).
- [127]A. P. Vassilopoulos. *Fatigue and Fracture of Adhesively-bonded Composite Joints Behaviour, Simulation and Modelling*. 2015 (cit. on p. 82).
- [128]T. Vu-Khanh. „Crack-arrest study in mode II delamination in composites“. In: *Polymer composites* 8 (1987), pp. 331–341 (cit. on p. 53).

- [129]H. Wang and T. Vu-Khanh. „Use of end-loaded-split (ELS) test to study stable fracture behaviour of composites under mode II loading“. In: *Composite Structures* 36.1-2 (1996), pp. 71–79 (cit. on pp. 5, 50, 53).
- [130]H. Wang, T. Vu-Khanh, and V. N. Le. „Effects of large deflection on mode II fracture test of composite materials“. In: *Journal of Composite Materials* 29.6 (1995), pp. 833–849 (cit. on pp. 5, 24, 50, 51, 53, 55).
- [131]W. Wang, Y. Takao, and M. Nakata. „Effects of Friction on the Measurement of the Mode II Interlaminar Fracture Toughness of Composite Laminates“. In: *Proceedings of the 14th International Conference on Composite Materials* (2003), pp. 14–18 (cit. on p. 6).
- [132]Y. Wang and J. G. Williams. „Corrections for mode II fracture toughness specimens of composites materials“. In: *Composites Science and Technology* 43.3 (1992), pp. 251–256 (cit. on p. 12).
- [133]J.G. Williams. „Large Displacement and End Block Effects in the 'DCB' Interlaminar Test in Modes I and II“. In: *Journal of Composite Materials* 21.4 (1987), pp. 330–347 (cit. on pp. 5, 24, 51, 55, 56).
- [134]J. Xavier, M. Oliveira, J.J.L. Morais, and M.F.S.F. de Moura. „Determining mode II cohesive law of Pinus pinaster by combining the end-notched flexure test with digital image correlation“. In: *Construction and Building Materials* 71 (2014), pp. 109–115 (cit. on p. 14).

Appendix. Generated papers

A

A.1 A data reduction method based on the J -integral to obtain the interlaminar fracture toughness in a mode II end-loaded split (ELS) test

M. Pérez-Galmés^a, J. Renart^a, C. Sarrado^a, A. Rodríguez-Bellido^b, J. Costa^a

^aAMADE, Mechanical Engineering and Industrial Construction Department, Universitat de Girona, Campus Montilivi s/n, Girona, Spain

^bComposite Technology, Materials and Processes, AIRBUS Operations SL, Paseo John Lenon s/n, E-28906 Getafe, Madrid, Spain

The paper has been published in *Composites Part A: Applied Science and Manufacturing Vol. 90 (2016) 670-677*.



A data reduction method based on the J -integral to obtain the interlaminar fracture toughness in a mode II end-loaded split (ELS) test



M. Pérez-Galmés^{a,*}, J. Renart^a, C. Sarrado^a, A. Rodríguez-Bellido^b, J. Costa^a

^a AMADE, Polytechnic School (II), University of Girona, Carrer Universitat de Girona, 4, E-17003 Girona, Spain

^b Composite Technology, Materials and Processes, AIRBUS Operations SL, Paseo John Lenon s/n, E-28906 Getafe, Madrid, Spain

ARTICLE INFO

Article history:

Received 5 April 2016

Received in revised form 3 August 2016

Accepted 17 August 2016

Available online 31 August 2016

Keywords:

B. Fracture toughness

B. Delamination

D. Mechanical testing

J -integral

ABSTRACT

Various difficulties arise in the data reduction of the end-loaded split (ELS) test. On one hand, a small Fracture Process Zone (FPZ) at the crack front is assumed in the existing mode II end-loaded split test methodologies based on Linear Elastic Fracture Mechanics (LEFM). However, mode II fracture has been reported to involve large FPZ and a fuzzy crack tip. Furthermore, the ELS test, is usually affected by geometrical non-linearities.

This work proposes a closed-form solution based on the J -integral to determine the interlaminar fracture toughness in an ELS test. This solution avoids the need to measure the crack length, and is applicable when a large FPZ is present, as occurs in adhesive bonded joints between CFRP. In addition, because the ELS test involves large vertical deflections, a correction of the formulation for large displacements has been implemented.

This new methodology has been compared to other methods available in the literature based on LEFM by means of an experimental campaign of delamination tests using unidirectional CFRP specimens in order to make a first validation of the method.

© 2016 Elsevier Ltd. All rights reserved.

1. Introduction

The end-loaded split (ELS) test is used to determine mode II fracture toughness in unidirectional fibre-reinforced polymer composites [1–3]. Among other mode II test methodologies, such as the End Notch Flexure (ENF) test [4,5] or the 100% mode II Mixed Mode Bending (MMB) test [6], the ELS has the advantage of stable crack growth [1–3,7]. According to the existing ISO 15114 standard [8], which is based on Linear Elastic Fracture Mechanics (LEFM), the crack length is a required parameter that must be either measured or calculated.

The main hypothesis behind LEFM is that the non-linear zone at the crack front, and thus also the Fracture Process Zone (FPZ), is small in comparison to any of the specimen's relevant dimensions (width, thickness or crack length). Mode II fracture has been reported to involve large FPZ, which in conjunction with the lack of crack opening, hinders measuring the crack length by visual inspection [9–11]. To overcome this, a method based on an effective crack length derived from the specimen's compliance

was proposed by Blackman et al. [2]. Even though this method has shown great success in measuring fracture toughness in mode II delamination, it is still based on corrected LEFM assumptions and, therefore, the analysis of those situations involving large FPZ may fall outside their scope [8]. Adhesively bonded joints have been reported to entail large FPZ due to the plasticity of the adhesive layer [12,13], so their analysis should be based on non-linear fracture mechanics data reduction methods.

One of the methods that has enjoyed greater success on the characterization of fracture in a non-linear fracture mechanics framework is the contour integral known as the J -integral. The J -integral was first developed by Rice [14] and has been used as a data reduction method to determine fracture toughness when LEFM assumptions do not hold true, e.g. when performing a mode II fracture test of an adhesive joint [15,16]. The J -integral has been also used to obtain fracture toughness closed-form solutions for pure mode II ENF [17] and MMB [18] tests. These closed-form solutions are derived by selecting a convenient integration path that allows the contour integral to be solved. Such J -integral closed-form solutions can be applied when large FPZ are present as they do not rely on LEFM assumptions and do not require a crack length measurement, so they are a good alternative for measuring fracture toughness when LEFM does not apply. Corleto [19] proposed

* Corresponding author.

E-mail addresses: magdalena.perez@udg.edu (M. Pérez-Galmés), jordi.renart@udg.edu (J. Renart), carlos.sarrado@udg.edu (C. Sarrado), ana.rodriguez@airbus.com (A. Rodríguez-Bellido), josep.costa@udg.edu (J. Costa).

a *J*-integral closed-form solution for the mode II ELS test, where evaluating the *J*-integral requires a calibration of the moment-curvature relationship for a given crack length before starting the test, making the method crack length dependent (unlike the *J*-integral solutions for ENF and MMB cited above [17,18]).

Most solutions for the *J*-integral are valid only under the assumptions of small displacements, where the crack front is perpendicular to the applied load [14,17,18]. However, the ELS test may involve large vertical deflections if the fracture toughness is high enough and/or thin specimens are used (e.g. in bonded joints with structural adhesives) [9,10,20].

Very few studies have dealt with large deflections in DCB [21] and ELS [19] tests, and those that do consider that the crack propagates through a horizontal plane parallel to the longitudinal axis following a straight pattern. By doing this, the problem becomes 1-dimensional, and the formulation developed by Rice [14] can be used to calculate the *J*-integral instead of using more general and complex approaches such as the vector *J*-integral [22].

This work presents a data reduction scheme for the ELS test based on the *J*-integral to extend the usefulness of this test to situations where the non-linear region cannot be neglected, i.e. where LEFM no longer applies. The method takes into account the large displacements involved in the ELS test and, unlike the method proposed by Corleto [19], the proposed closed-form solution does not depend on crack length.

In order to assess the correctness of the proposed procedure, the results of the *J*-integral and LEFM on delamination Carbon Fibre Reinforced Polymer (CFRP) specimens are compared. The two batches of specimens tested have different thickness in order to also compare the effect of large displacements on the results of the *J*-integral. For these specimens the non-linear zone is small and both LEFM and the *J*-integral should yield the same fracture toughness.

2. Analytical formulation

In the particular case of a two-dimensional elastic problem, the *J*-integral is defined as

$$J = \int_{\Gamma} \left[\omega dx_2 - T_k \frac{\partial u_k}{\partial x_1} ds \right] \quad (k = 1, 2) \tag{1}$$

where Γ is a closed path enclosing the crack tip and bounding a region R (see Fig. 1), u_k is the displacements vector, ds an infinitesimal arc length along Γ , and x_1 and x_2 are the horizontal and vertical coordinates, respectively. ω is the strain energy density, defined as

$$\omega = \int_0^{\epsilon_{ij}} \sigma_{ij} d\epsilon_{ij} \tag{2}$$

where σ_{ij} and ϵ_{ij} are the stress and strain tensors expressed in two dimensional form, respectively.

T_k is the tractions vector defined by

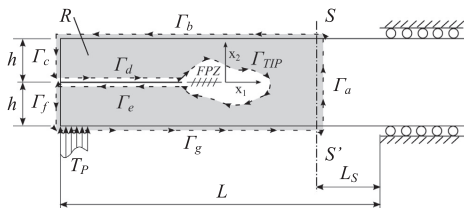


Fig. 1. Integration paths $\Gamma_a, \Gamma_b, \Gamma_c, \Gamma_d, \Gamma_e, \Gamma_f$ and Γ_g in the ELS specimen for derivation of *J*-integral equations.

$$T_k = \sigma_{ki} n_i \tag{3}$$

where n_i denotes the normal vector to the bounding path Γ .

For a fracture test specimen with an initial defect, the fracture toughness may be obtained by means of the *J*-integral computation along a remote arbitrary path Γ enclosing the crack tip [14], and in most cases the *J*-integral can be solved to obtain a closed-form solution [13,17,18].

If Γ is defined by the contour of the specimen edge, the traction vector T_k only takes into account the external forces applied to the specimen. In addition, when Γ does not cross the section of the specimen, the term of the strain energy density is zero. Therefore, the integral results in a simple expression that includes the loads applied and the rotation angles at the load application points and at the supports [18].

In the particular case of the ELS test, the specimen is loaded at the bottom arm of the pre-cracked end and clamped at the other end by a carriage, which allows unrestrained displacement along the longitudinal edge (x_1) but restricts the vertical displacement [8] (Fig. 1). The estimation of the reaction forces induced by the carriage is not straightforward because it is a contact problem that depends on many variables. Therefore, in order to simplify the calculation, the clamped region is excluded from the integration path, which is defined along the contour of the specimen by cutting a transversal section $S-S'$ outside the clamped end (Fig. 1).

Section $S-S'$ is located far enough from the clamping end (L_c) to prevent stress concentrations associated to the carriage. In addition, section $S-S'$ must be located as far as possible away from the initial crack tip to ensure that the path defined to calculate the *J*-integral encompasses the total FPZ involved. The integration path along the external contour of the specimen is $\Gamma = \Gamma_a \cup \Gamma_b \cup \Gamma_c \cup \Gamma_d \cup \Gamma_e \cup \Gamma_f \cup \Gamma_g$. The path independence property of the *J*-integral gives $J_{\Gamma} + J_{\Gamma_{IP}} = 0$, where the $J_{\Gamma_{IP}}$ is the *J*-integral calculated on a path, Γ_{IP} , surrounding the FPZ.

Taking into account the hypothesis of small displacements and that the crack front is parallel to x_1 , paths Γ_c and Γ_f of Fig. 1 run through an unloaded region of the specimen; path Γ_b runs through a free surface parallel to the crack direction, and given that friction has been shown to barely affect fracture toughness [8], paths Γ_d and Γ_e also run through a free surface parallel to the crack direction. Therefore,

$$J_{\Gamma_b} = J_{\Gamma_d} = J_{\Gamma_e} = 0 \quad (dx_2 = 0, T_k = 0) \tag{4}$$

$$J_{\Gamma_c} = J_{\Gamma_f} = 0 \quad (\omega = 0, T_k = 0) \tag{5}$$

$$J_{ELS} = J_{IP} = J_{\Gamma_a} + J_{\Gamma_g} \tag{6}$$

Path Γ_g runs through a free surface parallel to the crack tip ($dx_2 = 0$). Thus, J_{Γ_g} is zero everywhere except at the load introduction point, where an external traction is applied (T_P).

Considering the tractions in Fig. 1 as concentrated forces applied in an infinitesimal region dx_1 , $\int \sigma_{22} dx_1 = \frac{P}{b}$, where P is the external applied load and b the specimen width. These tractions can therefore be considered punctual forces, as in Fig. 2. The derivative of the displacements is

$$\frac{\partial u_k}{\partial x_1} = \begin{bmatrix} \frac{\partial u_1}{\partial x_1} \\ \frac{\partial u_2}{\partial x_1} \end{bmatrix} = \begin{bmatrix} \epsilon_{11} \\ \tan(\theta_p) \end{bmatrix} \tag{7}$$

where θ_p is the rotation angle at the load application point. The replacement of Eq. (7) into (1) reads:

$$J_{\Gamma_g} = \frac{P}{b} \tan(\theta_p) \tag{8}$$

Path Γ_a travels through a transversal section perpendicular to the crack tip. It is assumed that the strains ϵ_{22} are zero. Under the

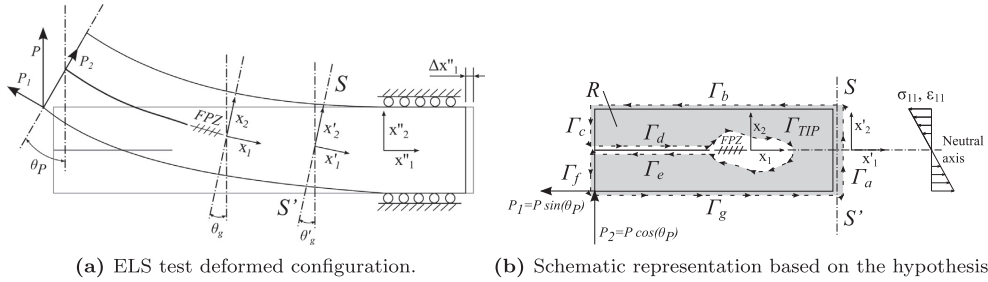


Fig. 2. Integration paths in the ELS specimen with large displacements assumption.

hypothesis of a linear elastic constitutive relationship between strains and stress, the strain energy density takes the form:

$$\omega = \frac{1}{2} \sigma_{ij} \epsilon_{ji} = \frac{1}{2} \sigma_{11} \epsilon_{11} + \sigma_{12} \epsilon_{12} \quad (9)$$

The normal vector to path Γ_a is $n_i = [1 \ 0]^T$, therefore the tractions vector in path Γ_a is

$$T_k = \sigma_{ki} n_i = \begin{bmatrix} \sigma_{11} & \sigma_{12} \\ \sigma_{12} & \sigma_{22} \end{bmatrix} \begin{bmatrix} 1 \\ 0 \end{bmatrix} = \begin{bmatrix} \sigma_{11} \\ \sigma_{12} \end{bmatrix} \quad (10)$$

The product between the tractions and the displacement gradients in path Γ_a is

$$T_k \frac{\partial u_k}{\partial X} = \begin{bmatrix} \sigma_{11} & \sigma_{12} \end{bmatrix} \begin{bmatrix} \epsilon_{11} \\ \tan \theta_g \end{bmatrix} = \sigma_{11} \epsilon_{11} + \sigma_{12} \tan \theta_g \quad (11)$$

where θ_g is the rotation at section $S-S'$.

Replacing (9) and (11) into (1) the contribution of path Γ_a to the J -integral is obtained:

$$J_{\Gamma_a} = \int_{-h}^h \left(-\frac{1}{2} \sigma_{11} \epsilon_{11} + \sigma_{12} (\epsilon_{12} - \tan \theta_g) \right) dx_2 \quad (12)$$

Assuming a UD laminate, plane strain, small strains and $\epsilon_{22} = 0$, Eq. (12) can be represented as a function of the strains as

$$J_{\Gamma_a} = \int_{-h}^h \left(-\frac{1}{2} E_{11} \epsilon_{11}^2 + G_{12} \epsilon_{12} (\epsilon_{12} - \tan \theta_g) \right) dx_2 \quad (13)$$

where E_{11} is the Young's modulus in the fibre direction, G_{12} is the shear modulus, h is half the specimen thickness and ϵ_{11} and ϵ_{12} are the longitudinal and shear strains along the section $S-S'$.

Eq. (13) can be solved by assuming a parabolic shear strain distribution along the thickness direction in section $S-S'$,

$$\epsilon_{12} = \frac{3P(h^2 - x_2^2)}{4bh^3 G_{12}} \quad (14)$$

By adding up expressions (8) and the solution of (13) the J -integral closed-form solution for the ELS test is obtained:

$$J_{ELS} = \frac{3}{5} \frac{P^2}{G_{12} b^2 h} + \frac{P}{b} (\tan \theta_p - \tan \theta_g) + \int_{-h}^h \left(-\frac{1}{2} E_{11} \epsilon_{11}^2 \right) dx_2 \quad (15)$$

The last term in Eq. (15) can be addressed in three ways:

Firstly, by integrating numerically the last term of a strain profile, which can be experimentally measured by means of, for example, a Digital Image Correlation system (DIC).

Secondly, under the assumption of a linear strain profile at section $S-S'$, this term can be solved by measuring the longitudinal strains at the top of section $S-S'$ with a longitudinal strain gauge. In that case Eq. (15) results in

$$J_{ELS} = \frac{3}{5} \frac{P^2}{G_{12} b^2 h} + \frac{P}{b} (\tan \theta_p - \tan \theta_g) - \frac{E_{11} h}{3} \epsilon_g^2 \quad (16)$$

where ϵ_g is the strain gauge measurement on the top face of section $S-S'$.

Thirdly, the longitudinal strain profile can be estimated by means of Simple Beam Theory, resulting in an expression that does not depend on the strains, but rather on the distances between the load application point and the clamp tool (L), and the distance between section $S-S'$ and the clamp tool (L_s), (Fig. 1):

$$J_{ELS} = \frac{3}{5} \frac{P^2}{G_{12} b^2 h} + \frac{P}{b} (\tan \theta_p - \tan \theta_g) - \frac{E_{11} h}{3} \left(\frac{3}{2} \frac{P(L-L_s)}{E_{11} b h^2} \right)^2 \quad (17)$$

The Young's modulus in the fibre direction (E_{11}) can be obtained from the calibration specified on the test standard [8], from a three point bending test, or from the difference between two rotated angles along the beam. In this work the Young's modulus is obtained by taking into account the difference in rotated angles between the load application point and section $S-S'$. Thus, the Young's modulus in the fibre direction (E_{11}) is obtained by applying the second Mohr's Theorem at the linear region of the load displacement curve (before the propagation starts) where the crack length is known:

$$E_{11} = \frac{-3P(3a_0^2 + (L-L_s)^2)}{4bh^3(\theta_p - \theta_g)} \quad (18)$$

where a_0 is the initial crack length. Measuring the angles at section $S-S'$ (θ_g) and at the load application point (θ_p) avoids using additional tests to obtain E_{11} .

2.1. Large displacements correction

This section presents an extension of the formulation to account for large displacements in the bending arms. In an ELS test the crack plane is not horizontal due to the bending of the specimen, but rather it is rotated an angle θ_g with respect to the horizontal axis (x'_1), as shown in Fig. 2. In addition, the applied load causes a vertical deflection and an horizontal displacement ($\Delta x'_1$) of the sliding fixture that tends to increase the stiffness of the system, see Fig. 2a.

With the aim of simplifying the calculation, the test set-up has been idealized by assuming three hypotheses (Fig. 2b): (i) the crack propagates along a straight line parallel to the x_1 axis; (ii) the difference in the rotation angles at section $S-S'$ and the crack front is negligible (i.e. x'_1 is parallel to x_1 , or $\theta_g = \theta'_g$) and; (iii) the specimen curvature is small compared to the length of the specimen and the strains caused by the horizontal component of load P (P_1) are

negligible compared to the rest of the deformation, so that it does not affect the position of the neutral axis. By assuming these hypotheses, Rice's J -integral [14] can be used instead of a more general and complex formulation such as the vector J -integral [22].

With regards to the second hypothesis, smaller curvature is produced on the uncracked region because of its higher moment of inertia. This was checked using Mohr's Second Theorem obtaining less than 3.2° difference between x_1 and x'_1 axis rotations before the crack starts to propagate. The third hypothesis is demonstrated from the DIC measured strain profile at section S - S' , where the neutral axis of the beam coincides with the zero intersection of the longitudinal strain profile ($\varepsilon_{11}(x'_2 = 0)$), as shown in Fig. 7.

Analogous to the situation of small displacements, from Fig. 2b and considering Eq. (1) $J_{I_a} = J_{I_c} = J_{I_d} = J_{I_e} = J_{I_f} = 0$, as these contours are either free surfaces or contact surfaces with no friction assumed. Therefore, only paths Γ_a and Γ_g contribute to the J -integral.

J_{I_g} is zero everywhere except at the load point. Considering the tractions as concentrated forces applied in an infinitesimal region:

$$\int T_i ds = \int \sigma_{ij} n_j ds = \frac{1}{b} \begin{bmatrix} -P_1 \\ P_2 \end{bmatrix} = \frac{1}{b} \begin{bmatrix} -P \sin \theta_p \\ P \cos \theta_p \end{bmatrix} \quad (19)$$

where $n_j = [-\sin \theta_p, -\cos \theta_p]^T$ is the normal vector to surface Γ_g at the load application point, θ_p is the rotation angle between the load P and n_i at the load application point, P_1 and P_2 are respectively, the tangent and normal components of the applied load. The derivative of the displacements is defined with respect to section S - S' , coordinate system (x'_1, x'_2):

$$\frac{\partial u_k}{\partial x'_1} = \begin{bmatrix} \varepsilon_{11} \\ \tan(\theta_p - \theta_g) \end{bmatrix} \quad (20)$$

where ε_{11} are the longitudinal strains in x'_1 direction and $\theta_g = \theta'_g$ is the rotation angle between section S - S' and axis x'_2 . According to the third hypothesis, the strains caused by the tangent component of load (P_1) are small compared to the rest of the deformations and can be dismissed ($\varepsilon_{11} \approx 0$). Furthermore, the bending moment at the load application point is zero. Therefore, J_{I_g} reads

$$J_{I_g} = \int -T_1 \frac{\partial u_i}{\partial x'_1} ds = \frac{P \cos(\theta_p)}{b} \tan(\theta_p - \theta_g) \quad (21)$$

Given the assumption of similar rotation between (x_1, x_2) and (x'_1, x'_2), in path Γ_a the strain energy density, the traction vector and the displacement gradients take the same form as in the small displacements formulation, so J_{I_a} can be obtained directly from Eq. (12). From the combination of Eqs. (12) and (21) a general solution for the J -integral with large displacements is obtained:

$$J_{EIS} = \frac{3(P \cos(\theta_p))^2}{5G_{12}b^2h} + \frac{P \cos(\theta_p)}{b} \tan(\theta_p - \theta_g) + \int_{-h}^h \left(-\frac{1}{2} E_{11} \varepsilon_{11}^2 \right) dx_2 \quad (22)$$

Note that the rotation angle θ_g is the same as θ'_g . Because of that, the partial derivative of displacements is $\frac{\partial u_k}{\partial x'_1} = [\varepsilon_{11} \ 0]^T$. It is worth mentioning that expression (22) is the same as (15) if small displacements are considered.

The last term of Eq. (22) can be addressed in the same way as in Eq. (15), i.e. numerically integrating the strain profile measured using DIC, as done in Eq. (16), i.e. under the assumption of a linear strain profile measured by a strain gauge placed on the top face of section S - S' or by estimating the strain profile from Simple Beam Theory, as done in Eq. (17).

3. Experimental campaign

The proposed methodology was validated with an experimental testing campaign. The results obtained from the J -integral closed-form solutions were compared to those provided by the methods available in the literature based on LEFM assumptions. In order to use the latter methods as a reference, the testing campaign consisted of delamination tests on unidirectional CFRP specimens, where small FPZ are expected. Therefore, the crack length could be either measured or calculated.

Two batches of 5 specimens of carbon fibre reinforced polymer (AS4/8852) unidirectional laminates were tested. The specimens in each batch differed in their total thickness (3 mm and 4.5 mm), but they had the same length (250 mm) and width (25 mm). The Young's modulus in the fibre direction (E_{11}) is 120.9 GPa and the in-plane shear modulus (G_{12}) is 4.6 GPa [23].

3.1. Test procedure

Before the ELS test, a clamp calibration was performed in accordance with the ISO 15114 standard [8]. This preliminary test was used to obtain the ELS clamp correction and the specimen flexural modulus (E_{11}), data required for the Simple Beam Theory (SBT) and the Corrected Beam Theory using Effective crack length (CBTE). For the J -integral method, the flexural modulus was obtained directly from the test by measuring the angles θ_p and θ_g , Eq. (18).

After the calibration, the specimen edges were prepared to be analyzed both by the J -integral and the data reduction required by the ISO15114 standard [8].

In this way, edge A, was prepared to monitor the crack length. A thin coat of white paint was applied and thin vertical crack length markers at 1 mm increments were drawn. Edge B, was prepared for the DIC measurement by applying a coat of white paint and a random black speckled pattern using an airbrush in the zone around section S - S' . Section S - S' was placed 7 mm away from the clamp fixture in order to avoid the clamping effects of the sliding fixture (carriage) and at 28 mm from the initial crack tip to make sure that the FPZ is encompassed during the test.

With the aim of avoiding an unstable crack initiation from the insert, a pre-crack in mode II was made according to the standard [8]. A load block was bonded to the specimen so that the initial crack length was 52.5 mm. After the pre-crack, the final crack length was measured with an optical microscope. The crack length after the pre-crack test was approximately 65 mm in all the specimens. Afterwards, edge A was marked every millimetre with a vertical line for the first 35 mm from the new crack tip.

The ELS test was performed in a test rig designed according to the requirements of the test standard [8]. The specimens were clamped in the sliding fixture of the test rig so that the distance between the clamping device and the load application point was of $L = 100$ mm. To ensure a stable propagation, the ratio between the crack length a and L has to be $a/L > 0.55$ [8]. In this work the ratio was set to $a/L = 0.65$.

The tests were carried out under displacement control at a crosshead displacement rate of 1 mm/min.

3.2. Instrumentation

During the test, the crack length was optically monitored at edge A with a video acquisition system consisting of a Canon 550D camera with a macro lens mounted on a travelling fixture. The longitudinal strains (ε_{11}) at section S - S' zone were measured using two methods: a 3 mm longitudinal strain gauge with a resistance of 350 Ω and a Digital Image Correlation (DIC) system.

The strain gauge was placed on topface of the specimen and it was centred at section $S-S'$. The DIC cameras were focused on a region near section $S-S'$ on edge B, covering the entire thickness of the specimen and a propagation zone of 17 mm. In order to obtain a stereoscopic image of section $S-S'$, two Stingray F504B ASG cameras with a resolution of 2452×2056 pixels were used. They were placed at a distance of about 250 mm away from the specimen edge B [24]. During the test, the data acquisition frequency of the images taken by the cameras was 2.5 Hz.

Two inclinometers were used to measure the rotation angles at section $S-S'$ (θ_s , inclinometer 2), and at the loading application point (θ_p , inclinometer 1). In order to correct the small rotation of the carriage, two additional inclinometers, named 03 and 04, were situated at the top and bottom part of the clamping tool on the carriage (see Fig. 3). The inclinometers used were the capacitive inclinometers NA3-30, from SEIKA Mikrosystemtechnik GmbH, with a resolution of 0.005° and a maximum linearity deviation over the whole measurement range ($\pm 30^\circ$) of 0.06° , in accordance with the manufacturer's specifications. A detail of the specimen instrumentation is shown in Fig. 3.

3.3. Data reduction

The fracture toughness was obtained from the three LEFM data reduction methods proposed in the ISO 15114 standard [8]: (i) Experimental Compliance Method (ECM), (ii) Simple Beam Theory (SBT) and (iii) Corrected Beam Theory using Effective crack length (CBTE). Following the standard, the values of G_{IIc} obtained from

these methods were corrected taking into account large deflections in the specimen and the stiffness induced by the loading blocks [8]. For comparative purposes, G_{IIc} was also obtained from the area method (AREA) [9].

With regards to the J -integral, three different methods were used to obtain the mode II fracture toughness: (i) a numerical integration of the strain profile at section $S-S'$ measured using Digital Image Correlation (DIC), Eq. (15); (ii) an estimation of the strain profile by means of the strain gauge (SG), Eq. (16); and (iii) an estimation of the strain profile from the Simple Beam Theory (BT), Eq. (17). Furthermore, the results were obtained from the same data reduction methods but including large displacements correction (DIC-LD, SG-LD and BT-LD).

The data reduction methods used, and their corresponding equations, are shown in Table 1.

4. Results

The load-displacement curve of one representative specimen is shown in Fig. 4. The load and displacement values of five propagation points are included in the curve. These points correspond to five propagation points (PROP₁, PROP₁₂, PROP₁₈, PROP₂₀ and PROP₂₈). The last propagation point coincides with the location of section $S-S'$, where the strain gauge is bonded and the DIC measurements are made. These points are taken as a reference and will be identified in the results for discussion purposes. Apart from these, other propagation points were obtained, but are not depicted for clarity.

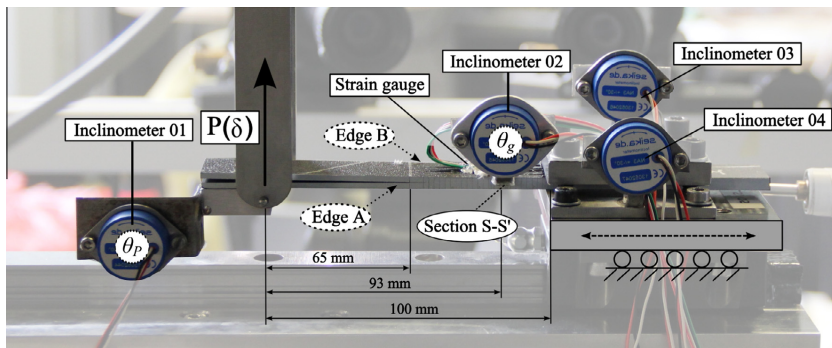


Fig. 3. Specimen instrumentation: inclinometers and strain gauge. Location of section $S-S'$ and edges A and B. (For interpretation of the references to colour in this figure legend, the reader is referred to the web version of this article.)

Table 1
Data reduction methods nomenclature.

Method	Method	Identifier code	Equation/reference
Linear Elastic Fracture Mechanics (G_{IIc})	Area	AREA	Hashemi et al. [9]
	Corrected Beam Theory using Effective crack length	CBTE	
	Experimental Compliance Method	ECM	
J -integral (Small Displacements)	Simple Beam Theory	SBT	ISO 15114 [8]
	Digital Image Correlation	DIC	
	Strain Gauge	SG	
J -integral (Large Displacements)	Beam Theory	BT	Eq. (15) Eq. (16) Eq. (17)
	Digital Image Correlation	DIC-LD	
	Strain Gauge	SG-LD	
	Beam Theory	BT-LD	Eq. (22) ^a Eq. (22) ^b

^a Last term of the equation addressed in the same way as in Eq. (16).

^b Last term of the equation addressed in the same way as in Eq. (17).

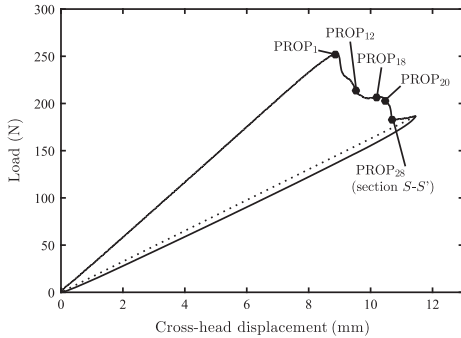


Fig. 4. Load-displacement curve of a 4.5 mm thick specimen. PROP_{*i*} point corresponds to a crack growth of *i* mm visually measured. The dotted line is a straight unloading curve from the maximum displacement point to the zero of load and displacement used in the AREA data reduction method.

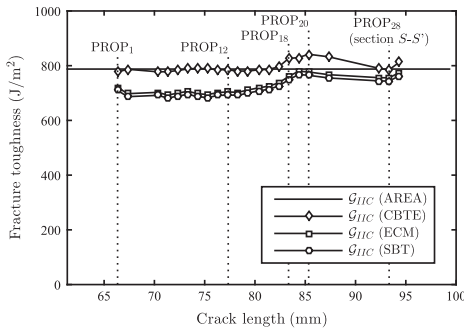


Fig. 5. LEFM-based methods fracture toughness results. 4.5 mm thick specimen.

Fig. 5 shows the R-curve of the same representative specimen used in Fig. 4, obtained from LEFM-based methods. The location of the propagation points previously marked in the load-displacement curve in Fig. 4 are indicated by vertical dotted lines.

During propagation G_{IC} (CBTE) remains around 800 J/m².

In terms of the data reduction methods, the SBT yields the lowest value of G_{IC} while the CBTE provides the highest. The difference between them is around 12% for the 3 mm thick specimens and 3% for the 4.5 mm thick specimens.

The ISO15114 standard [8] recommends using the values of G_{IC} obtained from CBTE data reduction method, because it has the best reproducibility. In Fig. 5, the results obtained from the CBTE data reduction method are very close to those from the area method. These two methods are used in the comparison to those obtained from the *J*-integral. The comparison between the *J*-integral and the LEFM data reduction methods is shown in Fig. 6 for the same specimen used in Figs. 4 and 5.

In spite of the fact that methods based on the *J*-integral do not make use of the crack length in the calculations, the fracture toughness in Fig. 6 is represented against the crack length *a* in order to be compared with the data reduction method CBTE, which is usually expressed in terms of crack length (*R*-curve). The vertical dotted lines represent the same propagation points indicated in Figs. 4 and 5.

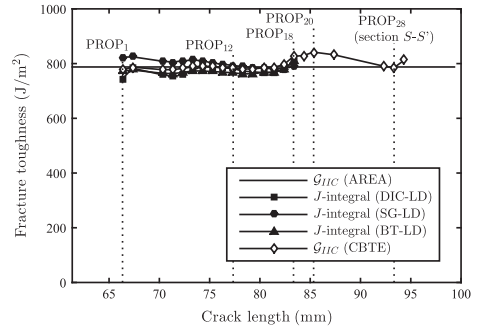


Fig. 6. Fracture toughness results using the *J*-integral (large displacements correction) and LEFM-based methods. Results from a 4.5 mm thick specimen.

The *J*-integral results are in close agreement with the CBTE and the AREA method during the first 18 mm of propagation, when section *S-S'* is situated 10 mm away from the optically measured crack length tip. At this plateau region the dispersion between the data reduction methods based on the *J*-integral (Fig. 6) is smaller than the dispersion between the methods based on the LEFM (Fig. 5).

5. Discussion

In Fig. 6, only the results of the first 18 mm of propagation have been represented because from this point on the values of the *J*-integral start to deviate from the other data reduction methods. This deviation is caused by the non-linearities in the strain profile at section *S-S'* caused by the crack front stresses. The closed-form solutions of the *J*-integral presented in this work are based on the hypothesis that the crack front is far enough from the integration contours so that the strain profile is linear, which means that the paths defined to calculate the *J*-integral encompass the total FPZ involved. Therefore, as the crack front approaches section *S-S'* and the strain profile loses its linearity, the formulations developed are no longer valid.

In order to further analyse this effect, a comparison between the strain profile at section *S-S'* for different propagation stages of the same specimen as before is shown in Fig. 7. The strain profile measured with DIC is compared to a linear estimation of the strain profile obtained from the strain gauge measurements (SG).

The whole strain profile along section *S-S'* cannot be obtained using DIC because of an inherent lack of measurement points near the edges of this technique. Only the central part is measured (80% of the strain profile) and the other 20% of the profile has to be estimated. The estimation of the strain at the top and bottom faces is carried out with a linear extrapolation of the last two external strain measurements taken with the DIC.

During the first 18 mm of propagation the strain profile is almost linear and there are no appreciable differences between the measured values (DIC) and the prediction (SG), Fig. 7. As the crack front approaches section *S-S'* (10 mm away, Fig. 7c), the strain profile tends to deviate from the linearity, as evidenced by the DIC and the strains measured with the strain gauge. From this point, despite capturing almost the full strain profile with the DIC, it is not possible to determine the fracture toughness by means of the proposed method because the strain at section *S-S'* is affected by the crack front stresses and, thus, part of the strain field generated by the FPZ falls outside the integration paths.

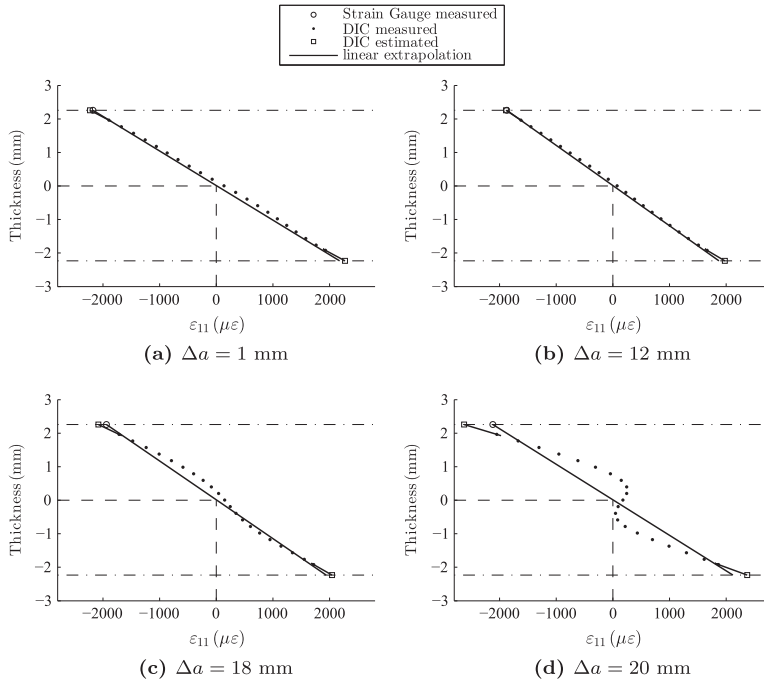


Fig. 7. Strain profiles at section *S-S'* measured with DIC and estimated from the strain gauge (ϵ_g) measurements for different propagation stages. Results from a 4.5 mm thick specimen.

Table 2

Fracture toughness propagation values obtained from different data reduction methods (LEFM and *J*-integral) from the batches with 3 mm and 4.5 mm thick specimens. Values obtained from the propagation range within points PROP₇ and PROP₁₅ of each specimen (propagation points at which the fracture toughness becomes constant). The values in brackets refer to the difference respect \mathcal{G}_{IC} (CBTE) in %.

Specimen thickness		\mathcal{G}_{IC}		<i>J</i> -integral (SD)			<i>J</i> -integral (LD)		
		AREA	CBTE	DIC	SG	BT	DIC	SG	BT
3 mm	Mean (J/m^2)	744 (3.4)	771	810 (5.1)	839 (8.9)	788 (2.3)	759 (1.5)	788 (2.2)	758 (1.7)
	St dev (J/m^2)	33.6	25.7	43.5	30.6	31.8	40.3	28.0	30.0
	CV (%)	4.5	3.3	5.4	3.6	4.0	5.3	3.6	4.0
4.5 mm	Mean (J/m^2)	789 (0.2)	791	823 (4.1)	807 (2.0)	795 (0.5)	797 (0.8)	781 (1.3)	775 (2.0)
	St dev (J/m^2)	47.8	29.9	33.3	63.5	34.7	31.8	61.8	33.6
	CV (%)	6.1	3.8	4.0	7.9	4.4	4.0	7.9	4.3

The average results of the propagation values of the \mathcal{G}_{IC} and *J*-integral for each 3 mm and 4.5 mm thick specimen batches are listed in Table 2. For each specimen, the average accounts for the propagation points in the range between $\Delta a = 7$ mm and $\Delta a = 15$ mm, see Figs. 5 and 6.

The difference between the CBTE data reduction method and the *J*-integral (DIC) diminishes when the large displacements correction is taken into account. The relative error between both data reduction methods (CBTE and *J*-integral (DIC-LD)) decreases from 5.1% to 1.5% for the 3 mm thick specimens, and from 4.1% to 0.8% for the 4.5 mm thick specimens.

A very good agreement is obtained between the results from the LEFM data reduction method \mathcal{G}_{IC} (CBTE) and the *J*-integral (LD),

having differences of less than 2.3%. With regards to the results of the *J*-integral (LD), the three proposed methodologies provide similar results of the mode II fracture toughness, having variation of less than 2.3% between them.

Furthermore, after comparing the results of the 3 mm and 4.5 mm thick specimens, it can be concluded that the results of the fracture toughness for the delamination in these specimens do not depend on specimen thickness. This is evidenced by all the data reduction methods. However, thinner specimens can cause larger deflections which then have to be taken into account in the data reduction methods.

The proposed data reduction methods are limited to unidirectional specimens. However, this work includes some general equa-

tions that can be particularized for the case of multidirectional laminates. To adapt the formulation to a multidirectional laminate, the path Γ_a in Eq. (12) has to be divided as a sum of integrations of each layer.

$$J_{\Gamma_a} = \sum_{j=1}^n \int_{-h_j}^{h_j} \left(-\frac{1}{2} \sigma_{11} \varepsilon_{11} + \sigma_{12} (\varepsilon_{12} - \tan \theta_g) \right) dx_2 \quad (23)$$

where σ_{11} , σ_{12} , ε_{11} and ε_{12} correspond to the layer stress and strain at the corresponding directions, n is the number of layers and h_j is the half thickness of the layer. The constitutive relationship between the stresses and the strains may be defined from the laminate theory.

With regards the data reduction methods based on the J -integral presented in this work, the simplest one is the J -integral based on Simple Beam Theory (BT-LD), where the last term in Eq. (22) is addressed by estimating the longitudinal strain profile at section S - S' by means of Simple Beam Theory without the need for extra equipment besides two inclinometers. With this method, similar results of fracture toughness from LEFM methods are obtained, with errors of less than 2%. From these experimental results, it can be asserted that this methodology (J -integral (BT-LD)) is a good candidate for determining fracture toughness in ELS tests, thus providing a suitable and robust method for an industrial environment. The methodology can be used in delamination tests of laminated composite materials, as well as adhesively bonded joints.

It is worth mentioning that the specimen dimensions are critical because section S - S' has to be situated far enough away from the FPZ. This means that the specimen dimensions depend on the expected FPZ length.

6. Conclusions

The end-loaded split (ELS) test, was recently standardized [8] as a result of its suitability for measuring mode II fracture toughness with stable crack growth. The standard method requires calibrating the clamp fixture beforehand and is based on LEFM assumptions, that is, the Fracture Process Zone (FPZ) ahead of the crack tip is small compared to the other dimensions of the problem. This paper presents a new methodology based on the J -integral which is not restricted to small FPZ, so it can be used, for example, to analyze adhesive joints.

The methodology relies on measuring load, displacement, rotation at the load application point and the section close to the clamping end (section S - S'), as well as the strain profile at this section. While the rotations may be measured in a simple way using inclinometers, three alternative methods are proposed for assessing the strain profile in section S - S' : (i) Digital Image Correlation (DIC), (ii) a Strain Gauge on the top face of the specimen and (iii) an estimation based on Simple Beam Theory assumptions.

This new method is more objective than LEFM based approaches as it requires neither directly measuring nor calculating crack length. It requires less preparation because it does not need the clamp fixture to be calibrated beforehand. The proposed formulation accounts for large deflections in the ELS test.

The outcome of the LEFM based scheme and J -integral methodology on the data reduction of delamination tests are compared to check for correctness of the proposed formulation (both methods should reproduce the same fracture toughness), and a difference of less than 2.3% between the CBTE and any of the J -integral methods has been observed. In addition, the different methods used to assess the strain profile in section S - S' result in a deviation in fracture toughness of less than 4%.

Acknowledgements

The authors would like to acknowledge the support of the Spanish government through the Ministerio de Economía y Competitividad under contract TRA2015-71491-R.

References

- [1] Davies P, Blackman BRK, Brunner A. Standard test methods for delamination resistance of composite materials: current status. *Appl Compos Mater* 1998;5 (Iso 4585):345–64. <http://dx.doi.org/10.1023/a:1008869811626>.
- [2] Blackman BRK, Brunner A, Williams J. Mode II fracture testing of composites: a new look at an old problem. *Eng Fract Mech* 2006;73(16):2443–55. <http://dx.doi.org/10.1016/j.engfractmech.2006.05.027>.
- [3] Brunner A, Blackman BRK, Davies P. A status report on delamination resistance testing of polymermatrix composites. *Eng Fract Mech* 2008;75(9):2779–94. <http://dx.doi.org/10.1016/j.engfractmech.2007.03.012>.
- [4] ASTM D7905M-14. Standard test method for determination of the mode II interlaminar fracture toughness of unidirectional fiber-reinforced polymer. *American Society for Testing and Materials*; 2014.
- [5] DIN EN 6034:1996. Aerospace series – carbon fibre reinforced plastics – test method – determination of interlaminar fracture toughness energy – mode II – GIIC. *Deutsches Institut für Normung*; 1996.
- [6] ASTM D6671/D6671M. Standard test method for mixed mode I-mode II interlaminar fracture toughness of unidirectional fiber reinforced polymer matrix composites. *American Society for Testing and Materials*; 2013.
- [7] de Morais A, de Moura M. Evaluation of initiation criteria used in interlaminar fracture tests. *Eng Fract Mech* 2006;73(16):2264–76. <http://dx.doi.org/10.1016/j.engfractmech.2006.05.003>.
- [8] ISO 15114:2014. Fibre-reinforced plastic composites – determination of the mode II fracture resistance for unidirectionally reinforced materials using the calibrated end-loaded split (C-ELS) test and an effective crack length approach. In: *International standard organization*. Geneva, Switzerland, p. 1–26 (1).
- [9] Hashemi S, Kinloch A, Williams J. The analysis of interlaminar fracture in uniaxial fiber-polymer composites. *Proc R Soc A* 1990;427:173–99. <http://dx.doi.org/10.1098/rspa.1990.0007>.
- [10] Wang H, Vu-Khanh T, Le VN. Effects of large deflection on mode II fracture test of composite materials. *J Compos Mater* 1995;29(6):833–49. <http://dx.doi.org/10.1177/002199839502900608>.
- [11] Brunner A. Experimental aspects of Mode I and Mode II fracture toughness testing of fibre-reinforced polymer-matrix composites. *Comput Methods Appl Mech Eng* 2000;185(2–4):161–72. [http://dx.doi.org/10.1016/S0045-7825\(99\)00257-1](http://dx.doi.org/10.1016/S0045-7825(99)00257-1).
- [12] Blackman BRK, Kinloch A, Paraschi M. The determination of the mode II adhesive fracture resistance, GIIC, of structural adhesive joints: an effective crack length approach. *Eng Fract Mech* 2005;72(6):877–97. <http://dx.doi.org/10.1016/j.engfractmech.2004.08.007>.
- [13] Högberg J, Sørensen B, Stigh U. Constitutive behaviour of mixed mode loaded adhesive layer. *Int J Solids Struct* 2007;44(25–26):8335–54. <http://dx.doi.org/10.1016/j.jisolsolstr.2007.06.014>.
- [14] Rice J. A path independent integral and the approximate analysis of strain concentration by notches and cracks. *J Appl Mech* 1968;35:379–86. <http://dx.doi.org/10.1115/1.3601206>.
- [15] Andersson T, Stigh U. The stress elongation relation for an adhesive layer loaded in peel using equilibrium of energetic forces. *Int J Solids Struct* 2004;41:413–34. <http://dx.doi.org/10.1016/j.jisolsolstr.2003.09.039>.
- [16] O'Brien T. Composite interlaminar shear fracture toughness, GIIC: shear measurement or shear myth? *ASTM STP* 1998;1330:3–18. <http://dx.doi.org/10.1520/STP13263S>.
- [17] Stigh U, Alfredsson K, Biel A. Measurement of cohesive laws and related problems. In: *IMECE2009: proceedings of the ASME international mechanical engineering congress and exposition*, p. 293–8 (11).
- [18] Sarrado C, Turon A, Renart J, Costa J. An experimental data reduction method for the Mixed Mode Bending test based on the J -integral approach. *Compos Sci Technol* 2015;117(117):85–91. <http://dx.doi.org/10.1016/j.compscitech.2015.05.021>.
- [19] Corleto C. Mode II delamination fracture characterization of fiber reinforced composite materials, a Ph.D. dissertation. Mechanical engineering, Texas A&M University; 1990.
- [20] Williams J. Large displacement and end block effects in the 'DCB' interlaminar test in modes I and II. *J Compos Mater* 1987;21(4):330–47. <http://dx.doi.org/10.1177/002199838702100403>.
- [21] Nilsson F. Large displacement aspects on fracture testing with double cantilever beam specimens. *Int J Fract* 2006;139(2):305–11. <http://dx.doi.org/10.1007/s10704-006-8376-3>.
- [22] Chen Z, Adams R, Da Silva LF. The use of the J -integral vector to analyse adhesive bonds with and without a crack. *Int J Adhes Adhes* 2011;31(1):48–55. <http://dx.doi.org/10.1016/j.jadhadh.2010.11.005>.
- [23] Renart J, Blanco N, Pajares E, Costa J, Lazzcano S, Santacruz G. Side Clamped Beam (SCB) hinge system for delamination tests in beam-type composite specimens. *Compos Sci Technol* 2011;71(8):1023–9. <http://dx.doi.org/10.1016/j.compscitech.2010.10.005>.
- [24] Correlated Solutions. Vic-3D Testing guide; 2010.

A.2 Suitable specimen dimensions for the determination of mode II fracture toughness of bonded joints by means of the ELS test

M. Pérez-Galmés ^a, J. Renart ^a, C. Sarrado ^a, J. Costa ^a

^aAMADE, Mechanical Engineering and Industrial Construction Department, Universitat de Girona, Campus Montilivi s/n, Girona, Spain

The paper has been submitted to *Engineering Fracture Mechanics*

Suitable specimen dimensions for the determination of mode II fracture toughness of bonded joints by means of the ELS test

M. Pérez-Galmés^a, J. Renart^a, C. Sarrado^a, J. Costa^a

^aAMADE, Polytechnic School, University of Girona, Carrer Universitat de Girona, 4.Campus de Montilivi, 17003-Girona, Spain

Abstract

The definition of the specimen dimensions in mode II fracture tests of bonded joints, where large Fracture Process Zones (FPZ) occur, is still an issue to be solved.

Several conditions shall be met in order to obtain propagation values in bonded joints testing; stability of the test, full FPZ formation, and avoidance of large deflections and adherend failure.

This work presents a methodology that indicates the specimen dimensions needed to obtain propagation values in End Loaded Split (ELS) tests.

In addition, suitable specimen dimensions for a wide range of thin bonded joints between CFRP adherends is presented, solving the issue of defining suitable specimen dimensions to test adhesives to ensure steady state propagation.

Keywords: Toughness testing, Bonded joints, Mode II, ELS

1. Introduction

The use of Fibre Reinforced Polymer composites (FRP) has become very popular in aerospace and automotive industries since their use results in the structure weight reduction. The joining of FRP parts through the use of adhesives instead of other mechanical fasteners is of great interest due to the adhesives capability to redistribute the loads, resulting in a reduction of the stress concentrations.

The adhesive bonded joints perform better in shear loading than under tensile or peel loadings, reason why they are designed such that the adhesive is mainly loaded in shear. Thus, the most relevant mechanical property in the FRP bonded joints design is the shear (mode II) fracture toughness of the bonded joint.

26 Several mode II tests have been developed in order to solve the main problem of mode II testing:
27 stability of the test. The highly used End Notched Flexure (ENF) test [1] is mainly unstable, and
28 other tests have been developed such as the tapered ENF (TENF) test [2], the stabilized ENF
29 (SENF) test [3], the Over-Notched flexure (ONF) test [4], the four ENF (4ENF) test [5] or the recent
30 inverse ELS test [6] among others, in order to achieve stable propagation. However, other problems
31 arise from this tests: specimen manufacturing (TENF), complex test set-up (SENF) or friction
32 (4ENF and ONF).

33 The end-loaded split (ELS) test is used to determine the mode II fracture toughness in unidirectional
34 Fibre-Reinforced Polymer composites (FRP). Unlike other tests, it has the advantage of stable crack
35 growth under displacement control if the ratio between the initial crack (a_0) and the span length (L)
36 is higher than 0.55 [7–11], allowing longer propagation length relative to the mode II ENF test case
37 [12].

38 According to ISO 15114 standard [13], the crack length is a required parameter that has to be either
39 measured or estimated during the test. In standard delamination tests it is assumed the existence of
40 a neat crack or, in its absence, that the non-linear zone at the crack front, the so called Fracture
41 Process Zone (FPZ), is small in comparison to any specimen relevant dimensions (width, thickness or
42 crack length) [14]. Therefore, the steady state propagation is reached just after the initiation values.

43 Generally, adhesively bonded joints have been reported to entail large FPZ under shear loadings,
44 compared to other specimen dimensions, induced by the plasticity of the adhesive layer [15, 16]. The
45 large FPZ involved, in conjunction with the lack of crack opening, hinders the measurement of the
46 crack length by visual inspection [7, 17, 18]. To overcome this, a method based on an effective crack
47 length (a_e) derived from the specimen compliance was proposed by Blackman et al. [10] and a non
48 crack dependant method, based on the J -integral, was later developed by Pérez-Galmés et al. [19].
49 Notwithstanding the improvement in fracture toughness calculation of bonded joints with methods
50 that do not depend on crack measurements, other problems arise when testing adhesives because of
51 the large FPZs involved. During the test, the energy release rate increases while the FPZ develops,

52 attaining its maximum value (G_{IIc}) when the FPZ has been totally formed. Thus, for large FPZs,
53 several millimeters of propagation region are required to reach the propagation steady state [12].
54 Taking into account the specimen dimensions recommended by ISO 15114 [13], the steady state is
55 not always achieved even after the crack front reaches the support, as occurs e.g. in bonded joints
56 with a high toughness adhesive. Several authors performed mode II tests of adhesives without
57 reaching the steady state propagation, either reporting propagation values that are below the self
58 similar ones, or just providing initiation values [14, 20–22]. Unfortunately, those initiation values lead
59 to very conservative results because they are several times lower than the propagation ones.
60 On the positive side, having large FPZ increases the stability of mode II tests. It allows the use of
61 smaller a_0/L ratios and consequently, the propagation region to develop the total FPZ becomes
62 larger (i.e. for a same L case, $L-a_0$ is increased). Such examples can be found in the works of different
63 authors who used the ENF test with ratios of a_0/L below 0.7 (the minimum stable ratio established
64 by Carlsson et al. [23]) in adhesive testing resulting in stable crack propagation [14, 20, 24–29].
65 Moreover, due to the high fracture toughness of the adhesives and/or the dimensions of the
66 specimens commonly used, the ELS test may involve Large Deflections (LD) [7, 17, 30]. Although
67 the effects of LD in fracture toughness measurement appears to be solved in the ISO 15114 standard
68 [13] by the use of the F correction factor proposed by Williams [30] or in other data reduction
69 methodologies such as the use of J -integral [19], these large deflections stiffen the system and the test
70 tends to be less stable. Regarding this, some authors have used thicker specimens to prevent
71 exceeding the LD limit of $\delta = 0.2L$ [31, 32].
72 The previous considerations of using larger and/or thicker specimens to let the FPZ to fully develop
73 or reach a steady-state crack propagation are intuitive and they follow a trial-and-error procedure.
74 For this reason, a prediction of the test configuration needed beforehand would avoid repeating the
75 tests. In this work, a method to predict the specimen dimensions and the test configuration to get
76 propagation values in ELS mode II fracture test, is proposed. The method establishes a design region
77 (working domain) , defined by four criteria: full development of FPZ, stability of the test, avoidance

78 of large deflections and prevention of adherend failure. The first three criteria are evaluated through
79 an analytical model based on the work of Alfredsson [24] which predicts the load-displacement curve
80 of an ENF test by assuming the adhesive behaviour with a linear cohesive law. The last criterion is
81 evaluated by considering Linear Elastic Fracture Mechanics (LEFM). A set of design regions is
82 proposed for a wide range of existing commercial adhesives. As a result, the method provides a
83 practical methodology for anyone who want to obtain the mode II fracture toughness in bonded
84 joints with the ELS test.

85 **2. ELS specimen design criteria**

86 To obtain crack propagation when testing adhesives with the ELS test, some conditions must be
87 accomplished. Firstly, to reach the steady-state crack propagation and thus the resistance curve
88 plateau, ensuring the formation of the whole FPZ (i), secondly, to guarantee the stability of the test
89 under displacement control (ii), thirdly, to avoid Large Deflections (LD) (iii) and, lastly, to prevent
90 the Adherend Failure (AF) during testing (iv).

91 All these conditions shall be met by adjusting the ELS geometry: span length (L), initial crack
92 length (a_0) and, if necessary, the specimen total thickness ($2H$).

93 *2.1. Full FPZ development criterion*

94 In order to obtain at least one propagation point, the propagation region ($L - a_0$) must be large
95 enough to let the FPZ fully develop. Based on a previous work [19] a minimum distance of 10 mm
96 have been be left in order to avoid clamping effects. The aforementioned conditions are satisfied if,

$$L - a_0 > l_{FPZ} + 10mm \quad (1)$$

97 where a_0 is the initial crack length, L is the span length and, l_{FPZ} is the length of the FPZ when the
98 propagation begins. It is worth mentioning that the pre-crack test has not been taken into account
99 in the previous condition (equation 1), since it is considered a previous test.

100 To define this criterion, the corresponding l_{FPZ} for a particular L and a_0 has to be estimated, which
101 can be done by means of the analytical model presented in section 3. It is worth noticing that, when
102 the end of the FPZ approximates the clamp tool, compressive stresses can influence the crack
103 propagation. On that account, the initial crack length (a_0) should be approximated to the minimum
104 allowed by the other criteria.

105 2.2. Stability criterion

106 When the test becomes unstable, the crack jumps, and propagation values can not be obtained.
107 Various studies dealt with the stability of ELS test under displacement control assuming Simple
108 Beam Theory (SBT) and Linear Elastic Fracture Mechanics (LEFM) and they concluded that the
109 propagation will be stable using a minimum a_0/L ratio of 0.55 [7, 8, 17, 33, 34]. The stability can be
110 improved by using larger a_0/L ratios, reducing however the length available for the crack to grow (or
111 by requiring a larger specimen to maintain the propagation distance, $L-a_0$)

112 In adhesive testing, test stability cannot be simply obtained under the assumptions of LEFM. By
113 studying the FPZ effect in mode II testing, several authors concluded that the closure stresses ahead
114 of the crack tip due to FPZ development contribute to the crack growth stability [20, 24, 25, 29].

115 Alfredsson [24] estimated, for an ENF test, a minimum a_0/L ratio by assuming an specific cohesive
116 law for the adhesive, and he demonstrated that the critical a_0/L ratio is less restrictive, when large
117 FPZ are involved, than the LEFM-based ENF stability limit $a_0/L > 0.7$ [23].

118 In order to explain how the FPZ improves the test stability, Figure 1 shows the schematic
119 Load-displacement ($P - \delta$) curves of two specimens with the same fracture toughness but different
120 l_{FPZ} .

121 In Figure 1, the dotted line marks the stability limit according to LEFM [17]. It is observed that a
122 test on a specimen with large FPZ can be stable even if the ratio of a_0/L is smaller than 0.55.
123 Therefore, in presence of large FPZ, the LEFM stability limit based on Griffith's energy balance
124 approach, $\partial\mathcal{G}/\partial a < 0$, is too conservative. A snap-back in the Load-displacement curve ($P - \delta$)
125 always occurs in an unstable test. Therefore, the proposed stability criterion relies on avoiding

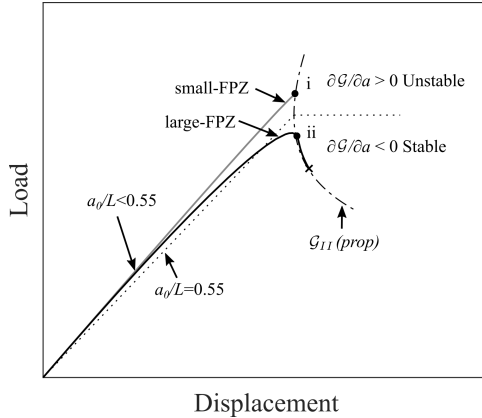


Figure 1: Schematic of LEFM $P - \delta$ curve. Example of FPZ effects in the stability.

126 snap-back in the Load-displacement curve. However, the only way to determine the stability limit is
 127 by predicting the $P - \delta$ curve beforehand, which in this work is done with an analytical model of the
 128 ELS test presented in section 3.

129 2.3. Large deflections criterion

130 In the case of specimens with thin adherends, the ELS test configuration results in Large Deflections
 131 (LD) [7, 17, 30]. In presence of LD, the compliance decreases with the displacement, and the test
 132 becomes less stable. To illustrate this behaviour, Figure 2 shows the schematic $P - \delta$ curves of two
 133 specimens with the same geometry but with different adhesive properties. The curves are represented
 134 assuming a LEFM approach.

135 Specimen 1 (Small Deflections) has stable propagation but specimen 2 becomes unstable due to LD
 136 effects (i.e. specimen stiffening).

137 As previously stated, the presence of FPZ reduces the stiffness of the specimen, so larger deflections
 138 for the same initial specimen geometry are produced. For this reason the analytical study of LD is
 139 not straightforward.

140 Williams [30] proposed a F correction factor that introduces the effect of the reduction on the
 141 moment arm due to large displacements in ELS test. The F correction factor used in this work has

152 *2.4. Adherend failure criterion*

153 When testing high fracture toughness adhesives, Adherend Failure (AF) can occur due to bending
 154 stresses, even before the crack starts to propagate.

155 As the compression strength is lower than the tensile value in unidirectional composite laminates, the
 156 maximum compression stress (σ_c) is considered as the critical parameter for the rupture of the
 157 specimen substrates.

158 The maximum compression stress may take place either at the top face near the clamp section or
 159 near the crack tip ($x = 0$ or $x = b$ in Figure 3). By considering that the maximum compressive
 160 stress at clamp end section (σ_c) must be smaller than the ultimate normal compression strength of
 161 the adherend ($\sigma_u \geq \sigma_c$), and assuming beam's theory and LEFM, the maximum compressive stress
 162 at clamp end section ($x = b$) can be expressed in function of the a_0/L ratio

$$\frac{a_0}{L} \geq \sqrt{\frac{E_{11}\mathcal{G}_{IIc}}{H\sigma_u^2}} \quad (3)$$

163 where H is the arm specimen thickness, E_{11} is the adherend longitudinal Young's modulus, \mathcal{G}_{IIc} is
 164 the adhesive fracture toughness, and σ_u is the normal compression strength of the adherend.
 165 On the other hand, the critical compression stress at the crack tip section ($x = 0$) defines the
 166 minimum thickness for each substrate to prevent its rupture

$$H \geq \frac{4E_{11}\mathcal{G}_{IIc}}{\sigma_u^2} \quad (4)$$

167 Moreover, shear stresses can also lead to adherend failure. Under the same assumptions than
 168 previous equations, a minimum value for a_0 is obtained:

$$a_0 \geq \frac{\sqrt{E_{11}\mathcal{G}_{IIc}H}}{2\tau_u} \quad (5)$$

169 where τ_u is the ultimate shear strength of the adherend laminate.

170 By assuming an specific failure strength of the adherends, a limit case can be set for each geometry,

171 based on equations (3), (4) and (5).

172 Equation (4) is independent of a_0 and L constraining the maximum \mathcal{G}_{IIc} that can be tested with a
 173 determined specimen thickness, while the other two, equations (3) and (5), restrict a_0 depending on
 174 the span length L .

175 3. Analytical model

176 The analysis of the stability of the test and evolution of FPZ formation criteria require the
 177 estimation of a Load-displacement curve accounting for the FPZ length. The most important
 178 parameter to describe the fracture process is the fracture toughness. If combined with the shear
 179 strength, both the energy dissipated and the length of the process zone can be controlled. These two
 180 parameters, represented in a linear cohesive law, can provide reliable descriptions of the fracture
 181 process. Using cohesive law shapes would complicate the analytical developments of the model, to
 182 obtain a small improvement in its accuracy. Furthermore, the adhesive properties available in the
 183 literature are mainly the shear fracture toughness and failure shear strength and very few
 184 information can be found about the cohesive law shape.

185 In this work, the Load-displacement curve is obtained from an analytical model adapted from the
 186 work of Alfredsson [24] to an ELS test configuration. The model simulates a mode II test of a
 187 bonded joint in which the adhesive is a thin layer capable to transmit pure shear.

188 The geometry considered for the ELS test is shown in Figure 3.

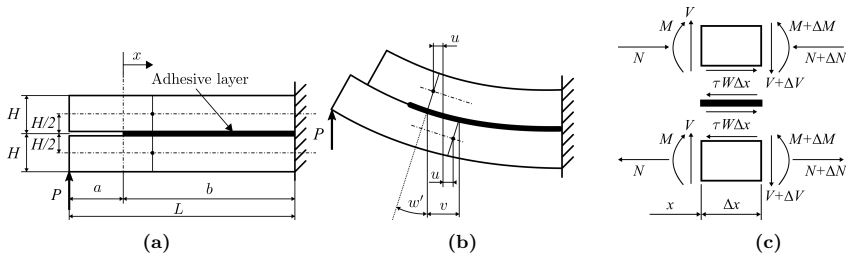


Figure 3: a) Undeformed geometry of ELS specimen; b) Deformed geometry of ELS specimen. v corresponds to the shear deformation of the adhesive layer and w to the deflection; c) Positive directions of sectional loads and adhesive stresses in the interval $x \in [0, b]$, where W corresponds to the specimen width.

189 For small values of the slope ($|w'| \ll 1$) the shear deformation $v(x)$ of the adhesive layer is given by

$$v(x) = 2u(x) + Hw'(x) \quad (6)$$

190 The constitutive behaviour of the adhesive layer is entirely described by a bilinear law (see Figure 4)

191 defined by,

$$\tau(v) = \begin{cases} kv & \text{for } 0 \leq v \leq v_a \\ \bar{k}(v_c - v) & \text{for } v_a \leq v \leq v_c \\ 0 & \text{for } v \geq v_c \end{cases} \quad (7)$$

192 being $k = \tau_{sh}/v_a$ and $\bar{k} = \tau_{sh}/(v_a - v_c)$.

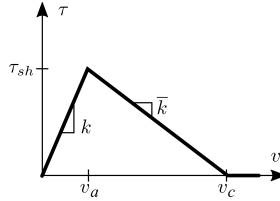


Figure 4: Bilinear constitutive relation of the adhesive layer.

193 The equilibrium equations obtained from the interval forces of two adjacent sections of the adhesive

194 layer, $x \in [0, b]$, are the same than in [24], see Figure 3c,

$$N'(x) = W\tau[v(x)] \quad (8a)$$

$$V'(x) = 0 \quad (8b)$$

$$V(x) = M'(x) + \frac{1}{2}WH\tau[v(x)] \quad (8c)$$

195

196 where geometric parameters, H , b , v and x are defined in Figure 3, W is the specimen width, $\tau[v(x)]$

197 is the constitutive relationship of the adhesive layer defined in equation (7), N denotes the normal
 198 force of the adherends, and M and V are the bending moment and shear force respectively.
 199 By assuming elastic adherend deformation and according to Euler-Bernoulli beam's theory, the
 200 normal force, the shear and the bending moment are given by [24],

$$N(x) = EWHu'(x) \quad (9a)$$

$$V(x) = \frac{P}{2} \quad (9b)$$

$$M(x) = -\frac{EWH^3}{12}w''(x) \quad (9c)$$

201

202 where E is the longitudinal Young's modulus of the adherend material and P is the applied load,
 203 represented in Figure 3.

204 Equations (6) to (9) define a system of two ordinary differential equations in $w(x)$ and $v(x)$ that
 205 describe the mathematical problem:

$$\begin{cases} EHv''(x) = 8\{\tau[v(x)] - 2\bar{\tau}\} & \text{for } 0 \leq x < b \\ EwH^3w''(x) = -6\{P(x+a) - HW \int_0^x \tau[v(\tilde{x})]d\tilde{x}\} & \text{for } -a \leq x < b \end{cases} \quad (10)$$

206 where $\bar{\tau} = 3P/(8WH)$ is the shear stress in solid beam sections (e.g. Beer et al., 2002 [36])

207 In order to obtain $v(x)$ and $w(x)$ the following boundary conditions are considered:

$$N(0) = 0 \quad (11a)$$

$$M(0) = Pa/2 \quad (11b)$$

$$v(b) = 0 \quad (11c)$$

$$w(b) = 0 \quad (11d)$$

$$w'(b) = 0 \quad (11e)$$

208

209 According to equation (7) the boundary conditions (equation (11)) transforms to

$$v'(0) = \frac{-16\bar{\tau}a}{EH} \quad (12)$$

210 Assuming the presence of a cohesive zone of length d at the crack tip ($d < b$), the general solution to
 211 the shear deformation equation (10) is:

$$v(x) = \begin{cases} A_1 \sin(\bar{\kappa}x) + A_2 \cos(\bar{\kappa}x) + v_c - 2\bar{\tau}/\bar{k} & \text{for } 0 \leq x \leq d \\ A_3 e^{\kappa x} + A_4 e^{-\kappa x} + 2\bar{\tau}/k & \text{for } d \leq x \leq b \end{cases} \quad (13)$$

212 where $\bar{\kappa} \equiv \sqrt{8\bar{k}/(EH)}$ and $\kappa = \sqrt{8k/(EH)}$.

213 The integration constants A_1, A_2, A_3 and A_4 are determined from boundary conditions (equation
 214 (11) and equation (12)) and the continuity equations at $x = d$, for $v(d)$ and $v'(d)$.

215 The solution of $v(x)$ is divided in 3 parts.

216 Firstly, when $v(0) \leq v_a$ the adhesive has a linear response and there is no FPZ, thus $d = 0$. Only the
 217 elastic part of $v(x)$ is considered:

$$v(x) = A_3 e^{\kappa x} + A_4 e^{-\kappa x} + 2\bar{\tau}/k \quad \text{for } 0 \leq x \leq b \quad (14)$$

218 Secondly, if $v_a \leq v(0) \leq v_c$ the FPZ is under development. A relationship between d and the applied
219 load, represented by $\bar{\tau}$, can be determined by knowing that the deformation of the right end of the
220 process zone is $v(d) = v_a$.

221 And thirdly, if the shear displacement $v(x)$ exceeds the critical value v_c , the crack propagates. The
222 crack growth length a is increased in equation (13) and a new size of the process zone, d , is
223 calculated using equation (13) and knowing the shear deformation of both sides of the FPZ;
224 $v(0) = v_c$, and $v(d) = v_a$. For each increment of a , a value of P is obtained.

225 It is worth noticing that in this later part d must be kept as a dependent value, because as it is
226 shown in [24] there is a small variation of d with the increment of the crack length, a .

227 Once $v(x)$ is known, $w(x)$ can be obtained by solving the differential equation (10) taking into
228 account boundary conditions (equations (11) and (12)). The displacement at the loading application
229 point is $w(-a)$.

230 A comparison between the analytical model and FEM for three different adhesive cohesive properties
231 is shown in Figure 5, demonstrating that $P - \delta$ curve from the analytical model fits well with the
232 FEM results.

233 The finite element model was developed in Abaqus implicit [37] using four-node, 2D plane strain
234 elements (CPE4). A row of zero-thickness four-node cohesive elements (COH2D4) was placed ahead
235 of the notch tip to model crack propagation. The same boundaries and cohesive properties used in
236 the analytical model were used in the FEM.

237 In the proposed analytical model the assumed boundaries do not take into account clamp effects,
238 caused by the imperfect encastre of the ELS test rig, because they have to be evaluated once the
239 specimen geometry is defined [13]. In Section 6 the clamp effects on the working domain definitions
240 are discussed. It is worth noticing that the analytical model do not take into account the shear
241 deformations of the adherends, since Euler Bernoulli assumptions are considered and the results show
242 good agreement.

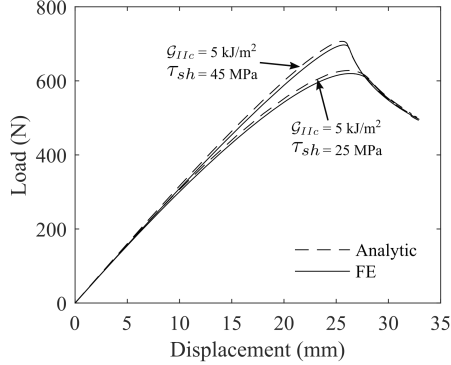


Figure 5: $P - \delta$ curve from a FE model and the proposed analytical model. Results from specimens with the same geometry ($a_0 = 80$ mm, $H = 3$ mm, $W = 25$ mm and $L = 150$ mm) but with different cohesive properties.

243 4. Definition of a working domain

244 4.1. Working domain for known adhesive properties.

245 Assuming the constitutive properties of the adhesive layer, τ_{sh} and \mathcal{G}_{IIc} , a specimen thickness, H ,
 246 and the mechanical properties of the adherends, we can define a relationship between a_0 and L for
 247 the specimen that fulfils the criteria defined in section 2.

248 Each criterion (Stability, full FPZ formation, LD: Large Deflections, AF: Adherend Failure) defines a
 249 boundary curve that, together, enclose a working domain defined by a_0 and L . These boundary
 250 curves are defined by using the analytical model described in section 3.

251 For a given adherend thickness H , a set of models with different span lengths L and a short a_0 are
 252 run. From the results, the a_0 at which the test is no longer stable (Stability criterion) is determined.

253 On the other hand, a set of geometries with different L and a_0 are defined for a given H and the
 254 corresponding initial l_{FPZ} and the displacement when the propagation starts (δ_{prop}) are obtained.

255 This data in combination with equations (1) and (2) define the onset of crack propagation (full FPZ
 256 formation criterion) and the values of a_0 for which the assumption of small deflections, is no longer
 257 valid (LD criterion).

258 Repeating this procedure for different H , the curves that define the Stability, full FPZ formation and
 259 LD criteria are obtained.

260 The AF criteria are represented directly on the a_0 vs. L or a_0 vs. a_0/L graphs from equations (3)
 261 and (5). Equation (4) defines the minimum thickness ($2H$) of the specimen to prevent the arm
 262 failure near the crack front before the propagation.

263 Figure 6a exemplifies how the ELS working domain is defined in an a_0 vs L plot. The grey area
 264 represents the working domain of a bonded joint with an adhesive with $\mathcal{G}_{IIC} = 8 \text{ kJ/m}^2$, $\tau_{sh} = 30$
 265 MPa, $k = 10^4 \text{ GN/m}^3$, $H = 6 \text{ mm}$, $E_{11} = 120 \text{ GPa}$, $\sigma_u = 1500 \text{ MPa}$ and $\tau_u = 100 \text{ MPa}$.

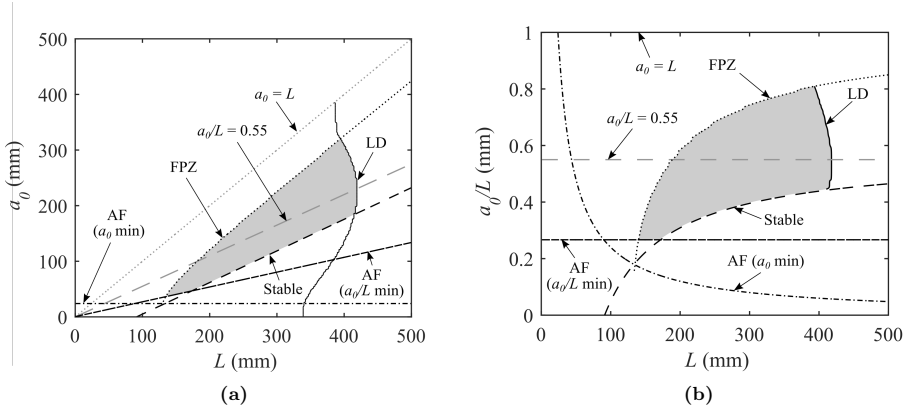


Figure 6: Working range of case 5 ($\mathcal{G}_{IIC} = 8 \text{ kJ/m}^2$ and $\tau_{sh} = 30 \text{ MPa}$). Specimens of 6 mm thickness.

266 The working domain is the area enclosed by all the criteria boundaries, each one represented by a
 267 curve, except the AF boundaries that are represented by 2 curves, defined by equations (3) and (5).
 268 In Figure 6a, equation (3) does not limit the working domain.

269 The same results are represented in a a_0/L versus L plot for an easier viewing of each limit, see
 270 Figure 6b.

271 Additionally, the propagation ($a_0 = L$) and the stability ($a_0/L \geq 0.55$) boundaries based on LEFM
 272 assumptions have been added to Figures 6a and 6b to highlight the effect of the FPZ on the working
 273 domain. In Figure 6b the boundaries based on LEFM define a domain for the ratio a_0/L from 0.55

Table 1: Mechanical properties (fracture toughness, shear failure strength and Young’s modulus) of common adhesives used in aeronautics.

Type	Name	Supplier	\mathcal{G}_{IIc} (kJ/m ²)	τ_{sh} (MPa)	E_{adh} (GPa)
Resin	TEXIPREG HS-160 RM	SEAL [®]	0.79 [38] ³ ; 0.84 [39]	80 [40] ³	-
	MCP1110	Maruhachi Corp.	1.89 [41]	49.9 [42]	3.2 [41]
	8551-7	Hexcel [®]	-	100-107 ¹	-
	8552	Hexcel [®]	1.33-1.76 [43]	128 ¹	-
	M21	Hexcel [®]	-	110 ¹	-
Paste	Araldite [®] 2015	Araldite [®]	3.18 [44], 4.3 [20], 4.7 [38] ³	17.9 [45], 22.8 [38] ³	1.85 [46]
	AV138/HV998	Araldite [®]	4.91 [20]	30.2 [47]	4.59 [45], 4.89 [46]
	EA 9361 (Hysol)	Henkel [®]	5.22 [48] ²	20.6 [48] ²	0.723 ¹ ; 0.67 [48]
Film	FM-300M	CYTEC	7.0 [28], 7.9 [49]	45 [28], 47.5 [49]	2.921 [49]
	EA9628	Henkel [®]	-	40-41.3 ¹	2.377 ¹
	EA9695	Henkel [®]	-	31.7-34.5 ¹	-

¹ Manufacturer’s data.

² The interlaminar shear strength reported in [48] depends on the adhesive thickness, so the value shown is the result of the linear extrapolation of the failure load to a zero adhesive thickness.

³ Data used in numerical modelling.

274 to 1, whereas when large FPZ applies, this domain is reduced and shifted down. The LD criterion
275 limits the maximum span length (L) that can be used.

276 4.2. Definition of a general domain

277 Figure 6 can only be obtained if the constitutive properties of the adhesive layer are known in
278 advance. In case they are not, they must be estimated.

279 Table 1 summarizes the cohesive properties of common adhesives used in aeronautics found in the
280 literature, they are divided into three main groups: resins, pastes and films.

281 It is observed that the paste and film adhesives have middle failure shear strengths ($\tau_{sh} = 17.9$ MPa
282 to 47.5 MPa) and middle to high fracture toughnesses ($\mathcal{G}_{IIc} = 2.18$ kJ/m² to 7.9 kJ/m²), while the
283 resins are of middle to high failure shear strengths ($\tau_{sh} = 49.9$ MPa to 128 MPa) and low fracture
284 toughnesses ($\mathcal{G}_{IIc} = 0.79$ kJ/m² to 1.89 kJ/m²).

285 Moreover, according to [40, 50, 51] the size of the FPZ is proportional to \mathcal{G}_{IIc} and inversely
286 proportional to τ_{sh} .

Table 2: Cohesive properties and geometries considered in the analytical model.

	\mathcal{G}_{IIc} (kJ/m ²)	τ_{sh} (MPa)
Case 1	0.7	110
Case 2	3	30
Case 3	5	45
Case 4	5	17
Case 5	8	30

287 By taking this into account, and based on the literature data presented in Table 1, typical
288 interlaminar constitutive behaviour of a bonded joint or an adhesive are represented by the 5 cases
289 presented in Table 2.

290 Cases 1 and 2 are a combination of the maximum and minimum properties of the resins of Table 1.
291 Cases 2 and 3 encompass the properties of low to medium toughness adhesives. And finally, cases 4
292 and 5 concern medium to high toughness adhesives. The combination of two cases can define an
293 overlapped working domain for an interface (adhesive / resin) with a wider range of properties.

294 5. Results

295 A series of working domains were defined for 3 different adherend thicknesses ($H = 1, 3$ and 6 mm)
296 and for each case of Table 2. The same width, W , was considered in all the cases (25 mm).

297 As not being crucial in fracture toughness calculation of a thin adhesive layer, k is fixed to 10^4
298 GN/m³ for all models, by considering a adhesive layer thickness of $t = 0.15$ mm and an adhesive

299 shear modulus of $G_{adh} = 1500$ MPa [45], and $k = G_{adh}/t$ according to Alfredsson [24]. The elastic
300 properties of the adherends considered are typical values of unidirectional CRFP: $E_{11} = 120$ GPa,
301 $E_{22} = E_{33} = 7.8$ GPa and $G_{12} = 4$ GPa [28], where subscript 1 denotes x direction (c.f. Figure 3).

302 The ultimate values considered to calculate the adherend failure limits are $\sigma_u = 1500$ MPa and $\tau_u =$
303 100 MPa.

304 To construct the domains, the span length was varied in the interval $L \in [50, 500]$ mm, and $a_0 \in [0,$
305 $L]$.

306 Figure 7 shows the working domains for the configurations described in Table 2. Each Figure

307 includes the working domains for the 3 different thicknesses, 1, 3 and 6 mm.
308 In case 1 (Figure 7a) the working domains of the three thicknesses intersect. In case 2 this
309 intersection does not occur due to the LD limitation in $2H = 2$ mm thick specimens. In cases 3, 4
310 and 5, for a $2H = 2$ mm thick specimens, the boundary criteria do not define a working domain and
311 they are not represented.
312 Figures 8, 9 and 10 show the intersection of two cases of Table 2 for the same adherend thickness. It
313 is worth noticing that indications of what criterion is defining each limit are made in Figure 6, but
314 not in Figures 7 to 10, since they only aim to show the working domain for the studied cases. Figure
315 8 shows the intersection between cases 1 and 2, defining a working domain for low toughness
316 adhesives (0.7 to 3 kJ/m²).
317 Figure 9 plots the intersection between cases 2 and 4, defining the working domain for medium
318 toughness adhesives (3 to 5 kJ/m²). Finally, Figure 10 shows the intersection between cases 3 and 5,
319 defining the working domain for high toughness adhesives (5 to 8 kJ/m²).
320 For each intersection only two thicknesses are considered: $H = 1$ and 3 mm in Figure 8; $H = 3$ and 6
321 mm in Figures 9 and 10. The thickness chosen depends on the LD and AF criteria.

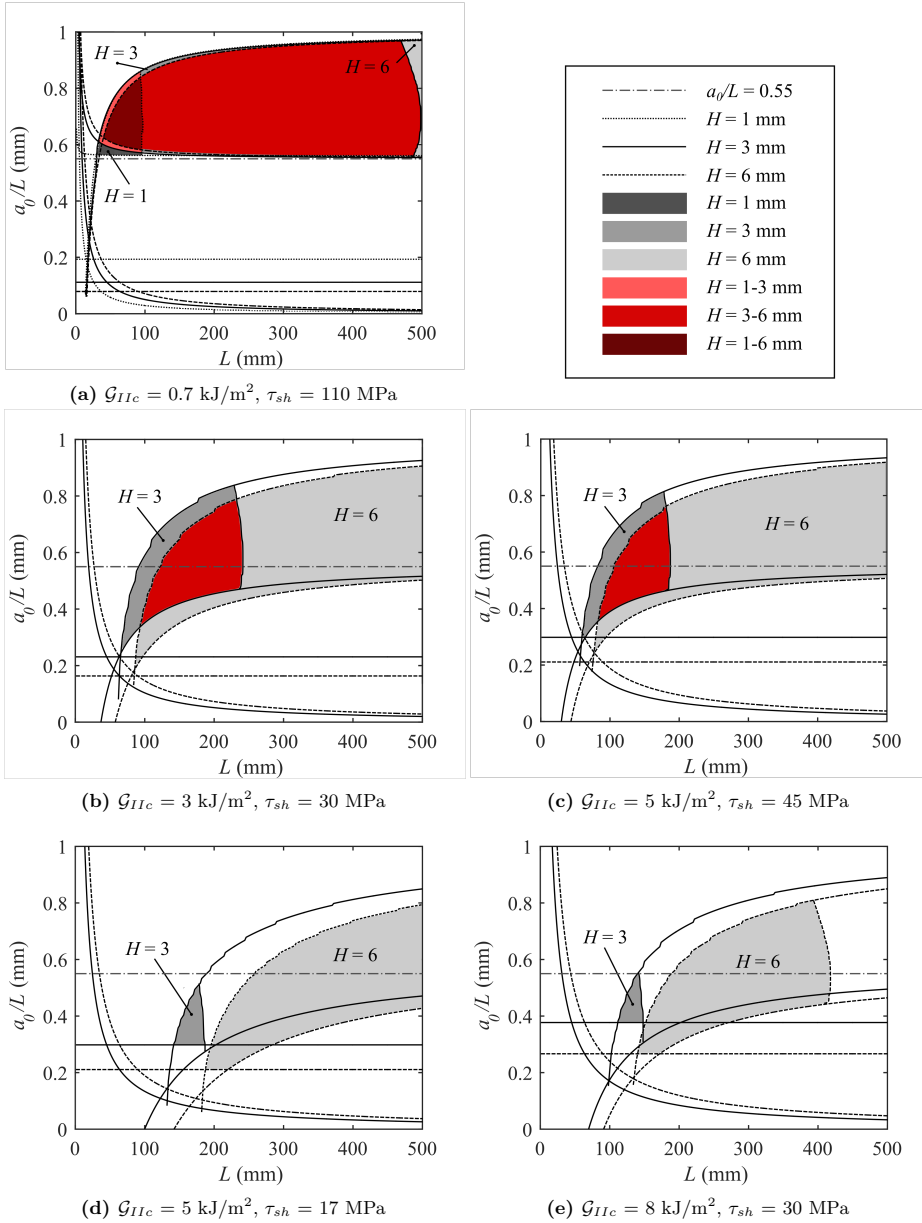
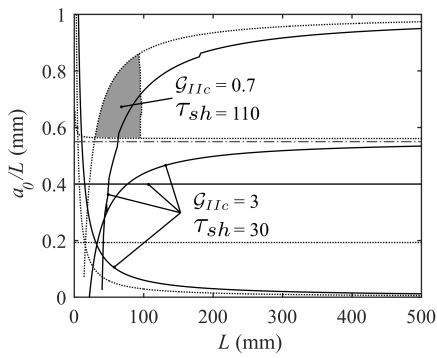
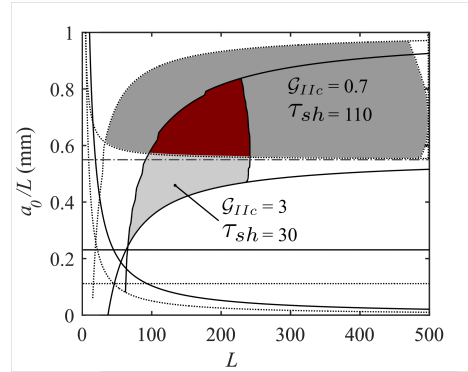


Figure 7: Working domain of each case study.

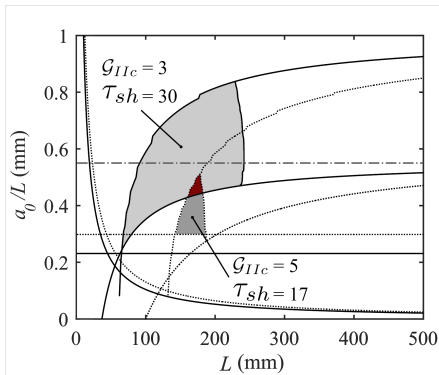


(a) $2H = 2$ mm

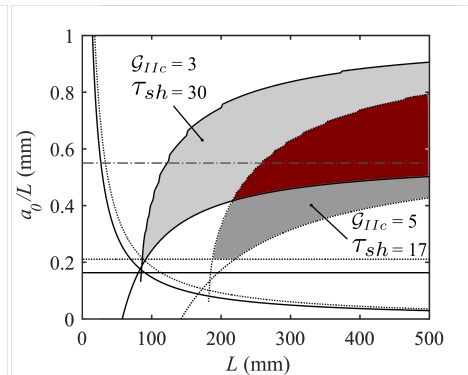


(b) $2H = 6$ mm

Figure 8: Working domain of resins of G_{IIc} between 0.7 kJ/m^2 and 3 kJ/m^2 and τ_{sh} between 30 MPa and 110 MPa . Relatives to cases 1 and 2.



(a) $2H = 6$ mm



(b) $2H = 12$ mm

Figure 9: Working domain of paste adhesives adhesives of G_{IIc} between 3 kJ/m^2 and 5 kJ/m^2 and τ_{sh} between 17 MPa and 30 MPa . Relatives to cases 2 and 3.

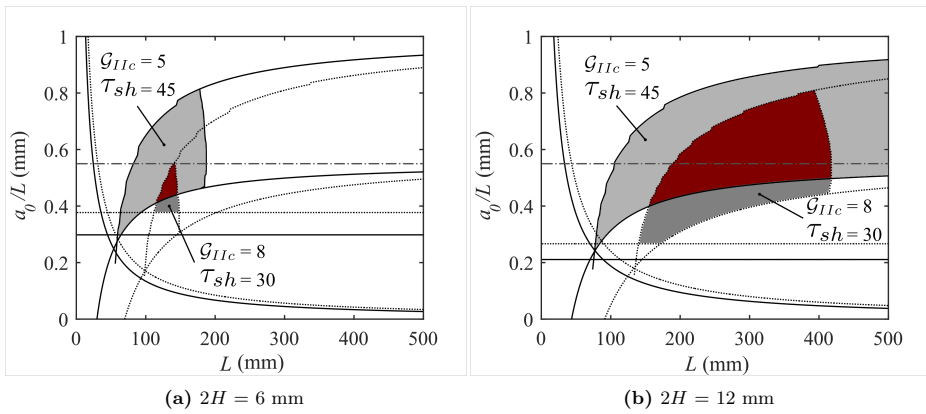


Figure 10: Working domain of film adhesives of \mathcal{G}_{IIC} between 5 kJ/m² and 8 kJ/m² and τ_{sh} between 30 MPa and 45 MPa. Relatives to cases 4 and 5.

322 6. Discussion

323 As it results in short FPZ lengths, the lower stable limit of case 1 ($\mathcal{G}_{IIc} = 0.7 \text{ kJ/m}^2$ and τ_{sh} 110
324 MPa, represented in Figure 7a) approximates the LEFM-based stable limit of $a_0/L = 0.55$ and the
325 higher FPZ formation limit approximates the geometric limit $a_0 = L$. Therefore, the recommended
326 geometries of the standard ISO 15114 [13] would be valid and only the LD limit must be taken into
327 account to define the specimen geometry.

328 In the general case of resins (Figure 8, combination of cases 1 and 2) the minimum a_0/L ratio to
329 maintain the stability is 0.55 and the full FPZ development criterion restricts the minimum L and
330 maximum a_0 . Furthermore, as including high toughness resins ($\mathcal{G}_{IIc} = 3 \text{ kJ/m}^2$), thicker specimens
331 must be used in order to reduce large deflections. Notice that there is not intersection of working
332 domains of cases 1 and 2 for thin specimens (c.f. Figure 8a).

333 On the other hand, the results of paste and film adhesives of high fracture toughness and low failure
334 shear strengths (cases 2 to 5) show that, when the l_{FPZ} is enlarged, the upper (full FPZ formation)
335 and lower (stability) domain boundaries decrease requiring the use of larger and thicker specimens.

336 In view of the results (Figures 7, 8, 9 and 10) effects on the proposed criteria can be described.

337 The \mathcal{G}_{IIc} value has significant effect on the LD and AF criteria because higher deflections are
338 produced before the propagation starts. This reduces the maximum span length (L) and minimum
339 specimen thickness ($2H$) allowed. The \mathcal{G}_{IIc} also restricts the minimum a_0/L ratio to avoid adherend
340 failure.

341 Low shear strengths, τ_{sh} , enlarge the FPZ length making the test more stable but limiting the
342 minimum span length L and maximum a_0/L ratio (uppermost full FPZ formation criterion).

343 The use of thick specimens enlarge the l_{FPZ} reducing the a_0/L ratio that allows the full FPZ
344 development criterion but relaxing the large deflections and adherend failure criteria (minimum a_0).

345 On the contrary, the use of thin specimens increase the minimum a_0 defined by the AF criteria.

346 Despite this, the AF criteria does not significantly limit any working domain.

347 Once the working domain is defined for a particular case, it is important to consider the physical

348 background of the domain boundaries in order to make a correct choice of an experimental ELS test
349 geometry.

350 First of all, the use of as small as possible geometries inside the working domain is recommended in
351 order to avoid the early onset of Large Deflections.

352 Secondly, the use of a_0/L ratios adjoining the lower stability criteria boundary is recommended
353 providing a larger propagation zone ($L - a_0$). As mentioned in Section 3 clamp effects are not taken
354 into account in the analytical model to define the working domain, since they can not be evaluated
355 before defining the specimen. Thus, before the test, a clamp calibration may be performed in order
356 to obtain Δ_{clamp} [13]. Then, the minimum initial crack length a_0 can be defined taking into account
357 that for the stable criterion limit, the considered L in the horizontal axis of the working domain plot
358 is $L + \Delta_{clamp}$.

359 Notice also that when approaching the upper full FPZ formation limit, any propagation of the crack
360 is accomplished and only the initiation range of the resistance curve is obtained, i.e. FPZ
361 development but there is no need of take into account the clamp effect.

362 7. Conclusions

363 The large FPZ involved in adhesive testing directly affects the suitability of the ELS test. This paper
364 presents a methodology to define the working domain of the ELS test based on four limiting criteria:
365 i) stability, ii) full FPZ formation, iii) Large Deflections and iv) Adherend Failure. The presented
366 methodology ensures successful tests by providing a tool for the design of specimens. To do so, an
367 analytical model that considers a linear constitutive relation in the cohesive zone expressed in terms
368 of fracture toughness (\mathcal{G}_{IIC}) and failure shear strength (τ_{sh}) is presented and used to evaluate the
369 proposed criterion.

370 With the presented methodology, suitable ELS specimens dimensions to ensure steady state
371 propagation in adhesive testing can be obtained by assuming the adherend properties and a range
372 the adhesive mechanical properties to be tested, i.e. the working domain of specimen dimensions to

373 perform the ELS test satisfactorily.

374 It has been shown that large FPZ make the LEFM based stable criterion less restrictive but demand
375 larger zones for the crack to propagate and may induce larger deflections. Therefore, in cases of small
376 FPZ, the standard ELS dimensions are suitable but larger FPZ demand the use of thicker and larger
377 specimens. On the other hand, high toughness adhesives demands the use of thicker and stronger
378 adherends since higher stresses are reached during the test.

379 Although particular cases have been studied (Table 2), the results presented in section 5 show the
380 working domains for a combination of resins, paste and film adhesive properties (Table 1). These can
381 be used as a guide, along with the recommendations presented in the discussion section 6, to define
382 ELS specimens dimensions to satisfactorily test a wide range of adhesives with no need of further
383 analysis. The present work therefore presents a practical methodology for all those who need to
384 obtain the mode II fracture toughness in bonded joints.

385 **8. Acknowledgements**

386 The authors would like to acknowledge the support of the Spanish government through the Ministerio
387 de Economía y Competitividad under the contracts TRA2015-71491-R and MAT2015-69491-C3-1-R.

388 **References**

- 389 [1] ASTM D7905M-14 . Standard Test Method for Determination of the Mode II Interlaminar
390 Fracture Toughness of Unidirectional Fiber-Reinforced Polymer. American Society for Testing
391 and Materials 2014;.
- 392 [2] Qiao P, Wang J, Davalos JF. Analysis of tapered ENF specimen and characterization of bonded
393 interface fracture under Mode-II loading. International Journal of Solids and Structures
394 2003;40(8):1865–84. doi:10.1016/S0020-7683(03)00031-3.
- 395 [3] JIS K 7086 . Testing methods for interlaminar fracture toughness of carbon fibre reinforced
396 plastics. Japanese Standard association 1993;.

- 397 [4] Tanaka K, Kageyama K, Hojo M. Prestandardization study on mode II interlaminar fracture
398 toughness test for CFRP in Japan. *Composites* 1995;26(4):243–55.
399 doi:10.1016/0010-4361(95)93668-A.
- 400 [5] Martin R, Davidson B. Mode II fracture toughness evaluation using four point bend, end
401 notched flexure test. *Plastics, Rubber and Composites* 1999;28(8):401–6. doi:ISSN 1465-8011.
- 402 [6] Jumel J, Budzik MK. Inverse end-loaded-split test analysis effect of small scale yielding.
403 *Theoretical and Applied Fracture Mechanics* 2017;(May):1–15. URL:
404 <http://dx.doi.org/10.1016/j.tafmec.2017.11.005>. doi:10.1016/j.tafmec.2017.11.005.
- 405 [7] Wang H, Vu-Khanh T, Le VN. Effects of large deflection on mode II fracture test of composite
406 materials. *Journal of Composite Materials* 1995;29(6):833–49. doi:10.1177/002199839502900608.
- 407 [8] Wang H, Vu-Khanh T. Use of end-loaded-split (ELS) test to study stable fracture behaviour of
408 composites under mode II loading. *Composite Structures* 1996;36(1-2):71–9.
409 doi:10.1016/S0263-8223(96)00066-9.
- 410 [9] Davies P, Blackman BRK, Brunner A. Standard test methods for delamination resistance of
411 composite materials: current status. *Applied Composite Materials* 1998;5(Iso 4585):345–64.
412 doi:10.1023/a:1008869811626.
- 413 [10] Blackman BRK, Brunner A, Williams J. Mode II fracture testing of composites: a new look at
414 an old problem. *Engineering Fracture Mechanics* 2006;73(16):2443–55.
415 doi:10.1016/j.engfracmech.2006.05.022.
- 416 [11] de Moraes A, de Moura M. Evaluation of initiation criteria used in interlaminar fracture tests.
417 *Engineering Fracture Mechanics* 2006;73(16):2264–76. doi:10.1016/j.engfracmech.2006.05.003.
- 418 [12] de Moura M, Dourado N, Moraes J, Pereira FAM. Numerical analysis of the ENF and ELS tests
419 applied to mode II fracture characterization of cortical bone tissue. *Fatigue and Fracture of*
420 *Engineering Materials and Structures* 2011;34(3):149–58. doi:10.1111/j.1460-2695.2010.01502.x.

- 421 [13] ISO 15114:2014 . Fibre-reinforced plastic composites - Determination of the mode II fracture
422 resistance for unidirectionally reinforced materials using the calibrated end-loaded split (C-ELS)
423 test and an effective crack length approach. International Standard Organization, Geneva,
424 Switzerland 2014;(1):1–26.
- 425 [14] Sarrado C, Turon A, Costa J, Renart J. On the validity of linear elastic fracture mechanics
426 methods to measure the fracture toughness of adhesive joints. *International Journal of Solids
427 and Structures* 2016;81:110–6. doi:10.1016/j.ijsolstr.2015.11.016.
- 428 [15] Blackman BRK, Kinloch A, Paraschi M. The determination of the mode II adhesive fracture
429 resistance, GIIC, of structural adhesive joints: an effective crack length approach. *Engineering
430 Fracture Mechanics* 2005;72(6):877–97. doi:10.1016/j.engfracmech.2004.08.007.
- 431 [16] Högberg J, Sørensen B, Stigh U. Constitutive behaviour of mixed mode loaded adhesive layer.
432 *International Journal of Solids and Structures* 2007;44(25-26):8335–54.
433 doi:10.1016/j.ijsolstr.2007.06.014.
- 434 [17] Hashemi S, Kinloch A, Williams J. The analysis of interlaminar fracture in uniaxial
435 fiber-polymer composites. *Proceedings of the Royal Society A* 1990;427:173–99.
436 doi:10.1098/rspa.1990.0007.
- 437 [18] Brunner A. Experimental aspects of Mode I and Mode II fracture toughness testing of
438 fibre-reinforced polymer-matrix composites. *Computer Methods in Applied Mechanics and
439 Engineering* 2000;185(2-4):161–72. doi:10.1016/S0045-7825(99)00257-1.
- 440 [19] Pérez-Galmés M, Renart J, Sarrado C, Rodríguez-Bellido A, Costa J. A data reduction method
441 based on the J-integral to obtain the interlaminar fracture toughness in a mode II end-loaded
442 split (ELS) test. *Composites Part A: Applied Science and Manufacturing* 2016;90:670–7.
443 doi:10.1016/j.compositesa.2016.08.020.
- 444 [20] da Silva L, de Magalhães FC, Chaves F, de Moura M. Mode II Fracture Toughness of a Brittle

- 445 and a Ductile Adhesive as a Function of the Adhesive Thickness. *The Journal of Adhesion*
446 2010;86(9):891–905. doi:10.1080/00218464.2010.506155.
- 447 [21] Floros IS, Tserpes KI, Löbel T. Mode-I, mode-II and mixed-mode I+II fracture behavior of
448 composite bonded joints: Experimental characterization and numerical simulation. *Composites*
449 *Part B: Engineering* 2015;78(October):459–68. doi:10.1016/j.compositesb.2015.04.006.
- 450 [22] Fernandes R, de Moura M, Moreira RF. International Journal of Adhesion & Adhesives Effect
451 of moisture on pure mode I and II fracture behaviour of composite bonded joints. *International*
452 *Journal of Adhesion and Adhesives* 2016;68:30–8. URL:
453 <http://dx.doi.org/10.1016/j.ijadhadh.2016.01.010>. doi:10.1016/j.ijadhadh.2016.01.010.
- 454 [23] Carlsson L, Gillespie J, Pipes R. On the Analysis and Design of the End Notched Flexure
455 (ENF) specimen for Mode II Testing. *Journal of Composite Materials* 1986;20(6):594–604.
456 doi:10.1177/002199838602000606.
- 457 [24] Alfredsson KS. On the instantaneous energy release rate of the end-notch flexure adhesive joint
458 specimen. *International Journal of Solids and Structures* 2004;41(16-17):4787–807.
459 doi:10.1016/j.ijsolstr.2004.03.008.
- 460 [25] de Moura M. Numerical simulation of the ENF test for the mode-II fracture characterization of
461 bonded joints. *Journal of Adhesion Science and Technology* 2006;20(1):37–52. URL:
462 <http://www.tandfonline.com/doi/abs/10.1163/156856106775212422>.
463 doi:10.1163/156856106775212422.
- 464 [26] de Moura M, Chousal J. Cohesive and continuum damage models applied to fracture
465 characterization of bonded joints. *International Journal of Mechanical Sciences* 2006;48:493–503.
466 doi:10.1016/j.ijmecsci.2005.12.008.
- 467 [27] de Morais A, Pereira AB. Application of the effective crack method to mode I and mode II

- interlaminar fracture of carbon/epoxy unidirectional laminates. *Composites Part A: Applied Science and Manufacturing* 2007;38(3):785–94. doi:10.1016/j.compositesa.2006.09.001.
- [28] Leone F. Progressive Damage Analysis of Bonded Composite Joints. NASA/TM-2012-217790 2012;.
- [29] Azevedo J, Campilho R, da Silva F, Faneco T, Lopes R. Cohesive law estimation of adhesive joints in mode II condition. *Theoretical and Applied Fracture Mechanics* 2015;80:143–54. doi:10.1016/j.tafmec.2015.09.007.
- [30] Williams J. Large Displacement and End Block Effects in the 'DCB' Interlaminar Test in Modes I and II. *Journal of Composite Materials* 1987;21(4):330–47. doi:10.1177/002199838702100403.
- [31] de Moura M, de Morais A. Equivalent crack based analyses of ENF and ELS tests. *Engineering Fracture Mechanics* 2008;75(9):2584–96. URL: <http://linkinghub.elsevier.com/retrieve/pii/S0013794407001063>. doi:10.1016/j.engfracmech.2007.03.005.
- [32] Silva M, Morais J, de Moura M, Lousada J. Mode II wood fracture characterization using the ELS test. *Engineering Fracture Mechanics* 2007;74(14):2133–47. doi:10.1016/j.engfracmech.2006.10.012.
- [33] Vu-Khanh T. Crack-arrest study in mode II delamination in composites. *Polymer composites* 1987;8:331–41.
- [34] Davies P, Blackman B, Brunner A. Mode II delamination. In: Moore D, Pavan A, Williams J, editors. *Fracture mechanics Testing Methods for Polymers, Adhesives and Composites*; chap. 4.2. Elsevier. ISBN 0 08 043689 7; 2001, p. 307–33. doi:10.1016/S1566-1369(01)80039-X.
- [35] ISO 25217:2014 . Adhesives - Determination of the mode I adhesive fracture energy of structural adhesive joints using double cantilever beam and tapered double cantilever beam specimens. International Organization for Standardization, Geneva, Switzerland 2009;.

- 492 [36] Beer, F. P., Johnson, E. R., DeWolf JT. Mechanics of Materials. third ed.; New York:
493 McGraw-Hill; 2002. ISBN 10: 0073659355.
- 494 [37] Abaqus . 6.12. Documentation. Dassault Systèmes Simulia Corp., Providence. 2012.
- 495 [38] Campilho R, de Moura M, Ramantani D, Morais J, Domingues J. Buckling Behaviour of
496 Carbon-Epoxy Adhesively-Bonded Scarf Repairs. Journal of Adhesion Science and Technology
497 2009;23:1493 –513. doi:10.1163/156856109X433045.
- 498 [39] Campilho R, de Moura M, Pinto A, Ramantani D. Interlaminar Fracture Characterization of a
499 Carbon-Epoxy Composite in Pure Mode II. Materials Science Forum 2010;636 - 637:1518 –24.
500 doi:10.4028/www.scientific.net/MSF.636-637.1518.
- 501 [40] Soto A, González EV, Maimí P, Turon A, Sainz de Aja JR, de la Escalera FM. Cohesive zone
502 length of orthotropic materials undergoing delamination. Engineering Fracture Mechanics
503 2016;159:174–88. URL: <http://dx.doi.org/10.1016/j.engfracmech.2016.03.033>.
504 doi:10.1016/j.engfracmech.2016.03.033.
- 505 [41] Ma Y, Yang Y, Sugahara T, Hamada H. A study on the failure behavior and mechanical
506 properties of unidirectional fiber reinforced thermosetting and thermoplastic composites.
507 Composites Part B 2016;99:162–72. URL:
508 <http://dx.doi.org/10.1016/j.compositesb.2016.06.005>.
509 doi:10.1016/j.compositesb.2016.06.005.
- 510 [42] Landis C, Beyerlein I, McMeeking R. Micromechanical simulation of the failure of fiber
511 reinforced composites. Journal of the Mechanics and Physics of Solids 2000;48:621 –48.
512 doi:[http://doi.org/10.1016/S0022-5096\(99\)00051-4](http://doi.org/10.1016/S0022-5096(99)00051-4).
- 513 [43] Hansen P, Martin R. DCB , 4ENF and MMB delamination Characterisation of S2 / 8552 and
514 IM7 / 8552 MERL Report No. N68171-98-M-5177 1999;

- 515 [44] Campilho R, Leitão A, Fernandes R, Azevedo J, Banea M. Cohesive law estimation in mode II
516 of a ductile adhesive. *Annals of "Dunarea de Jos" University of Galati, Fascicle XII, Welding*
517 *Equipment and Technology* 2015;26:27–32.
- 518 [45] da Silva L, da Silva R, Chousal J, Pinto A. Alternative Methods to Measure the Adhesive Shear
519 Displacement in the Thick Adherend Shear Test. *Journal of Adhesion Science and Technology*
520 2008;22:15 – 29. doi:10.1163/156856108X292241.
- 521 [46] Campilho R, Pinto A, Banea M, Silva R, da Silva L. Strength Improvement of
522 Adhesively-Bonded Joints Using a Reverse-Bent Geometry Strength Improvement of
523 Adhesively-Bonded Joints Using. *Journal of Adhesion Science and Technology*
524 2011;25:23510–02368. doi:10.1163/016942411X580081.
- 525 [47] Marques E, da Silva L. Joint Strength Optimization of Adhesively Bonded Patches. *The Journal*
526 *of Adhesion* 2008;84:915 –34. doi:10.1080/00218460802505275.
- 527 [48] da Silva L, Rodrigues T, Figueiredo M, de Moura M, Chousal J. Effect of Adhesive Type and
528 Thickness on the Lap Shear Strength. *The Journal of Adhesion* 2006;82(November
529 2012):1091–115.
- 530 [49] Sarrado C. Experimental characterization and numerical simulation of composite adhesive joints
531 using the cohesive zone model approach (PhD thesis), University of Girona 2015;.
- 532 [50] Bažant Z, Planas J. *Fracture and size effect in concrete and other quasibrittle materials*. CRC
533 Press LLC; 1998. ISBN 0-8493-8284-X.
- 534 [51] Turon A, Dávila C, Camanho P, Costa J. An engineering solution for mesh size effects in the
535 simulation of delamination using cohesive zone models. *Engineering Fracture Mechanics*
536 2007;74:1665–82.

A.3 Towards a consensus on mode II adhesive fracture testing: experimental study

M. Pérez-Galmés ^a, J. Renart ^a, C. Sarrado ^a, A.J. Brunner ^b, A. Rodríguez-Bellido ^c

^aAMADE, Mechanical Engineering and Industrial Construction Department, Universitat de Girona, Campus Montilivi s/n, Girona, Spain

^bEmpa, Swiss Federal Laboratories for Materials Science and Technology, Laboratory for Mechanical Systems Engineering, Überlandstrasse 129, CH-8600 Dübendorf, Switzerland

^cComposite Technology, Materials and Processes, AIRBUS Operations SL, Paseo John Lenon s/n, E-28906 Getafe, Madrid, Spain

The paper has been submitted to *Theoretical and Applied Fracture Mechanics*

Towards a consensus on mode II adhesive fracture testing: experimental study.

M. Pérez-Galmés^{a,*}, J. Renart^a, C. Sarrado^a, A. J. Brunner^b, A. Rodríguez-Bellido^c

^aAMADE, Polytechnic School, University of Girona, Carrer Universitat de Girona, 4.Campus de Montilivi, 17003-Girona, Spain

^bEmpa, Swiss Federal Laboratories for Materials Science and Technology, Laboratory for Mechanical Systems Engineering, Überlandstrasse 129, CH-8600 Dübendorf, Switzerland

^cComposite Technology, Materials and Processes, AIRBUS Operations SL, Paseo John Lenon s/n, E-28906 Getafe, Madrid, Spain

Abstract

Mode II fracture toughness is crucial in the design of structural bonded joints between fibre reinforced polymers (FRP). This is mainly because adhesives are designed to work under shear, rather than peel, loading. However, one of the main problems encountered in mode II experimental testing is the poor reproducibility between the most common test methodologies: End-Notched Flexure (ENF), End-Load Split (ELS), 4-point End-Notched Flexure (4ENF), and the Mixed Mode Bending (MMB) test at 100% of mode II.

The objective of this work is to define reliable test methodologies and data reduction methods to obtain comparable results among the aforementioned tests.

For this reason, an experimental test campaign consisting of the abovementioned four mode II test methods was carried out. The J -integral was implemented in all the tests as a data reduction method, and it was compared to the data reduction methods based on Linear Elastic Fracture Mechanics (LEFM). The results obtained from the J -integral based methods were independent from the test methodology and obtained very good agreement among the tests.

In addition, from the experimental results the advantages and drawbacks of the different test procedures are analysed and discussed, concluding that the ELS test is the most suitable to measure mode II fracture toughness.

Keywords: Mode II fracture toughness, Bonded joints, J -integral, FRP, Mechanical testing

*Corresponding author. Tel.: +34 972 418 817

Email addresses: magdalena.perez@udg.edu (M. Pérez-Galmés), jordi.renart@udg.edu (J. Renart)